CRITICAL SCATTERING OF NEUTRONS FROM IRON

By

STEPHEN CHARLES GEORGE BORONKAY, B.Sc.,M.Sc.

A Thesis

Submitted to the Faculty of Graduate Studies

in Partial Fulfilment of the Requirements

for the Degree

Doctor of Philosophy

McMaster University

May, 1973

CRITICAL SCATTERING OF NEUTRONS FROM IRON

DOCTOR OF PHILOSOPHY (1973) McMASTER UNIVERSITY
(Physics) Hamilton, Ontario

TITLE: Critical Scattering of Neutrons from Iron

AUTHOR: Stephen Charles George Boronkay, B.Sc. (Hons.)
(Monash University), M.Sc. (Monash University)

SUPERVISOR: Dr. M. F. Collins

NUMBER OF PAGES: xi, 133

ABSTRACT:

Dynamical critical phenomena in iron were studied by the technique of inelastic neutron scattering.

Over the range of wave vector and temperature measured the spin-wave energy varied as the square of the wave vector and as the reduced temperature raised to the power 0.36 ± 0.03. The spin-wave damping diverged as the critical temperature is approached from below according to a simple power law with exponent -0.96 ± 0.10. The wave vector dependence of the damping was proportional to the fourth power of the wave vector. These results are in good agreement with the predictions of dynamic scaling and hydrodynamic theory. Anomalous damping was observed at the largest wave vector measured, 0.26 A^{-1}; this is tentatively ascribed to the effect of a Fermi surface minimum at wave vector 0.25 A^{-1}.

The spin waves became over-critically damped a few degrees below the critical temperature. At the critical temperature the scattering was diffusive in character with no

evidence of remnant spin waves; the energy width varied as a simple power of the wave vector with the exponent predicted by dynamic scaling. Above the critical temperature the width agreed with the general prediction of dynamic scaling and with the detailed numerical calculations of Résibois and Piette.

Below the critical temperature there was no evidence in the scattering of longitudinal spin fluctuations. This is in accord with other observations on isotropic ferromagnets; such a result is not physically understood at the present time.

ACKNOWLEDGEMENTS

I am particularly grateful to my research supervisor, Dr. M. F. Collins for his continuous guidance and encouragement. He has contributed greatly to my interest and knowledge in the field of solid state physics and of the techniques of neutron spectroscopy.

I would also like to thank Professor B. N. Brockhouse, F.R.S., for the use of his neutron spectrometers at McMaster University and at Chalk River Nuclear Laboratories.

To my colleagues in the neutron scattering groups at McMaster University: Mr. J. Couper, Mr. R. R. Dymond, Mr. G. S. Gill, Mr. G. Griffin, Mr. T. Johnston, Mr. W. A. Kamitakahara, Mr. J. Khatamian, Mr. A. Larose, Dr. H. C. Teh, and Mr. V. K. Tondon, go my sincere thanks for providing a congenial atmosphere, for many valuable discussions and for assistance throughout the course of this work.

This work was made possible through the financial support of an Alfred P. Sloan Fellowship award, the McMaster University Physics Department, the National Research Council of Canada, the Ontario Graduate Fellowship program and by the provision of research facilities by the Atomic Energy of Canada Limited, Chalk River, Ontario.

To Mrs. H. Kennelly go my sincere thanks for her accurate typing of this thesis, and finally to my wife, Françoise for constant encouragement during the course of my studies and for drawing the figures of this thesis.

TABLE OF CONTENTS

LIST OF ILLUSTRATIONS

LIST OF TABLES

CHAPTER I

INTRODUCTION

A. Introduction to Critical Phase Transitions

In recent years much interest has been shown in the study of critical phase transitions. Experiments have shown that ferromagnets, antiferromagnets, fluids, binary liquids, binary alloys, superconductors, ferroelectrics and superfluids all behave, near some transition temperature qualitatively and often quantitatively, in analogous ways. Because of the similarity in the nature of the phase transitions of such diverse systems it is speculated that the physical principles governing phase transitions are largely system independent.

This thesis reports on the study of one of these phase transitions, the ferromagnetic transition in iron. In view of this, the language and notation suitable for discussing magnetic properties will be adopted. It should not be forgotten however that this is just one special case of a more general problem. In fact one ultimate aim of research into critical phenomena is to give a theory which is set in sufficiently general terms as to include all the many types of systems that show critical phase transitions.

Some of the known properties of ferromagnets are considered first. A useful and powerful way of investigating magnetic systems is to apply a magnetic field H as an external probe and to

observe the resultant magnetization M, defined as the magnetic moment per unit volume, which is the response of the system to the probe. This is parametrized by the magnetic susceptibility χ that is a response function defined by

$$\chi = \frac{dM}{dH} \quad . \qquad \text{(I-1)}$$

The response is said to be linear when χ is independent of H.

A typical sketch of the magnetization M plotted against the temperature T for zero magnetic field H is given in Figure I-1a. Figure I-1a shows that above a certain temperature the magnetization is zero, while below that temperature there is a non-zero magnetization which increases monotonically as the temperature decreases. The temperature in question is known as the critical temperature T_c. The existence of a quantity which is non-zero below the critical temperature and zero above it is a common feature associated with all the different types of critical phase transitions. The quantity is known generally as the order parameter and is a measure of the amount and kind of ordering of the system; for a ferromagnetic critical transition the magnetization M is the order parameter. Below the critical temperature the system is said to be in the ordered or the ferromagnetic phase while above this temperature the system is in the disordered or paramagnetic phase.

Figure I-1b gives a typical sketch of the magnetization M plotted against the magnetic field H for different temperatures. It shows that when the temperature is much greater than the critical

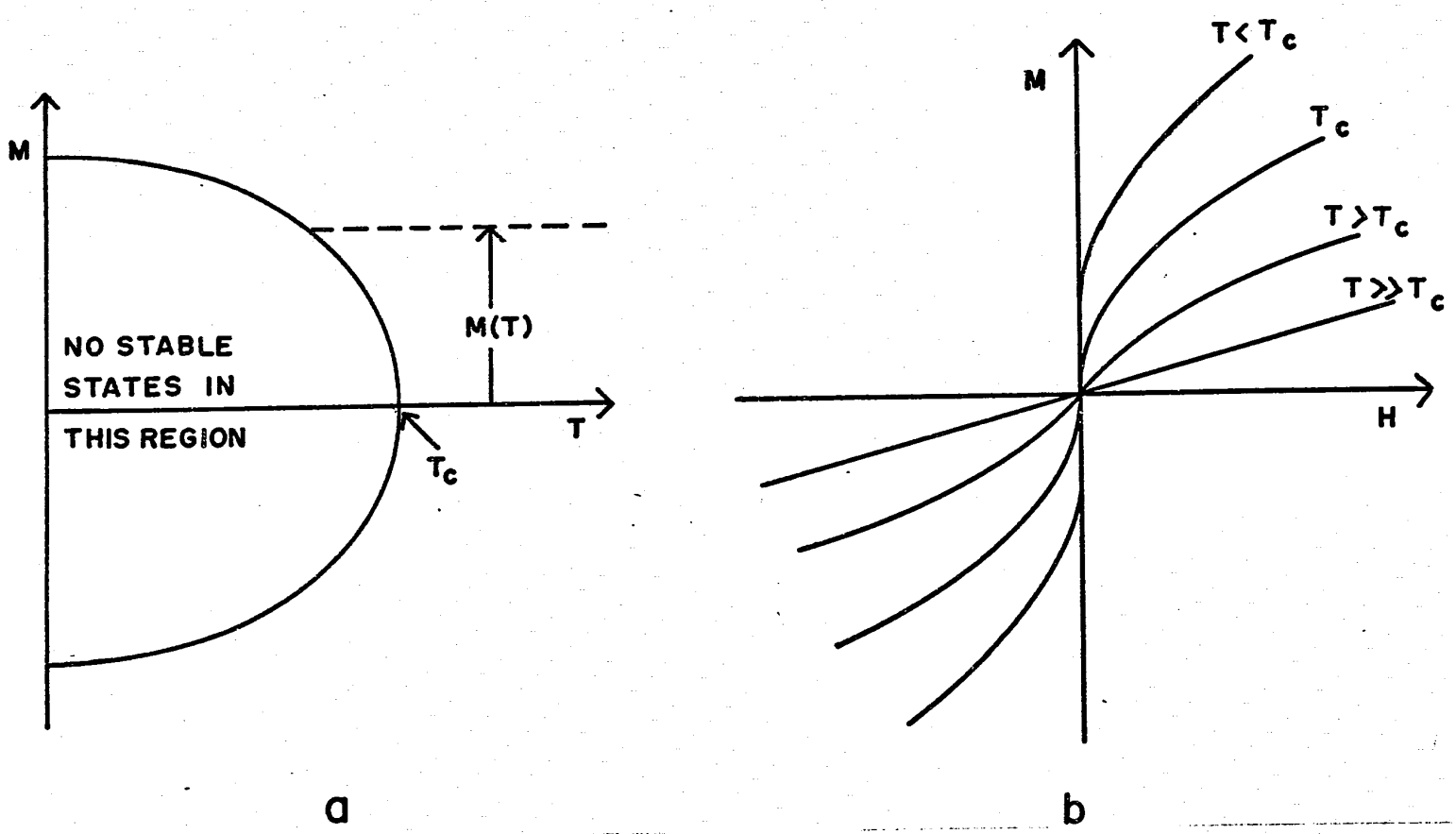

Figure I-1

(a) A typical sketch of the magnetization M plotted against the temperature T for zero magnetic field H.
(b) A typical sketch of the magnetization M plotted against the magnetic field H for different temperatures above and below the critical temperature T_c.

temperature the isotherm of the magnetization M plotted against the magnetic field H approaches a straight line. Thus the susceptibility χ is independent of the magnetic field which is the same behaviour as for the non-interacting magnetic system. This is expected since in this temperature range the individual magnetic moments or spins are randomly oriented as in a paramagnet.

As the temperature approaches the critical temperature from above, the isotherm ceases to be a straight line. Close to zero magnetic field its slope increases, and the susceptibility increases. In fact the slope becomes infinite at a temperature equal to the critical temperature in zero magnetic field so that the susceptibility becomes infinite. The increase in the susceptibility is accompanied by the appearance of small regions of correlated spins which increase in size as the critical temperature is approached. The linear size of these regions is known as the correlation range and is denoted by ξ. The regions of correlated spin result in fluctuations in space of the magnetization throughout the system. It is said that the system possesses short range order. However the magnetization of the system as a whole at and above the critical temperature is zero in zero magnetic field, i.e. there is no long range order. When the temperature is equal to the critical temperature, and the magnetic field is equal to zero, the correlation range ξ becomes infinite.

As the temperature is reduced from the critical temperature the large fluctuations in the magnetization decrease, and the

correlation range ξ also decreases. Now there is an excess of spins pointing in one direction compared with the other resulting in a net magnetization of the system even in zero magnetic field (Figures I-1a and I-1b). When the temperature is much smaller than the critical temperature the alignment is almost complete and when the temperature is equal to zero all the spins are pointing in the same direction.

Thus the ferromagnetic phase transition can be characterized by the magnetization which goes to zero and by the susceptibility and correlation length which diverge at the critical temperature for zero magnetic field. Another physical quantity that characterizes critical phase transitions is the specific heat which also diverges at the critical temperature in zero magnetic field.

The first phenomenological theories of phase transitions were by Van der Waals (1873) for the liquid-gas system and by Weiss (1907) for a ferromagnet. These theories are equivalent and were generalized by Landau (Landau and Lifshitz, 1969). They are now called mean-field theories. In a ferromagnet it is assumed that the mean field acting on each magnetic moment due to its neighbours is proportional to the magnetization of the system as a whole. However the quantitative predictions of the mean-field theory do not agree with the experimental observations on magnetic systems.

More realistic descriptions of interacting magnetic systems usually start from the Ising or the Heisenberg models. In

the Ising model the magnetic moments or spins denoted by S_ℓ^z are situated on each of the lattice sites denoted by ℓ. The direction that each moment can point is only up or down along the z axis. If an external magnetic field H is applied along the z direction then the Hamiltonian H_{ISING} of the Ising model is given by

$$H_{ISING} = - \sum_{\ell n} J_n S_\ell^z S_{\ell+n}^z - g\mu_B H \sum_\ell S_\ell^z \qquad \text{(I-2)}$$

where J_n is the exchange constant between the spins situated on the lattice sites denoted by ℓ and $\ell+n$, g is the Landé splitting factor and μ_B is the Bohr magneton.

The Heisenberg model regards the magnetic moments as being related to three component spin operators $\underline{S}_\ell$ situated on each of the lattice sites denoted by ℓ. It is assumed that the energy is proportional to the scalar product of the operators. The Hamiltonian H_{HEIS} of the Heisenberg model is given by

$$H_{HEIS} = - \sum_{\ell n} J_n \underline{S}_\ell \cdot \underline{S}_{\ell+n} - g\mu_B H \sum_\ell S_\ell^z \qquad \text{(I-3)}$$

where J_n is the exchange constant between the spins situated on the lattice sites denoted by ℓ and $\ell+n$, g is the Landé splitting factor, μ_B is the Bohr magneton and H is the magnetic field the direction of which defines the z axis.

Because of the relative simplicity of these Hamiltonians compared to those belonging to other systems much effort has been devoted to finding their solution. It is hoped that the Ising and the Heisenberg models can be used not only to attempt to

understand their magnetic phase transitions but also those of other systems as well. For the majority of magnetic systems the Heisenberg Hamiltonian is most appropriate. The theoretical predictions from the Heisenberg model will be compared with the experiments presented in this thesis.

Fluid systems exhibit similar behaviour to the magnetic systems and can be described in terms of the lattice gas model which is analogous to the Ising model. This model considers that the volume V of the fluid is partitioned into fixed cells of volume v that is the size of the molecules and an occupied cell corresponds to the spin up case in the Ising model. In this case one would find large fluctuations in the density very close to the critical temperature and when the correlation length becomes comparable to the wavelength of light, light is scattered strongly. This phenomenon is called critical opalescence. Large fluctuations in the magnetization of a ferromagnet near the critical temperature scatter thermal neutrons strongly in analogy with critical opalescence in a fluid system.

Since the Ising model gives a critical transition and can be used to describe a number of real systems it was a great milestone in the theory when the exact solution of two-dimensional Ising model in zero magnetic field was obtained by Onsager (1944). The solution did in fact show the existence of a critical phase transition at a non-zero temperature. This was significant since the exact solution of the one-dimensional Ising model does not

yield a phase transition at a non-zero temperature (Ising, 1925). Another important result of the solution of the two-dimensional Ising model was that the magnetization, susceptibility and correlation length varied as $|T_c-T|/T_c$ to the power 1/8,-7/4 and-1 respectively.

A number of experiments on widely differing critical phase transitions showed that many physical properties varied as $|T_c-T|/T_c$ raised to some power. These power laws were obeyed over several decades of variation of (T_c-T) and strongly suggested that the correct description of critical phenomena is in such terms. Since Onsager's solution also gives results of the power-law type it has become common to describe critical processes in this way with the exponents of the power laws known as critical exponents.

The critical exponent of the order parameter is called β and it is usual to write the variation of the order parameter near the critical temperature as ε^{β}, where ε is the reduced temperature defined by

$$\varepsilon \equiv \frac{|T_c-T|}{T_c} \quad . \qquad \text{(I-4)}$$

Although the physical quantities involved in the phase transitions obey simple power laws in the vicinity of the critical temperature they also contain other terms which are significant if the temperature is sufficiently far away from the critical temperature. However the range of validity of the power laws is usually large (several decades of the reduced temperature). The width of this

range is believed to be linked to the range of interactions in the critical system. For systems with short range interactions (e.g. magnetic systems) the critical properties dominate when the reduced temperature ε is less than 0.1 while for systems with long range interactions (e.g. superconductors, ferroelectrics) the range of validity of the power laws is much more restricted.

The critical exponent β could be defined more accurately as

$$\beta \equiv \lim_{\varepsilon \to o} \frac{\ell n\ M}{\ell n\ \varepsilon} . \qquad \text{(I-5)}$$

Other important critical exponents are for the susceptibility χ which varies as the reduced temperature to the power $-\gamma$ and $-\gamma'$ for temperatures above and below the critical temperature respectively and for the correlation range ξ which varies as the reduced temperature to the power $-\nu$ and $-\nu'$ for temperatures above and below the critical temperature respectively.

Unlike for the case of the one and two-dimensional Ising models no exact solutions exist for the three-dimensional Ising or Heisenberg models. However using series-expansion techniques a number of critical exponents have been calculated that are quite close to the experimental values. The critical exponent β was calculated to be 0.315 for the Ising model (Fisher, 1967) and Als-Nielsen and Dietrich (1967) found 0.305±0.005 for the order-disorder transition in the binary alloy β-brass.

For the Heisenberg ferromagnet Stephenson and Wood (1970) calculated that β = 0.38 and Ferer, Moore and Wortis (1971) calculated that β = 0.373±0.014. Experimental values are 0.367±0.008

for EuO (Als-Nielsen, Dietrich,Kunmann and Passell, 1971), 0.389±0.005 for Fe from magnetization measurements (Arajs, Tehan, Anderson and Stelmach, 1970), 0.342±0.004 for Fe using Mössbauer effect (Preston, 1968) and 0.386 for Ni (Noakes and Arrott, 1968).

A further development in the understanding of critical phenomena was the Scaling hypothesis suggesting that there exist relations among the critical exponents (Widom, 1965; Domb and Hunter, 1965; Kadanoff, 1966; Kadanoff et al. 1967; Halperin and Hohenberg, 1969). The Scaling hypothesis is supported by considerable evidence as well as by the exact prediction of the two-dimensional Ising model and the approximate series-expansion calculations for the three-dimensional Ising and Heisenberg models.

Recently a new theoretical approach was taken by Wilson and Fisher (1972) who calculated critical exponents for the Ising and Heisenberg models using renormalization group techniques for dimension $d = 4 - \varepsilon_W$ with ε_W small. For dimensions equal to or greater than four the critical exponents were found to be mean-field exponents independent of ε_W. However below d=4 they were found to vary continuously with ε_W. Wilson (1972) calculated the critical exponent γ exactly to order ε_W to be 1.244 and 1.347 for the three-dimensional Ising and Heisenberg models respectively. These are close but not exactly equal to 1.250 for the Ising model (Moore,Jasnow and Wortis, 1969), and 1.375±0.010 (Bowers and Woolf, 1969) and 1.405±0.020 (Ferer, Moore and Wortis) for the Heisenberg model, obtained by series-expansion methods.

An attractive feature of the theory of Wilson and Fisher

is that it applies for a wide range of systems that exhibit critical phase transitions. The only adjustable parameters are the lattice dimensionality and the spin dimensionality. The latter determines to which specific system the predictions apply. The Ising model, superfluid ^{4}He and the Heisenberg model correspond to spin dimensionality of one, two and three respectively. The general nature of this theory is what one is looking for in a theory of critical phase transitions because of the experimentally observed similarity between the phase transitions of a wide variety of systems. In fact this is the only general theory going beyond Landau's simple mean-field theory that is applicable to many different systems.

The magnetic phase transition is not only reflected in the rapid changes with temperature near the critical temperature of static quantities like magnetization and susceptibility but also in the rapid changes in the spin dynamics. Therefore a complete understanding of phase transitions necessitates the study of both the static and dynamic properties.

When studying the dynamics of a system one is interested in the time-dependent as well as the space-dependent properties, that is the motion of the constituents of the system and also their position or orientation. Because of the additional variable time, the study of dynamic properties of systems is more difficult than that of the static properties. As a consequence much less is known about the time-dependent aspects of critical phenomena.

However what is evident from both experiment and theory is that the dynamic properties are not system independent. For example the theoretical predictions of the spin dynamics of the Ising and the Heisenberg models are qualitatively different. This is in contrast to the static properties predicted by the two models that are qualitatively the same and are only quantitatively different. As was seen before, the only difference between the predictions of the static magnetic properties by the two models was the different numerical values of the critical exponents. However with regard to dynamic properties the Ising model unlike the Heisenberg model predicts neither the existence of spin waves nor spin diffusion.

In order to learn more about the dynamical aspects of critical phenomena there has been a great deal of interest in this field in the last few years. The experiments presented in this thesis were performed in order to study the behaviour of the spin dynamics in the vicinity of the critical phase transition in the isotropic ferromagnet iron. Although iron is a metal and its magnetic d electrons take part in electrical conduction its known magnetic properties can be adequately described by the Heisenberg model.

In a ferromagnetic material that can be described by the Heisenberg model the motion of the magnetic moments, unlike their orientation, is correlated at all temperatures. This is because the motion of each magnetic moment is influenced by the orientation of its neighbours with which it interacts.

At low temperatures in the ordered phase the elementary excitations of a Heisenberg ferromagnet are propagative modes called spin waves whose energy depends on their momentum in reciprocal space. At temperatures much less than the critical temperature there are not many spin wave modes present and the probability of scattering between spin waves is small so that they have a long lifetime and a well defined energy. As the temperature approaches the critical temperature from below ,the number of spin waves increases and the scattering between spin waves becomes more important; lifetimes decrease and the energy ceases to be well defined. That is spin waves will be damped and in addition their energies will change. At very high temperatures compared with the critical temperature in the disordered phase there are no propagative modes present, only diffusive modes.

As yet there exist no detailed theories of the spin dynamics in the vicinity of the critical temperature. The Heisenberg model gives predictions of the dynamic properties at temperatures very small or very large compared to the critical temperature. The only predictions concerning the behaviour of the spin dynamics near the critical temperature are given by dynamic scaling which attempts to generalize the static scaling approach to the case of dynamic critical phenomena. Also most of the experiments measuring the dynamic properties of magnetic materials have been performed at temperatures very small or very large compared to the critical temperature. Therefore it is not yet completely understood how the spin dynamics changes near the critical temperature; the subject will be discussed further from a theoretical

and experimental viewpoint in Chapters II and IV.

The dynamic behaviour of a system is reflected in its energy spectrum which can be measured directly using the technique of inelastic neutron scattering. The measurement is possible if the energies involved are the same order as that of the neutron. The excitation energies of a magnetic system due to the interaction of the magnetic moments depends on the strength of the exchange constant J_n given in equation (I-3). As an approximate rule the excitation energies of magnetic systems increase with increasing critical temperature. Reactors produce neutrons with energies distributed about k_BT, where the temperature T is approximately 375°K. Hence it is possible to use the method of inelastic neutron scattering to measure dynamic critical phenomena in magnetic materials whose critical temperature is approximately within an order of magnitude of 375°K. Iron,of which the critical temperature is 1044°K (Noakes, Tornberg and Arrott, 1966), falls in this range.

B. Organization of the Thesis

This thesis reports on experiments that measured the spin dynamics in iron near the critical temperature using the technique of neutron scattering.

Chapter II discusses the theory needed to analyze the experimental data and will include the neutron scattering cross-section, scaling hypothesis as well as the spin dynamics and wave-vector-dependent susceptibility of Heisenberg ferromagnets near the critical temperature. A historical survey of the measurements

of the spin dynamics by neutron scattering, with special emphasis on the experiments on iron, will also be given.

The description of the vacuum furnace, the experimental techniques and the instrumental resolution will comprise chapter III.

Chapter IV will present the results of the critical neutron scattering experiments in iron. It is divided into two main parts corresponding to temperatures less than and to temperatures equal to or greater than the critical temperature. For temperatures less than the critical temperature the observed behaviour of the spin-wave energy, damping and the susceptibility will be discussed in comparison with theoretical predictions and with other critical scattering experiments on ferromagnets. For temperatures equal to or greater than the critical temperature there were no spin-wave modes observed, only diffusive modes; the scattering will be compared with the theoretical predictions and with other experiments.

In Chapter V the conclusions reached from the experimental observations will be presented.

CHAPTER II

THEORY AND HISTORICAL SURVEY

A. Neutron Scattering Cross-section

Neutron scattering is a very useful technique in the study of condensed matter because of the following basic properties:

a) the neutrons are neutral particles and can penetrate deeply into solids in contrast with, for example, electrons,

b) neutrons are scattered by nuclei and by magnetic atoms; the latter because neutrons have a magnetic moment,

c) the wavelength of thermal neutrons is of the same order of magnitude as the distance between atoms, while their energy is in the same range as that of elementary excitations in solids, e.g. phonons and magnons. Thus, by measuring the angular and energy distribution of scattered neutrons, one can find information about the dynamics of materials.

The following discussion will include only the magnetic scattering of neutrons, and it is assumed that the atoms are stationary on the sites of the crystal lattice.

The scattering cross-section of neutrons is calculated using the first Born approximation with the incident and scattered beam represented by plane waves. The use of this approximation is justified because of the property a) above, which ensures that the scattered neutron's wave function is small compared

to the incident wave function.

The magnetic part of the interaction between the neutron and the unpaired electrons in an atom is written as

$$- \sum_i \gamma \mu_N \underline{\sigma} \cdot \underline{H}_i \qquad \text{(II-1)}$$

where $\underline{\sigma}$ is a vector whose components σ^α are the Pauli spin matrices for the neutron. $\underline{H}_i$ is the magnetic field of a single electron, moving with velocity $\underline{v}_{e_i}$, given by Dirac's theory of the electron.

The unpaired electrons in an atom usually combine to give non-zero orbital and spin angular momentum. However, in the following discussion of the neutron scattering cross-section, it is assumed that the orbital angular momentum is quenched so that it does not contribute to the scattering. This is a reasonable assumption for the case of transition metals like iron.

For spin-only scattering by identical magnetic atoms of spin S forming a Bravais lattice, the neutron scattering cross-section per unit solid angle Ω and per unit outgoing neutron energy E' is given by (Marshall and Lovesey, 1971)

$$\frac{d^2\sigma}{d\Omega dE'} = \left(\frac{\gamma e^2}{m_e c^2}\right)^2 |F(\underline{Q})|^2 \frac{k'}{k} \sum_{\alpha\beta} (\delta_{\alpha\beta} - \hat{Q}_\alpha \hat{Q}_\beta) S^{\alpha\beta}(\underline{Q},\omega) \qquad \text{(II-2)}$$

where $\alpha, \beta = x,y,z$ and

$$S^{\alpha\beta}(\underline{Q},\omega) = \sum_{if} p_i \sum_{\ell\ell'} \exp(i\underline{Q}\cdot(\underline{R}_\ell - \underline{R}_{\ell'})) \langle i|S^\alpha_\ell|f\rangle\langle f|S^\beta_{\ell'}|i\rangle \delta(\hbar\omega + E_i - E_f) \qquad \text{(II-3)}$$

S^α_ℓ is the α component of the spin operator S on the lattice site denoted by ℓ. The first term in brackets in equation (II-2)

has a numerical value of 0.292 b, and $F(\underline{Q})$ is the atomic form factor. Since it is assumed that the orbital angular momentum is quenched, the Landé splitting factor g was taken to have its spin only value of g = 2 when writing equation (II-2).

$\hbar\underline{Q}$ and $\hbar\omega$ which are the change in momentum and energy of the scattered neutron are defined by the momentum and energy conservation laws,

$$\underline{Q} = \underline{k} - \underline{k}' = \underline{\tau} + \underline{q} \qquad \text{(II-4a)}$$

$$\hbar\omega = (\hbar^2/2m)\ (k^2 - k'^2) \qquad \text{(II-4b)}$$

$\underline{k}$ and $\underline{k}'$ are the incident and scattered neutron wave vectors respectively. $\underline{\tau}$ is a reciprocal lattice vector and $\underline{q}$ is a wave vector that is restricted to the first Brillouin zone of the target material. $\hat{Q}_\alpha$ is the α direction cosine of $\underline{Q}$. $|i\rangle$ and $|f\rangle$ are the initial and final states of the target with corresponding energies E_i and E_f. p_i is the probability that the target spin system is in the initial state $|i\rangle$.

$$p_i = \frac{\exp(-E_i/k_BT)}{\sum_i \exp(-E_i/k_BT)} \qquad \text{(II-5)}$$

k_B is Boltzmann's constant and T is the absolute temperature. Using equation (II-5), the expectation value of an operator A is given by

$$\langle A \rangle = \sum_i p_i \langle i|A|i\rangle \ . \qquad \text{(II-6)}$$

For an isotropic Heisenberg ferromagnet, whose Hamiltonian was given in equation (I-3), not all the terms in the sum $\sum_{\alpha\beta}$ of equation (II-2) contribute to the cross-section. The ones that do

can be found from equation (II-3). Taking the z direction as the direction of magnetization and substituting for S^x and S^y in terms of spin creation and annihilation operators using the relations

$$S^x = \frac{1}{2}(S^+ + S^-) \quad \text{and} \quad S^y = \frac{1}{2i}(S^+ - S^-),$$

it is found that

$$S^{\alpha z}(\underline{Q},\omega) = S^{zz}(\underline{Q},\omega)\delta_{\alpha z}$$

because if $\alpha = x$ or y, then for the matrix element $\langle i|(S^+ + S^-)|f\rangle$ to be non-zero one must have f = (i+1) or (i-1), in which case the matrix element

$$\langle i\pm 1|S^z|i\rangle = 0.$$

Thus, $S^{xz}(\underline{Q},\omega) = S^{yz}(\underline{Q},\omega) = S^{zx}(\underline{Q},\omega) = S^{zy}(\underline{Q},\omega) = 0.$ (II-7)

Using similar arguments it can be shown that

$$S^{xy}(\underline{Q},\omega) = -S^{yx}(\underline{Q},\omega) \qquad \text{(II-8)}$$

so that the net contribution to the scattering from these terms is zero. Therefore the only non-zero terms in the cross-section are $S^{zz}(\underline{Q},\omega)$, $S^{xx}(\underline{Q},\omega)$ and $S^{yy}(\underline{Q},\omega)$. Furthermore in an isotropic Heisenberg ferromagnet the directions x and y are equivalent at all temperatures. Hence, utilizing the symmetry of the Heisenberg Hamiltonian fully, the cross-section given in equation (II-2) can be written as

$$\frac{d^2\sigma}{d\Omega dE'} = \left(\frac{\gamma e^2}{m_e c^2}\right)^2 |F(\underline{Q})|^2 \frac{k'}{k}[(1-\hat{Q}_z^2)S^{zz}(\underline{Q},\omega)+(1+\hat{Q}_z^2)S^{xx}(\underline{Q},\omega)] \qquad \text{(II-9)}$$

In equation (II-3) the δ function can be written in integral representation

$$\delta(\hbar\omega+E_i-E_f) = \frac{1}{\hbar}\int_{-\infty}^{\infty} dt\, \exp(-it(\hbar\omega+E_i-E_f)/\hbar)$$

so that equation (II-3) can be written as

$$S^{\alpha\alpha}(\underline{Q},\omega) = \frac{1}{\hbar}\sum_{\ell\ell'}\exp(i\underline{Q}\cdot(\underline{R}_\ell-\underline{R}_{\ell'}))\int_{-\infty}^{\infty} dt\,\exp(-i\omega t)$$

$$\times \sum_i p_i \langle i|S_\ell^\alpha \exp(iHt/\hbar) S_{\ell'}^\alpha \exp(-iHt/\hbar)|i\rangle \qquad \text{(II-10)}$$

This was obtained by utilizing first the fact that $\exp(itE_f/\hbar)$ is just a number so that it commutes with $S_{\ell'}^\alpha$, and second the relation

$$\exp(iHt/\hbar)|i\rangle = \exp(iE_i t/\hbar)|i\rangle$$

Using the definition of a time-dependent operator

$$S_{\ell'}^\alpha(t) = \exp(iHt/\hbar) S_{\ell'}^\alpha \exp(-iHt/\hbar)$$

and equation (II-6), then equation (II-10) can be written as

$$S^{\alpha\alpha}(\underline{Q},\omega)=\frac{1}{\hbar}\sum_{\ell\ell'}\exp(i\underline{Q}\cdot(\underline{R}_\ell-\underline{R}_{\ell'}))\int_{-\infty}^{\infty} dt\,\exp(-i\omega t)\langle S_\ell^\alpha(o) S_{\ell'}^\alpha(t)\rangle. \qquad \text{(II-11)}$$

So that the neutron scattering cross-section (equation (II-9)) is directly proportional to the Fourier transform in time and space of the time-dependent spin-spin correlation function

$$\langle S_\ell^\alpha(o)\ S_{\ell'}^\alpha(t)\rangle.$$

Neutron scattering is a suitable technique for studying dynamic critical phenomena in magnetic systems because the rapid change in the spin dynamics near T_c is reflected in the time-

dependent spin-spin correlation function.

Although equation (II-11) presents a very useful physical picture, it is not always easy to calculate the time-dependent spin-spin correlation function . To represent critical scattering the Fourier transform in space of the spin-spin correlation function is commonly used. The spatial Fourier transform S_q^α of the spin operator S_ℓ^α is defined by

$$S_q^\alpha = \sum_\ell S_\ell^\alpha \exp(-i\underline{q}\cdot\underline{R}_\ell) \qquad \text{(II-12)}$$

so that,summing over ℓ and ℓ',equation (II-11) becomes

$$S^{\alpha\alpha}(\underline{Q},\omega) = \frac{1}{h}\int_{-\infty}^{\infty} dt \exp(-i\omega t) \langle S_Q^\alpha(o)\ S_{-Q}^\alpha(t)\rangle. \qquad \text{(II-13)}$$

Equation (II-13) can be further transformed using linear response theory (Kubo, 1957). Linear response theory considers the neutron beam as a sinusoidally-varying magnetic field in both space and time that perturbs the system. Using this theory it is found that the neutron scattering cross-section can be written in the form that will be used to interpret the experimental data presented in this thesis. This is (Marshall and Lovesey, 1971)

$$\frac{d^2\sigma}{d\Omega dE'} = \left(\frac{\gamma e^2}{m_e c^2}\right)^2 |F(\underline{Q})|^2 \frac{k'}{k} \frac{\omega \exp(\hbar\omega/k_B T)}{\exp(\hbar\omega/k_B T)-1} \frac{N}{(g\mu_B)^2}$$

$$\times [(1-\hat{Q}_z^2)\chi^{zz}(q)F_q^{zz}(\omega) + (1+\hat{Q}_z^2)\chi^{xx}(q)F_q^{xx}(\omega)]. \qquad \text{(II-14)}$$

N is the number of spins in the system and the Bohr magneton μ_B is defined as $e\hbar/2\ m_e c$. $F_q^{\alpha\alpha}(\omega)$ is a spectral shape function that depends on the energy $\hbar\omega$ and the wave vector q that were

defined by equations (II-4b) and (II-4a). It is an even function of ω and is normalized to unity.

$$\int_{-\infty}^{\infty} F_q^{\alpha\alpha}(\omega)\,d\omega = 1 \qquad \text{(II-15)}$$

$\chi^{\alpha\alpha}(q)$, in equation (II-14), is a wave-vector-dependent susceptibility and is the Fourier transform of the response function of the spin system to a spatially varying magnetic field. The Fourier transform of the magnetic field and the magnetization are given by $H^{\alpha}(q)$ and $M^{\alpha}(q)$ respectively and the susceptibility $\chi^{\alpha\alpha}(q)$ is defined by the following relation

$$M^{\alpha}(q) = \chi^{\alpha\alpha}(q)\ H^{\alpha}(q). \qquad \text{(II-16)}$$

The form of the cross-section given by equation (II-14) is useful because, as will be shown later, $F_q^{\alpha\alpha}(\omega)$ and $\chi^{\alpha\alpha}(q)$ are quantities which it is natural to calculate in theoretical treatments that interpret the scattering in the vicinity of the critical temperature.

At small wave vectors q, near the critical temperature of iron, the neutron energy change $\hbar\omega$ is much smaller than $k_B T$

$$\therefore \frac{\omega \exp(\hbar\omega/k_B T)}{\exp(\hbar\omega/k_B T)-1} \sim \frac{k_B T}{\hbar}$$

hence integrating the cross-section (equation (II-14)) and using equation (II-15), one finds that

$$\int_{-\infty}^{\infty} d\omega \frac{d^2\sigma}{d\Omega dE} \propto \frac{k_B T}{\hbar} \sum_{\alpha} \chi^{\alpha\alpha}(q) \ . \qquad \text{(II-17)}$$

Thus the wave-vector-dependent susceptibility $\chi^{\alpha\alpha}(q)$ can be found experimentally by integrating the area under the energy spectrum of scattered neutrons. If in addition, the energy of the neutron E is much greater than the energy change on scattering $\hbar\omega$ so that the static approximation conditions

$$k'(\omega) \simeq k \qquad \text{(II-18a)}$$

and

$$q(\omega) \simeq q(\omega=0) \qquad \text{(II-18b)}$$

are satisfied, then equation (II-17) can be written as

$$\frac{d\sigma}{d\Omega} \propto \frac{k_B T}{\hbar} \sum_{\alpha} \chi^{\alpha\alpha}(q) \ . \qquad \text{(II-19)}$$

Now integrating over ω in equation (II-13) one obtains

$$\frac{d\sigma}{d\Omega} \propto \sum_{\alpha} \langle S^{\alpha}_{q}(o) S^{\alpha}_{-q}(o) \rangle \qquad \text{(II-20)}$$

so that $\chi^{\alpha\alpha}(q)$ is directly proportional to the Fourier transform in space of the time-independent spin-spin correlation function.

The majority of the previous experiments on iron measured $\frac{d\sigma}{d\Omega}$ near the critical temperature, however, the experiments reported in this thesis measured $\frac{d^2\sigma}{d\Omega dE'}$.

B. Scaling Hypothesis

The important assumption of the scaling hypothesis is that thermodynamic and correlation functions describing the phase transitions are homogeneous functions (Widom, 1965). The discussion is started with a brief review of the properties of homogeneous functions (Stanley, 1971).

A function f(x) is by definition homogeneous if for all values of the parameter λ

$$f(\lambda x) = g(\lambda) f(x). \qquad \text{(II-21)}$$

A homogeneous function f(x) has the property that, if its value at a point $x = x_o$ as well as the functional form of $g(\lambda)$ is known, the function is known everywhere. This follows because every value of x can be written in the form λx_o, and

$$f(\lambda x_o) = g(\lambda) f(x_o)$$

so that the value of f(x) at any point is related to $f(x_o)$ by a simple change of scale that is in general not linear.

Furthermore the function $g(\lambda)$ must be of the form

$$g(\lambda) = \lambda^p. \qquad \text{(II-22)}$$

A particular feature of homogeneous functions that will be useful in later discussion is now described considering a homogeneous function of two variables

$$f(\lambda x, \lambda y) = \lambda^p f(x,y) \ . \qquad \text{(II-23)}$$

Since equation (II-23) is valid for all values of the parameter λ (equation (II-21)), it holds for the particular choice $\lambda = 1/y$,

$$\therefore \ f(x/y,1) = y^{-p} f(x,y) \ . \qquad \text{(II-24)}$$

f(x/y,1) is formally a function of two variables with the second variable fixed at the value unity. Hence it can be denoted by a function of a single variable, defining the function

$$F(x/y) \equiv f(x/y,1).$$

Hence

$$f(x,y) = y^{p}F(x/y). \qquad \text{(II-25)}$$

In this thesis the scaling hypothesis as formulated by Halperin and Hohenberg (1969) will be outlined because it is suitable for interpreting critical neutron scattering experiments on magnetic systems.

The natural space to discuss the neutron scattering cross-section and the spin dynamics of magnetic systems is momentum-energy space. The formulation of the scaling hypothesis will also be given in momentum-energy space. The coordinates in momentum-energy space are the wave vector $\underline{q}$ and frequency ω which are the Fourier transforms of the coordinates $\underline{r}$ and t in position-time space.

A variable that is a function of the coordinates of one space can also be changed into a function of the coordinates of the other space by Fourier transformation. The Fourier transform in space for the spin operator S_{ℓ} is given by equation (II-12). A property of Fourier transformation is that small wave vectors q in momentum or reciprocal space correspond to large distances in position or real space. Similarly large wave vectors q in reciprocal space correspond to small distances in real space.

For diffusive type motion such as occurs above the critical temperature the spin-spin correlation function in real space decays monotonically with increasing distance between the spins. At a particular temperature it has a characteristic length called the correlation length ξ, that was discussed in Chapter I. The

Fourier transform of the spin-spin correlation function also decays monotonically with increasing wave vector q in reciprocal space. At a particular temperature it has a characteristic length in reciprocal space called the inverse correlation length $\kappa_1 \equiv \xi^{-1}$.

(i) Static scaling

Halperin and Hohenberg (1969) formulated static scaling by assuming that the inverse correlation length in reciprocal space κ_1 contains the dominant effects of critical fluctuations. In zero external magnetic field, κ_1 is assumed to go to zero at T_c as

$$\kappa_1 \propto \varepsilon^{\nu'} \quad \text{for T less than } T_c \qquad \text{(II-26a)}$$

$$\kappa_1 \propto \varepsilon^{\nu} \quad \text{for T greater than } T_c \qquad \text{(II-26b)}$$

Halperin and Hohenberg discussed the significance of the inverse correlation length κ_1 with the aid of a graph in reciprocal space (Figure II-1) where the wave vector q forms the ordinate and the inverse correlation length κ_1 forms the abscissa.

In Figure II-1, region I, where q is much smaller than κ_1 and the temperature is less than the critical temperature, is called the macroscopic or hydrodynamic region in the ordered phase. This is because in real space it corresponds to phenomena occurring over distances that are large compared to the correlation length ξ. Similarly region III, where the temperature is larger than the critical temperature, is the hydrodynamic region in the disordered phase. Region II, where the temperature

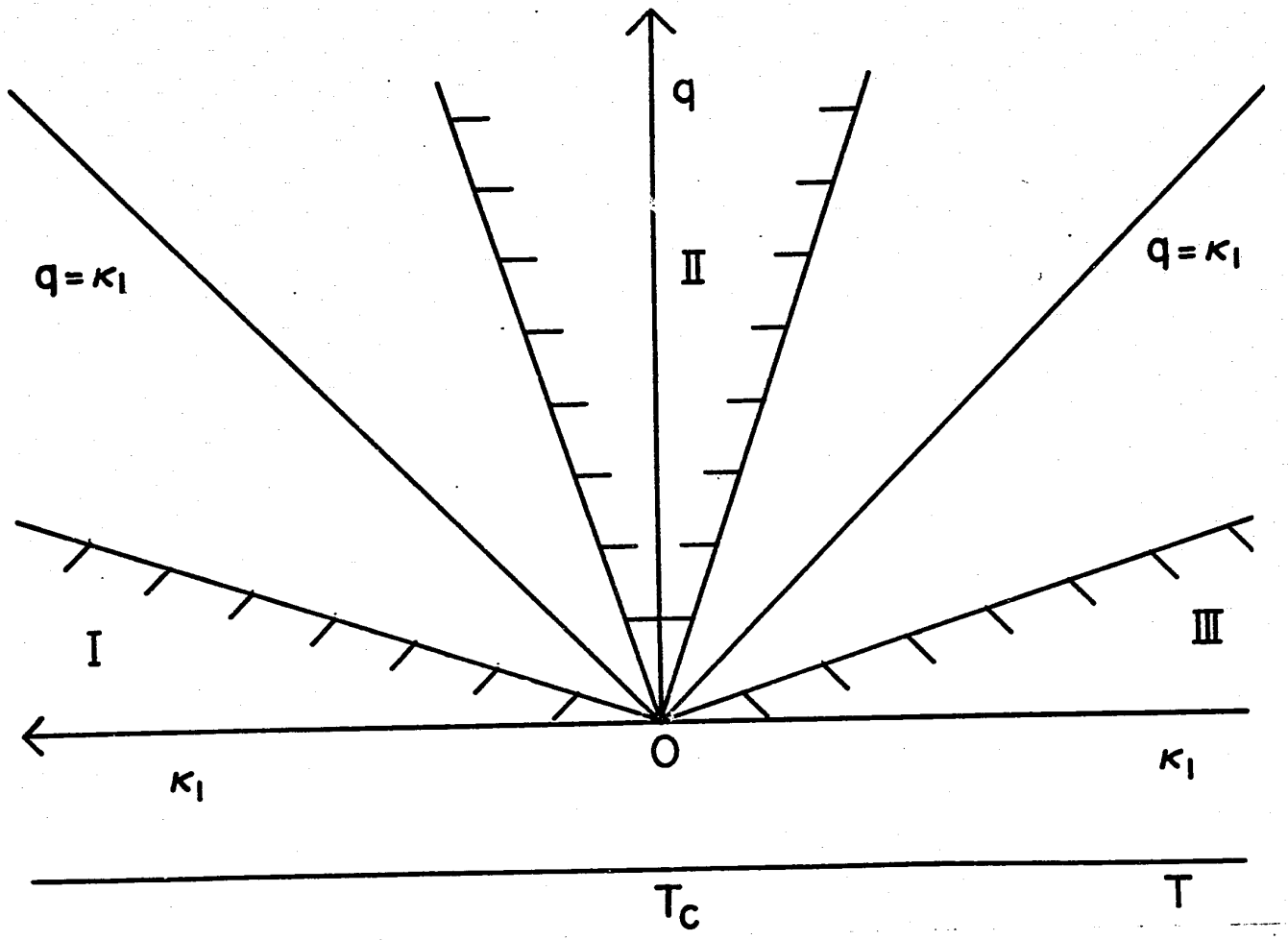

Figure II-1.

Representation of three asymptotic regions labelled I, II and III, in the q-κ_1 plane of reciprocal space, where the spin-spin correlation function has different characteristic behaviour.

is approximately equal to the critical temperature but where q is very much bigger than κ_1, is called the critical region which describes phenomena occurring over distances small compared to ξ.

The static spin-spin correlation function $C^{\alpha\alpha}_{\kappa_1}(q)$ is defined by

$$C^{\alpha\alpha}_{\kappa_1}(q) = \langle S^{\alpha}_{q}(o) S^{\alpha}_{-q}(o) \rangle \qquad \text{(II-27)}$$

so that from equation (II-19) and (II-20) $C^{\alpha\alpha}_{\kappa_1}(q)$ is directly proportional to the susceptibility $\chi^{\alpha\alpha}(q)$.

The static scaling hypothesis assumes that the spin-spin correlation function $C^{\alpha\alpha}_{\kappa_1}(q)$ varies smoothly in the q-κ_1 plane (Figure II-1) except for the singularity at the origin and that it is determined by its limiting but different behaviour in the above-mentioned three asymptotic regions. Furthermore since the correlation function is assumed to be a homogeneous function, it can be described by a function in the q-κ_1 plane that depends only on the ratio κ_1/q (equation (II-25)), given by

$$C^{\alpha\alpha}_{\kappa_1}(q) = q^{y} g^{+}(\kappa_1/q) \text{ , T greater than } T_c \qquad \text{(II-28a)}$$

$$C^{\alpha\alpha}_{\kappa_1}(q) = q^{y} g^{-}(\kappa_1/q) \text{ , T less than } T_c \qquad \text{(II-28b)}$$

(y depends on the dimensionality of the system; for three dimensions y=2). For finite q there is no discontinuity at the critical temperature so that $g^{+}(o) = g^{-}(o)$.

Since the spin-spin correlation function $C^{\alpha\alpha}_{\kappa_1}(q)$ depends only on the ratio κ_1/q (equations (II-28a) and (II-28b)), it

seems reasonable that its functional form is determined by whether q is much bigger or much smaller than the inverse correlation range κ_1.

The assumptions above give rise to functional relations between critical exponents, in particular that they can all be expressed in terms of two or three fundamental exponents. Two relations are that the critical exponents of the susceptibility χ and of the inverse correlation range κ_1 below the critical temperature are equal to the respective exponents above

$$\gamma = \gamma' \qquad \text{(II-29a)}$$

$$\nu = \nu' \ . \qquad \text{(II-29b)}$$

Scaling hypothesis does not predict the basic two or three critical exponents. However the relations predicted between critical exponents are in good agreement with experiment for a wide variety of systems. All the theoretical models commonly used to describe critical properties (c.f. Chapter I) give results in agreement with the scaling hypothesis. Hence the scaling hypothesis is believed to be correct and is useful in the study of critical phenomena.

(ii) Dynamic scaling

Dynamic scaling, in analogy with static scaling, assumes that the form of the dynamic correlation function is characterized by its behaviour in the three limiting regions in Figure II-1.

Halperin and Hohenberg defined the dynamic correlation function $S^{\alpha\alpha}_{\kappa_1}(q,\omega)$ of the neutron scattering cross-section

(equation (II-2)) to be in the form

$$S^{\alpha\alpha}_{\kappa_1}(q,\omega) = \frac{2\pi}{\omega_{\kappa_1}(q)} \; C^{\alpha\alpha}_{\kappa_1}(q) f^{\alpha\alpha}_{\kappa_1,q} \left(\frac{\omega}{\omega_{\kappa_1}(q)}\right) \qquad \text{(II-30)}$$

$S^{\alpha\alpha}_{\kappa_1}(q,\omega)$ is the Fourier transform in time and space of the time-dependent spin-spin correlation function.

Comparing $S^{\alpha\alpha}_{\kappa_1}(q,\omega)$ (equation (II-30)) with the neutron scattering cross-section in the form given by equation (II-14), one finds that when $\hbar\omega$ is much less than $k_B T$

$$F^{\alpha\alpha}_{q}(\omega) = \frac{1}{\omega_{\kappa_1}(q)} \; f^{\alpha\alpha}_{\kappa_1,q} \left(\frac{\omega}{\omega_{\kappa_1}(q)}\right). \qquad \text{(II-31)}$$

This was obtained using the result that $C^{\alpha\alpha}_{\kappa_1}(q)$ is directly proportional to $\chi^{\alpha\alpha}(q)$. Equations (II-31) and (II-15) imply that

$$\frac{1}{\omega_{\kappa_1}(q)} \int_{-\infty}^{\infty} d\omega \; f^{\alpha\alpha}_{\kappa_1,q} \left(\frac{\omega}{\omega_{\kappa_1}(q)}\right) = 1 \qquad \text{(II-32)}$$

Equation (II-32) defines the characteristic frequency $\omega_{\kappa_1}(q)$. The dynamic scaling assumptions are:

a) The characteristic frequency is a homogeneous function of q and κ_1. For the Heisenberg ferromagnet it was found to be of the form (c.f. equation (II-25))

$$\omega_{\kappa_1}(q) = c \; q^{5/2} \; f(\kappa_1/q). \qquad \text{(II-33)}$$

b) The dimensionless spectral weight function

$$f^{\alpha\alpha}_{\kappa_1,q} \left(\frac{\omega}{\omega_{\kappa_1}(q)}\right)$$

depends only on the quotient κ_1/q and not on q and κ_1 separately

$$\therefore f^{\alpha\alpha}_{\kappa_1,q}\left(\frac{\omega}{\omega_{\kappa_1}(q)}\right) = f^{\alpha\alpha}_{\frac{\kappa_1}{q}}\left(\frac{\omega}{\omega_{\kappa_1}(q)}\right). \qquad \text{(II-34)}$$

The above scaling assumptions have an important consequence on the frequency dependence of the dynamic correlation function $S^{\alpha\alpha}_{\kappa_1}(q,\omega)$: the shape of $S^{\alpha\alpha}_{\kappa_1}(q,\omega)$ will be the same along any straight line through the origin in the q-κ_1 plane apart from a change in scale determined by equations (II-28a and b) and (II-33).

C. Spin Dynamics

(i) Temperatures smaller than the critical temperature

For a Heisenberg ferromagnet at low temperatures the spin fluctuations are in the x-y plane and are described by spin-wave theory. A spin wave is a propagative excitation with wave vector q, and energy E_q. At limitingly low temperatures spin-wave theory is exact, but as the temperature is raised spin waves become damped and their energy varies with temperature. To describe the damping, a damping coefficient Γ_q for the spin waves is introduced so that the time-dependent transverse spin-spin correlation function can be written as

$$\begin{aligned} &\langle S^x_q(o) S^x_{-q}(t)\rangle \\ &= \langle S^x_q(o) S^x_{-q}(o)\rangle \left[\exp(iE_q t/\hbar)+\exp(-iE_q t/\hbar)\right]\exp(-\Gamma_q t). \end{aligned} \qquad \text{(II-35)}$$

Comparing the Fourier transform in time of this spin-spin correlation function with the neutron scattering cross-section (equation II-14)) for $\hbar\omega$ much less than $k_B T$, the spectral shape function $F^{xx}_q(\omega)$ can be shown to have a double-Lorentzian form

given by

$$F_q^{xx}(\omega) = \frac{\frac{1}{2}\Gamma_q}{(\omega-E_q)^2 + \Gamma_q^2} + \frac{\frac{1}{2}\Gamma_q}{(\omega+E_q)^2 + \Gamma_q^2} . \qquad \text{(II-36)}$$

This form of the damping has been commonly used in the past for interpreting experimental data. However Halperin and Hohenberg (1969) have given a somewhat different expression derived from hydrodynamic theory. They write

$$F_q^{xx}(\omega) = \frac{\gamma_q E_q^2}{(\omega^2-E_q^2)^2 + \gamma_q^2 E_q^2} \qquad \text{(II-37)}$$

For this expression the damping coefficient is denoted by γ_q.

The double-Lorentzian expression (equation (II-36)) brought to a common denominator can be written as

$$\frac{\Gamma_q(\Gamma_q^2 + \omega^2 + E_q^2)}{(\omega-E_q)^2(\omega+E_q)^2 + \Gamma_q^4 + 2\Gamma_q^2(\omega^2+E_q^2)} .$$

When the spin-wave damping Γ_q is much smaller than the energy E_q and ω is near resonance (i.e. $\omega^2 \simeq E_q^2$) the expression becomes,

$$\sim \frac{2\Gamma_q E_2^2}{(\omega^2-E_q^2)^2 + 4\Gamma_q^2 E_q^2} ,$$

which is just the Halperin and Hohenberg expression. Thus the two spectral shape functions are nearly identical with $\gamma_q = 2\Gamma_q$ if Γ_q is much smaller than E_q and with ω near resonance.

In Figure II-2, the two spectral shape functions are plotted for different values of the energy and damping coefficients with the constraint that $\gamma_q = 2\Gamma_q$ for each pair of spectra. Figure II-2 shows that both forms display a peak when ω equals

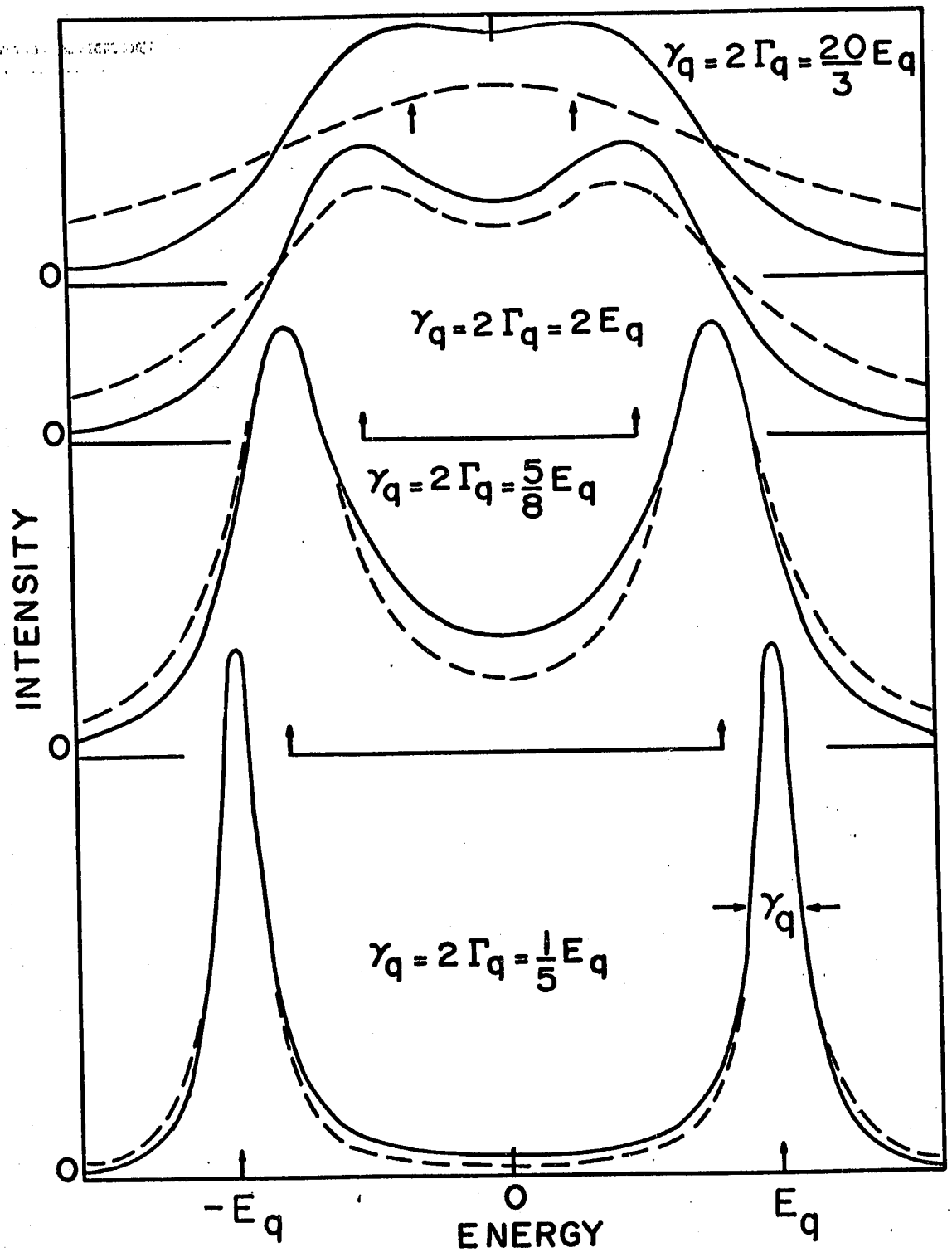

Figure II-2

Energy spectra predicted by the Halperin and Hohenberg (solid line) and the double-Lorentzian (dashed line) spectral shape functions for different values of the spin-wave energy and damping coefficients.

$\pm E_q$, corresponding to spin-wave annihilation and creation, so long as the damping is not too large compared to the energy. It also shows that the width of the peaks depends on the damping and the condition that the peaks are well resolved is that the damping coefficient is less than the spin-wave energy.

Different theories use either the form (II-36) or (II-37) to describe the damping. When analyzing the experiments the two spectral forms will be individually fitted to the data. The spin-wave energy and damping are expected to vary with temperature and the optimum values of the parameters for which the appropriate spectral form best fits the data will be found for each temperature. For well separated and sharp spin waves, the spectral forms should give approximately the same values for the damping and for the energy. However Figure II-2 shows that when the damping becomes of the order E_q the two spectral forms are different and therefore will not necessarily give the same values for the corresponding fitted parameters.

Lowest order spin-wave theory, considering terms only up to quadratic in spin operators (Holstein and Primakoff, 1940; Dyson, 1956) gives that at low temperatures and in the long-wavelength limit, for a cubic ferromagnet

$$E_q = Dq^2 \quad . \qquad \text{(II-38)}$$

When terms only up to quadratic in spin operators are considered in the Hamiltonian, the solution yields no interaction between spin waves. If there is no interaction between spin

waves then they are not damped and their energy does not depend on the temperature. Considering also terms of higher order than quadratic in the Hamiltonian, the solution of spin-wave theory does yield interactions between spin waves; it is called the dynamical interaction.

Spin-wave theory gives the temperature variation of the spin-wave energy due to the dynamical interaction as

$$E_q(T) = E_q(o)(1 + cT^{5/2}) \quad . \qquad \text{(II-39)}$$

The damping was calculated by Harris (1968) using perturbation theory, for spin waves with energy less than k_BT, taking into account all two magnon processes for the dynamical interaction. He predicts that the spin-wave damping is proportional to

$$q^4T^2\left(\frac{1}{6}\,\ell n^2\,\frac{k_BT}{Dq^2} + \frac{5}{9}\,\ell n\,\frac{k_BT}{Dq^2} - 0.05\right) \qquad \text{(II-40)}$$

the first term of which is the same as that obtained by Vaks, Larkin and Pikin (1968).

The above results of spin-wave theory for the temperature dependence of the energy and damping are not expected to be valid near T_c because the theory is effectively a low temperature expansion for the spin-wave properties. Another reason for the breakdown of spin-wave theory is that it ignores the kinematical interaction (Dyson, 1956) between magnons. The origin of this interaction is that no more than 2S spin deviations can exist on a single atom. The kinematical interaction is proportional to $\exp(-J/k_BT)$, where J is the exchange constant given in equation

(I-3). It is not expected to be significant at low temperatures (Dyson, 1956) and it cannot be expressed as a power series in $k_B T$.

Using another approach, namely hydrodynamic theory, Halperin and Hohenberg predicted that the spin-wave energy and damping in the hydrodynamic region below T_c are given by

$$E_q = Dq^2 \tag{II-41}$$

and

$$\gamma_q = \gamma' q^4 \ . \tag{II-42}$$

Furthermore they calculated that the spin-wave constant

$$D = \rho_s / \langle M \rangle$$

where ρ_s is a stiffness constant for variations in the direction of the spin orientation. Close to T_c the average magnetization $\langle M \rangle$ is proportional to ε^β and the stiffness constant ρ_s is proportional to κ_1. Using equation (II-26a)

$$D \propto \kappa_1 \, \varepsilon^{-\beta} = \varepsilon^{\nu' - \beta} . \tag{II-43}$$

From equations (II-31) and (II-37) we have that

$$f_{\frac{\kappa_1}{q}}\left(\frac{\omega}{E_q}\right) = \frac{\gamma_q / E_q}{\left(\frac{\omega^2}{E_q^2} - 1\right)^2 + \left(\gamma_q / E_q\right)^2} .$$

The dynamic scaling assumption b) (equation (II-34)) gives that $f_{\frac{\kappa_1}{q}}\left(\frac{\omega}{E_q}\right)$ depends only on the quotient $\frac{\kappa_1}{q}$

$$\therefore \frac{\gamma_q}{E_q} = \frac{\gamma' q^2}{D} \propto \left(\frac{q}{\kappa_1}\right)^2$$

Using equations (II-26a) and (II-43), then near T_c

$$\gamma' \propto \kappa_1^{-2} D = \varepsilon^{-\nu'-\beta}. \qquad \text{(II-44)}$$

So far, in the discussion of the spin dynamics below T_c, only spin fluctuations in the x-y plane have been considered. According to spin-wave theory there are no spin fluctuations along the direction of magnetization at very low temperatures. However at higher temperatures there are also spin fluctuations in the z direction.

One possibility is that the fluctuations in the z direction decay monotonically with a certain characteristic time that might change rapidly near T_c. In this case the energy spectrum would be a broad peak centered at zero energy and the width of the peak would depend on the characteristic decay time of the fluctuations.

Another possibility is that the fluctuations in the z direction oscillate so they can propagate. If these oscillations decay with time then they would give rise to damped waves. The energy spectrum would be qualitatively similar to that of the spin fluctuations in the x-y plane. However, the quantitative behaviour of the spin fluctuations in the z direction would be different. Such fluctuations are known as second magnons since they can be regarded as temperature oscillations in analogy with second phonons. Forney and Jäckle (1972) predicted that second magnons may occur over a limited frequency range at temperatures well below the critical temperature but not near T_c. Gulayev (1965) and Reiter (1968) have speculated their existence at higher temperatures. As yet there is no experimental evidence to support their existence at any temperature.

(ii) Temperatures equal to or greater than the critical temperature

As mentioned in Chapter I, the magnetization in a ferromagnet above T_c is zero in zero magnetic field. Therefore the directions x, y and z are equivalent for systems with an isotropic Hamiltonian like Heisenberg ferromagnets and the spin fluctuations in all the directions are the same.

Halperin and Hohenberg suggested that:

a) at temperatures equal to or greater than T_c the spin dynamics can be described using a spectral shape function that is given by a Lorentzian

$$F_q^{\alpha\alpha}(\omega) = \frac{\Gamma_T(q)}{\omega^2 + \Gamma_T^2(q)} \qquad \text{(II-45)}$$

b) the width parameter $\Gamma_T(q)$ is equal to the characteristic frequency defined by equation (II-33)

$$\therefore \Gamma_T(q) = cq^{5/2} f(\kappa_1/q) \qquad \text{(II-46)}$$

c) at T_c, $f(\kappa_1/q) = 1$

$$\therefore \Gamma_{T_c}(q) = cq^{5/2}. \qquad \text{(II-47)}$$

In the hydrodynamic region above T_c, Halperin and Hohenberg found that

$$f(\kappa_1/q) = (\kappa_1/q)^{1/2} \qquad \text{(II-48)}$$

$$\therefore \Gamma_T(q) = c\,\kappa_1^{1/2}\, q^2 = \Lambda q^2 \qquad \text{(II-49)}$$

and $c\,\kappa_1^{1/2}$ is defined to be the spin-diffusion constant Λ.

Hence Λ should vary as the reduced temperature ε to the power $\nu/2$ (equation (II-26b)).

Résibois and Piette (1970) calculated the scaling function $f(\kappa_1/q)$ between the critical region and the hydrodynamic region.

Just above T_c there exist regions of correlated spin although the net magnetization of the system is zero. In these regions the spin fluctuations may possibly give rise to damped spin waves in addition to the diffusive peak given in equation (II-45). However as the regions of correlated spin decrease rapidly with increasing temperature so would the damped spin-wave component of the energy spectrum.

These predictions are for Heisenberg ferromagnets where it is assumed that the spins are localized around the magnetic atoms. Since iron is a metal and its magnetic d electrons take part in the conduction it would not be correct to assume that the spins are localized. Recently, Hertz (1971) investigated the properties of spin fluctuations at and above T_c in itinerant ferromagnets and came to the conclusion that they are identical to those in a localized spin ferromagnet, namely that in the critical region the characteristic frequency varies as $q^{5/2}$ and in the hydrodynamic region the spin diffusion constant Λ is proportional to $\kappa_1^{1/2}$.

Experimental results on iron bear out the predictions of Hertz in as much as the metallic properties in iron are not evident, since the spin waves at low temperatures and the critical properties behave in a manner that might be expected for a Heisenberg ferromagnet.

D. Susceptibility

(i) Temperatures greater than the critical temperature

Above T_c in an isotropic ferromagnet all directions are equivalent. The Ornstein-Zernike approximation as applied to the Heisenberg ferromagnet (see Stanley, 1971) predicts that for small wave vectors q with respect to the first Brillouin zone boundary, the susceptibility $\chi(q)$ is given by

$$\chi(q) \sim \frac{1}{r_1^2(\kappa_1^2+q^2)} \qquad \text{(II-50)}$$

where κ_1 is the inverse correlation length and r_1 is the effective interaction range of the time independent correlation function. The asymptotic form of the time independent correlation function is given by the Ornstein-Zernike approximation

$$\langle S_{\ell}(o)S_{\ell'}(o)\rangle \sim \frac{1}{r_1^2}\ \frac{\exp(-\kappa_1 r)}{r}, \text{ where } r = |\underline{\ell}-\underline{\ell}'| \qquad \text{(II-51)}$$

(ii) Temperatures smaller than the critical temperature

The low-temperature form of the neutron scattering cross-section for a Heisenberg ferromagnet gives a transverse susceptibility $\chi^{xx}(q)$, which varies as k_BT/Dq^2 if the thermal energy k_BT is much greater than the spin-wave energy Dq^2. This theory neglects the kinematical interaction and assumes that all the terms higher than quadratic in spin operators in the Hamiltonian are involved only in the renormalization of the spin-wave constant D.

$$\therefore\ \chi^{xx}(q) \sim k_BT/Dq^2\ . \qquad \text{(II-52)}$$

A different form was predicted by Marshall and Murray (1969) considering the kinematical as well as the dynamical spin-wave interactions. They found that for the same conditions as above

$$\chi^{xx}(q) \sim \langle S^z \rangle k_B T/Dq^2. \qquad \text{(II-53)}$$

Near T_c longitudinal spin fluctuations may also exist. Assuming that the z component of the spins have an inverse correlation range κ_1, then the longitudinal susceptibility $\chi^{zz}(q)$ may have the Ornstein-Zernike form given in equation (II-50).

E. Historical Survey

The critical properties of iron have been studied by neutron scattering more extensively than any other ferromagnet, and in this section the highlights of earlier work are described. The first observations of critical scattering of neutrons in iron were by Palevsky and Hughes (1953), and by Squires (1954), from the study of the transmission of long wavelength neutrons. They found an anomalous increase in the total cross-section near the critical temperature.

Wilkinson and Shull (1956) found additional diffuse magnetic scattering near T_c that was most intense at the smallest angle measured and decreased with increasing angle. They found that at a fixed angle the additional magnetic scattering increased with temperature to a maximum in the vicinity of T_c and then decreased with increasing temperature. This appearance of a pronounced maximum at T_c in the small angle scattering suggested that it arises from the spontaneous fluctuations in the magnetic

moment density, which increases in magnitude as T_c is approached (Van Hove, 1954).

Jacrot, Konstantinovic, Parette and Cribier (1963) using a polycrystalline specimen of iron and neutrons of wavelength 4.75 A measured the differential cross-section $\frac{d\sigma}{d\Omega}$ above T_c.

It was seen that if the static approximation is obeyed (equations (II-18a and b)), the differential cross-section $\frac{d\sigma}{d\Omega}$ is proportional to the susceptibility $\chi(q)$ (equation (II-19)). Also, above T_c for the Ornstein-Zernike approximation, $\chi(q)$ is proportional to $\frac{1}{r_1^2(q^2+\kappa_1^2)}$ (equation (II-50)), so that the inverse correlation length κ_1 can be found directly by extrapolating the curve of the inverse scattered intensity plotted against q^2.

Jacrot et al. observed that even at T_c the scattering was inelastic and that the energy spectra of scattered neutrons could be fitted satisfactorily by a Lorentzian,

$$F_q(\omega) \sim \frac{\Lambda q^2}{\omega^2+\Lambda^2 q^4} \qquad \text{(II-54)}$$

with only a weak temperature variation of the spin-diffusion coefficient Λ. Therefore the second condition (equation (II-18b)) of the static approximation probably does not hold. Nevertheless Jacrot et al. found κ_1 directly, neglecting the inelasticity of the scattering. Their results were consistent with the values of κ_1 found previously by Ericson and Jacrot (1960).

Passell, Blinowski, Brun and Nielsen (1965) measured the small angle scattering from a polycrystalline sample of iron with 4.28 Å neutrons above T_c. In agreement with Jacrot et al., they found that the energy spectrum of the scattered neutrons could be fitted satisfactorily by the function $\frac{\Lambda q^2}{\omega^2 + \Lambda^2 q^4}$ (equation (II-54)). They determined the Ornstein-Zernike correlation function parameters κ_1 and r_1 in a similar fashion to Jacrot et al. However, they used the spectral form given above (equation (II-54)) to correct for the inelasticity of the scattering and obtained more accurate values of κ_1. They observed that the inverse of the resolution-corrected intensity plotted against q^2 deviated from a straight line at large wave vectors, and concluded that the form of the susceptibility $\chi(q)$ is only a Lorentzian (equation (II-50)) at small wave vectors. This deviation at large wave vectors did not affect their determination of κ_1 and $\chi(o)$. For the temperature range $(T-T_c)$ greater than 5°K they found that the inverse static susceptibility

$$\chi(o)^{-1} \sim T(\kappa_1^2 r_1^2) \sim (T-T_c)^{\gamma}$$

with $\gamma = 1.30 \pm 0.04$.

Spooner and Averbach (1966) showed that the diffuse magnetic scattering in a single crystal of iron is spherically symmetric about the origin at large wavelengths. They measured the scattering in the complete first Brillouin zone and obtained the spin-correlation coefficients above T_c from the

Fourier transform of the scattered intensity. Their treatment neglects inelasticity and hence must be somewhat questioned, although, with the short wavelength (1.38 A) neutrons they used, the correction is not as large as was involved in the long wavelength experiments.

Bally, Grabcev, Lungu, Popovici and Totia (1967) measured the temperature variation of small angle scattering of 1.25 A neutrons by a polycrystalline sample of iron and found that at very small wave vectors the scattering peaked at T_c, while at large wave vectors the peak was not as sharp and it shifted to higher temperatures. They determined κ_1 and r_1 after correcting for the inelasticity of the scattering and concluded that the Ornstein-Zernike time independent correlation function (equation (II-51)) is only valid for distances greater than 15 A. For smaller distances they claimed that the correlation has the form $\langle S_{\underline{\ell}}(o)\ S_{\underline{\ell}'}(o)\rangle \propto \exp(|\underline{\ell}'-\underline{\ell}|/\delta)$ that agreed with the findings of Spooner and Averbach. The critical exponent γ of the susceptibility $\chi(o)$ above the critical temperature was found to be 1.30 ± 0.04.

Stringfellow (1968) using a scattering surface technique near the forward direction, studied the spin dynamics from low temperatures up to the critical temperature. He found that in a polycrystalline iron specimen magnetized with a 3000 Oe magnetic field, the spin-wave constant D could be described satisfactorily using itinerant electron theory up to 0.4 T_c,

by the expression $D = D_o - D_1 T^2 - D_2 T^{5/2}$. However above 0.4 T_c, D decreased considerably faster than was predicted. Stringfellow found that the spin-wave cross-section increased with increasing temperature up to 0.7 T_c.

A comprehensive experiment that measured the spin dynamics in iron close to the critical temperature was performed by Collins, Minkiewicz, Nathans, Passell and Shirane (1969). They concentrated on very small wave vectors q both above and below T_c to try to satisfy the hydrodynamic condition, q much smaller than the inverse correlation range κ_1. The experiment confirmed two of the dynamic scaling predictions of Halperin and Hohenberg; firstly, the spin-wave constant D is renormalized to zero energy as the reduced temperature ε to the power 0.37±0.03 and secondly,in the critical region (q much larger than κ_1) the width parameter $\Gamma_{T_c}(q)$ of the diffusive peak varies as q to the power 2.7±0.3. Theory predicts that the critical exponent $(\nu'-\beta)$ of the spin wave constant D is 0.31±0.10 and that $\Gamma_{T_c}(q)$ should vary as q to the power 2.5. Since their measurements below T_c were at small wave vectors, the broadening of the magnons due to the instrumental resolution was comparable with or larger than their intrinsic width. Consequently the experiment of Collins et al. was not able to make any quantitative conclusions about the spin-wave damping.

Above the critical temperature, they found that the spin-diffusion constant Λ varied as the reduced temperature ε to the power 0.14±0.04 which is considerably smaller than the predicted value of 0.35±0.01 (equation (II-49) ,Bowers and Woolf,

1969; Ferer, Moore and Wortis, 1971). However their findings are in much closer agreement with those of Jacrot et al. (1963) and Passell et al. (1965) who did not find any temperature dependence of Λ at larger wave vectors. Above the critical temperature, the susceptibility $\chi(o)$ was found to vary as the reduced temperature ε to the power $\gamma = 1.30\pm0.06$ in good agreement with previous measurements. Another of the findings of Collins et al. was the absence of a zero energy peak below the critical temperature, that was expected from the longitudinal spin fluctuations.

It should be mentioned that for a real ferromagnet, a term corresponding to the dipole-dipole interaction should be added to the Heisenberg Hamiltonian (equation (I-3)) that would affect the predicted critical properties near T_c. Considering the dipole-dipole interaction, Holstein and Primakoff (1940) found that at low wave vectors the spin-wave energy E_s becomes

$$E_s = (D^2q^4 + 4\pi M_o \sin^2\theta_q g\mu_B D q^2)^{1/2} , \qquad \text{(II-55)}$$

θ_q is the angle between q and the z axis and M_o is the magnetization in zero magnetic field. M_o is predicted to vary with temperature similarly to D. Thus it is expected that at a given q the fractional shift of the spin-wave energy due to the presence of dipole-dipole forces will be temperature independent.

Collins et al. found that at room temperature the dipole-dipole interaction dominates the spin-wave energy at wave

vectors less than 0.02 A^{-1}. Arrott, Heinrich and Noakes (1972) found from magnetization measurements that the dipole-dipole interaction dominated the critical properties at ± 0.1°K from T_c. Since the determinations of the critical exponent γ by neutron scattering were at temperatures greater than 5°K above T_c and at wave vectors greater than 0.02 A^{-1}, it is not expected that the resulting exponents would be affected. Also the experiments reported in this thesis were at wave vectors greater than $q = 0.14\ A^{-1}$, so that the results are not expected to be affected by the dipole-dipole interaction.

The agreement between the values of the critical exponent γ of iron determined by the different neutron scattering experiments is excellent, and the mean value of γ is 1.30±0.03. They also agree within experimental error with those found by other techniques, namely 1.333±0.015 (Noakes, Tornberg and Arrott, 1966), 1.33±0.03(Develey, 1965) and 1.33 (Arajs and Colvin, 1964). The experimental values of γ are close to 1.347 predicted by Wilson (1972). However the theoretical predictions of 1.375±0.010 (Bowers and Woolf, 1969) and 1.405±0.020 (Ferer, Moore and Wortis, 1971), using high temperature series-expansion technique, are outside the range of the experimental values of γ; this discrepancy is not understood.

Résibois and Piette (1970) calculated numerically the scaling function $f(\kappa_1/q)$ (equation (II-46)) of the width parameter above T_c for a Heisenberg ferromagnet and antiferromagnet. They showed that the width of the diffusive peak is proportio-

nal to the hydrodynamic form $\kappa_1^{1/2}q^2$ (equation (II-49)) only when the ratio κ_1/q is larger than 4.

Als-Nielsen (1970) re-analyzed the experiments above T_c of Collins et al. (1969), Bally et al. (1967) and of Passell et al. (1965) using the scaling function calculated by Résibois and Piette (1970). He found that:

a) The disagreement between the values of the critical exponent of Λ predicted theoretically (0.35) and that found experimentally by Collins et al. (0.14±0.04) was because their measurements were not in the hydrodynamic region. This was revealed by the theoretical calculations of Résibois and Piette who defined more precisely the extent of the hydrodynamic region. However the measured width of the diffusive peak agrees with the predictions of Résibois and Piette for the region outside the hydrodynamic limit. The experiment in fact gives strong support to the theory of Résibois and Piette.

b) The apparent deviation from a straight line when plotting the reciprocal intensity against q^2 (Passel et al., 1965; Bally et al., 1967) was because they corrected for the inelasticity of the scattering assuming the hydrodynamic form of the energy spectrum (equation (II-54)). Using $f(\kappa_1/q)$ calculated by Résibois and Piette to correct for the inelasticity of the data of Passell et al., Als-Nielsen (1970) found that $\chi(q)$ plotted against q^2 is a straight line over the complete range of wave vectors measured. Hence the Lorentzian form of $\chi(q)$

(equation (II-50)) satisfactorily describes the scattering. Therefore the conclusion of Spooner and Averbach (1966) and Bally et al. (1967) that the Ornstein-Zernike form of the pair correlation function breaks down at small distances is questionable.

c) The flatness of the intensity maximum above T_c at a fixed scattering angle and the shift to higher temperatures with increasing q (Bally et al., 1967) is a direct result of the form of $f(\kappa_1/q)$.

Parette and Kahn (1971) verified experimentally the prediction of Résibois and Piette for the form of $f(\kappa_1/q)$ for larger values of κ_1/q than Als-Nielsen (1970). Their experiment also indicated that in the hydrodynamic region, the spin-diffusion constant Λ is proportional to $\kappa_1^{1/2}$ as predicted by Halperin and Hohenberg using dynamic scaling.

Recently there have been measurements of spin dynamics by neutron scattering in other magnetic systems.

Passell, Als-Nielsen and Dietrich (1972) measured the relaxation and renormalization of spin waves in the isotropic Heisenberg ferromagnet EuO over a range of wave vectors below T_c. Their results will be compared with the measurements presented in this thesis later on. Minkiewicz, Collins, Nathans and Shirane (1969) measured the critical and spin wave fluctuations in nickel. Tucciarone, Lau, Corliss, Delapalme and Hastings (1971) performed extensive measurements in the isotropic Heisenberg antiferromagnet $RbMnF_3$. Schulhof, Nathans,

Heller and Linz (1971) measured the spin dynamics in the uniaxial antiferromagnet MnF_2. Collins and Saunderson (1970) measured the spin dynamics in the ferrimagnet Fe_3O_4. Minkiewicz, Gesi and Hirahara (1971) measured the critical neutron scattering in the anisotropic ferromagnet MnP.

In the antiferromagnets it was observed that, for finite wave vectors, damped spin waves exist even at temperatures slightly above the critical temperature. In contrast, in ferromagnets and the ferrimagnet Fe_3O_4 it was observed that the spin waves are renormalized to zero energy at the critical temperature and in fact become over-critically damped at a temperature slightly below the critical temperature.

Another difference was the absence of the diffusive peak below the critical temperature in the isotropic ferromagnets and Fe_3O_4 that was clearly observed in the antiferromagnets and in the anisotropic ferromagnet MnP.

At the critical temperature, the wave-vector dependence of the width of the diffusive peak follows the predictions of dynamic scaling in both ferromagnets and antiferromagnets. The absence of any dynamic scaling prediction for ferrimagnets precludes the comparison of the results for Fe_3O_4 with the theory, but it was observed that at the critical temperature the wave-vector dependence of the width of the diffusive peak was like that of the antiferromagnets.

For temperatures greater than the critical temperature in $RbMnF_3$ and MnF_2 the behaviour of the characteristic frequency $\omega_{\kappa_1}(q)$ is consistent with the predictions of dynamic scaling. The plot of $\omega_{\kappa_1}(q)$ against κ_1/q at temperatures greater than the critical temperature for $RbMnF_3$ agreed well with the theory of Résibois and Piette (1970) for antiferromagnets but not so well for MnF_2 (because the anisotropy has to be taken into account).

In Ni above the critical temperature, Minkiewicz et al. (1969) found that in the hydrodynamic region the spin-diffusion constant Λ and the susceptibility $\chi(o)$ are proportional to the reduced temperature ε to the power 0.44 ± 0.07 and 1.58 ± 0.05 respectively. Further Minkiewicz (1971) found that the inverse correlation range κ_1 is proportional to the reduced temperature to the power 0.96 ± 0.25. Thus for temperatures greater than the critical temperature, all the critical exponents for Ni in the hydrodynamic region appear to be anomalous when determined by a scattering experiment performed at small energy transfers. The relationships between the critical exponents however are consistent with the scaling hypothesis.

CHAPTER III

EXPERIMENTAL APPARATUS AND TECHNIQUES

A. Specimen and Furnace

The specimen was a single crystal of iron* of nominal purity 99.99% and with a mosaic spread of less than 5 minutes. It had a cylindrical shape of diameter 0.25 inches and length 1.5 inches. It was mounted with the $[1\bar{1}0]$ axis vertical, which involved tilting the crystal 27 degrees from its cylindrical axis. Some of the general properties of iron are listed in Table III-1.

In experiments measuring critical phenomena, as it has been indicated in Chapter II, physical quantities of interest often diverge or go to zero as a function of the reduced temperature, so that large fractional changes occur in these quantities at temperatures very close to the critical temperature. Thus it is desirable to build a furnace with a high degree of temperature stability and specimen temperature uniformity so that reliable results can be taken close to the critical temperature T_c.

The difficulties in design arise in large part from the necessity of having thin walls around the specimen in the horizontal plane so that there is little scattering of neutrons except by the iron sample. This precludes the possibility of

*obtained from Metals Research Limited, Melbourn, Herts, England.

Table III-1. General Properties of Iron

Critical temperature[a] T_c	1044.0°K
Crystal Structure: 0-1180°K[b] - body centered cubic	
Lattice constant: at room temperature[b]	2.86645 A
At T_c[c]	2.898 A
Thermal neutron cross-section	
Nuclear coherent scattering[d]	10.6±0.4 barns
Nuclear incoherent scattering[d]	0.43 barns
Absorption[d] for 25 meV neutrons	2.55±0.05 barns
Magnetic scattering length p[e]	0.60×10^{-12} cm at $\theta=0$
	0.35×10^{-12} cm at $\frac{\sin\theta}{\lambda} = 0.25$ A^{-1}

[a] S. Arajs and R. V. Colvin, J. Appl. Phys. 35, 2424 (1964). J. E. Noakes, N. E. Tornberg, and A. Arrott, J. Appl. Phys. 37, 1264 (1966).

[b] W. B. Pearson, Vol. 2, A handbook of Lattice Spacings and Structures of Metals and Alloys. Pergamon Press (1967).

[c] N. Ridley and H. Stuart, J. Phys. D. (Appl. Phys.) 1,1291 (1968).

[d] Neutron Cross Sections, BNL 325, Second edition, Supplement No. 2. Vol. II A.

[e] G. E. Bacon, Neutron Diffraction, 2nd. ed. Oxford (1962).

surrounding the specimen by materials with high thermal capacity to improve temperature stabilization. Since the furnace is to be rotated about the vertical axis during the experiment, it is desirable that the material in the neutron beam is the same at any angular position. This can be achieved by constructing the furnace in a cylindrical form. Another limitation is that for the McMaster University spectrometers the middle of the neutron beam is 6 inches above the spectrometer table. Thus a very long cylindrical heater could not be used to minimize the temperature gradient along the cylinder axis near the centre of the cylinder.

The schematic diagram of the furnace constructed to meet the above requirements is shown in Figure III-1. It was evacuated by an oil diffusion pump to prevent the sample from oxidizing. The heater arrangement consisted of a vertical cylindrical heater supplying most of the heat and two small auxiliary heaters situated at the top and bottom of the former to reduce the temperature gradient of the specimen. The power to all the heaters was controlled by a proportional temperature controller.

The main heater element had a cylindrical form; height 6 inches, diameter 3.5 inches. Since the neutron beam passed through the heater element, it had to be of thin material. At first 0.005 inches thick molybdenum foil was used. Slots were cut into the element to increase the resistance to approximately 0.1 Ω. However it was difficult to cut the slots

Figure III-1

Schematic diagram of the vacuum furnace, with the important components numbered in the following order.

1. Specimen
2. Main heater
3. Electrode and support for main heater
4. Teflon vacuum seal and electrical insulation
5. Auxiliary heater
6. Copper cylinder
7. Specimen support
8. Radiation shields
9. Chromel-Alumel thermocouple measuring specimen temperature
10. Swagelock fitting
11. Flange
12. Cooling pipe
13. Thermocouple providing reference signal to temperature controller
14. Thermocouple acting as sensor to cut power to furnace in case of overheating
15. O ring vacuum seal
16. Vacuum line to diffusion pump.

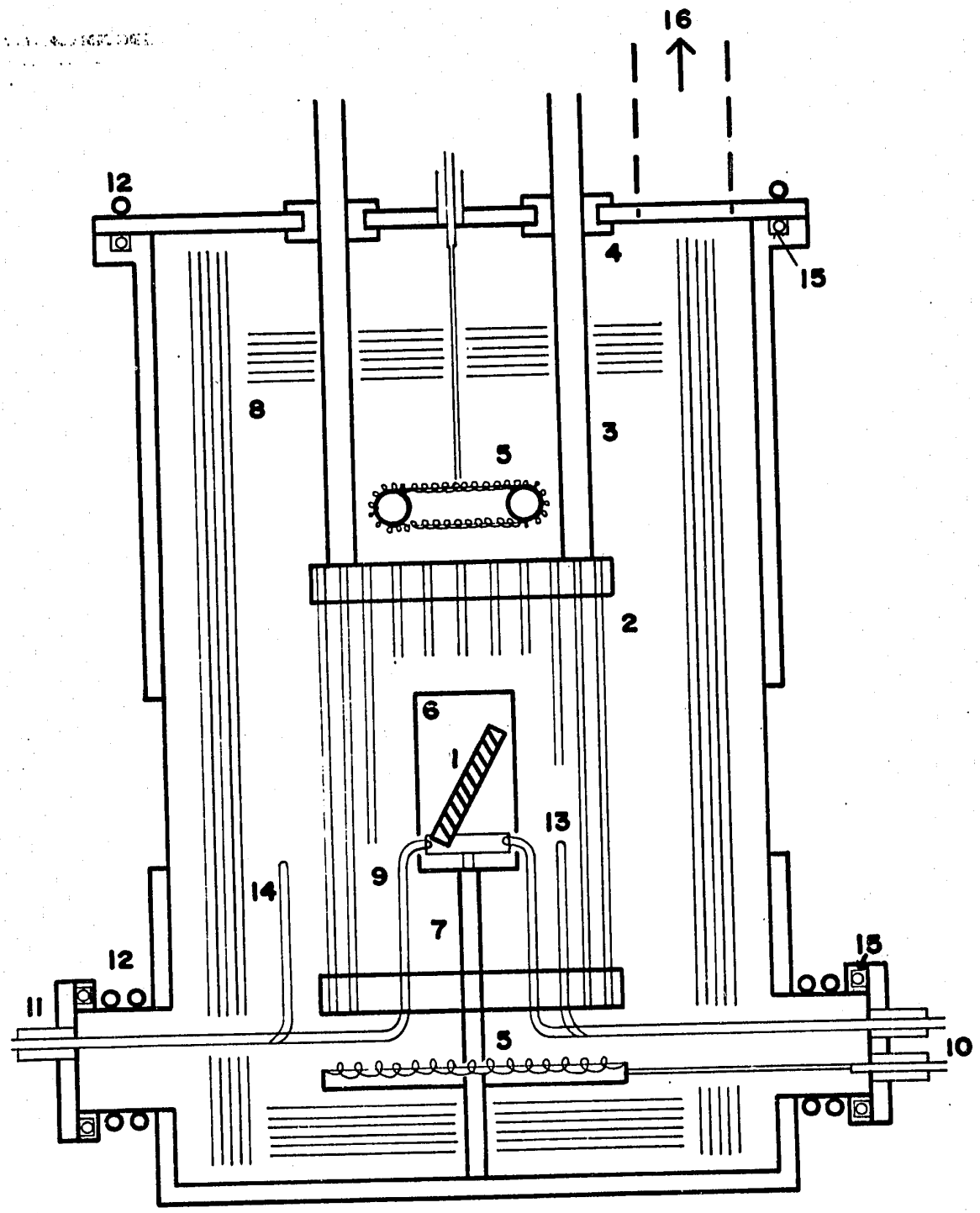
16
12
4
15
8
3
5
2
6
1
13
9
14
7
12
15
11
10
5

and cracks always appeared, decreasing the lifetime of the element. The element was replaced in the later part of the experiment by Kanthall Al strip 3 mm wide and 0.33 mm thick wired in a parallel arrangement of 15 strips with resistance 0.1 Ω.

Electrical conductors from outside the furnace to the main heater were iron rods 3/8 inches diameter. They also acted as mechanical supports for the heater (Figure III-1). They were of large diameter so that their electrical resistance was very small compared with that of the heater element. The rods were secured vertically in the lid of the furnace by a set of teflon rings that acted as an insulator and held the O ring for the vacuum seal. As the heater resistance was very small a large stepdown transformer (220 V primary, 14 V secondary; 2 KVA) was placed after the temperature controller.

The two auxiliary heaters situated above and below the main heater cylinder were of Kanthall Al wire. Their resistance was 25 Ω, with each having a separate variable transformer power supply connected to the temperature controller. The power to the auxiliary heaters could be adjusted independently to minimize the axial temperature gradient in the specimen.

The auxiliary heater terminals were 1/8 inch diameter brass rods secured into flanges using nylon Swagelock fittings. The nylon fittings acted both as insulator and as vacuum seal. The flanges were attached by screws near the base of the furnace using O rings for vacuum seals (Figure III-1). All the O ring seals on the furnace were water cooled.

Even with auxiliary heaters the thermal radiation incident on the specimen is not completely isotropic. To further reduce the temperature gradient, the specimen was mounted inside a hollow copper cylinder 2.5 inches long, 1.25 inches diameter and 1/16 inches thick that was enclosed at both ends. Thermal conductivity made the temperature of the copper cylinder more uniform so that it radiated the specimen with more isotropic radiation than that incident from the heaters. The copper cylinder with the specimen inside was attached on the end of a ceramic tube fixed to the bottom of the furnace. The ceramic tube had a low thermal conductivity so that the sample was thermally isolated from the outside.

The heaters were enveloped by five cylindrical stainless steel shields whose axes were along that of the main heater, and by six shields positioned above and below the heaters (Figure III-1). The 0.002 inches thickness of the shields at the side did not attenuate the neutron beam to any significant extent. The power dissipated in the furnace, with the specimen temperature around 800°C was approximately 0.8 KW and as a consequence the outside wall was quite hot. It was constructed of stainless steel and at the height of the neutron beam the wall thickness was machined down to less than 0.02 inches.

The temperature of the specimen was measured using an ungrounded Chromel-Alumel thermocouple enclosed in a 1/8 inches diameter stainless-steel sheath. There were altogether four such thermocouples inside the furnace; of these two were in thermal contact with the sample. The cold junctions of all the

thermocouples were kept at 0°C by an ice-point reference unit that was stable to better than 0.1°K over long periods.

The voltage of the specimen thermocouple was measured using a six-digit D.C. differential voltmeter. The absolute accuracy of the instrument was 4 μV corresponding to an accuracy of the temperature measurement of 0.1°K. The amplified output of the error signal, from the balance voltage of the voltmeter, was fed into a chart recorder to give a record of the specimen temperature during an experiment.

The temperature was controlled by a proportional temperature controller (Figure III-2) with a continuously variable setpoint between 15 mV and 35 mV (∿ 650°K to ∿ 1150°K). The setpoint could be set with an accuracy of 4 μV (0.1°K). The feedback signal to the temperature controller was provided by a Chromel-Alumel thermocouple, which was positioned between the main heater and the copper cylinder enclosing the specimen so that it could monitor the incident radiation. The power input to the heaters was varied by the controller in proportion to the difference between the thermal emf. of the feedback thermocouple and the setpoint voltage. When the difference was zero the power to the heaters had a pre-set constant value. With this arrangement the stability of the specimen temperature near T_c was 0.2-0.3°K over 24 hours and the response-time to a change in the setpoint was less than 1 minute.

There were three safety trips that could switch off the power to the heaters. These trips were installed to protect

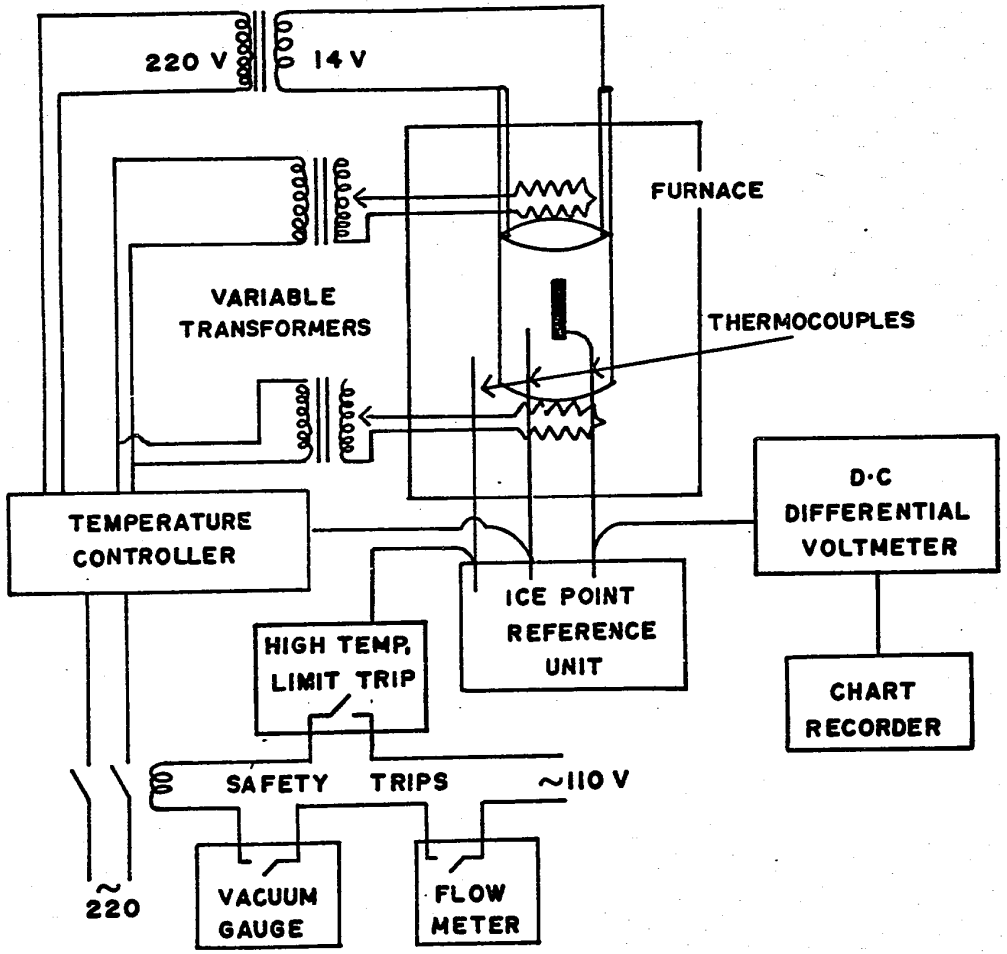

Figure III-2

Schematic diagram of the temperature control and measurement apparatus as well as the power supply and safety trips.

the crystal and the furnace from a deterioration of the vacuum, a decrease in the water flow to cool the O ring seals, and from overheating of the crystal. In iron there is a phase transition at $\sim$ 1180°K, i.e. only approximately 136°K above T_c. This is a b.c.c to f.c.c. phase transition and if the temperature was raised above this value the single crystal would be ruined. The temperature sensor for this trip was the fourth Chromel-Alumel thermocouple.

The temperature gradient in the specimen was measured before the start of the experiment. A Chromel-Alumel differential thermocouple was used to measure the temperature across the sample. Near T_c it was found that the auxiliary heaters were required to provide about 4% of the total power each. This gave a temperature gradient of the specimen which was approximately 0.2°K.

B. Triple Axis Spectrometer

The experiment was performed using the McMaster University E2 triple axis spectrometer (Figure III-3) (Brockhouse, deWit, Hallman and Rowe, 1968) installed at the NRU reactor, Chalk River.

The spectrometer has the unusual feature of a double monochromator situated within the reactor wall in which the monoenergetic beam of neutrons is reflected in succession from two matched parallel copper crystals.

The monochromator crystals were deformed by bending to increase their reflectivity without increasing appreciably

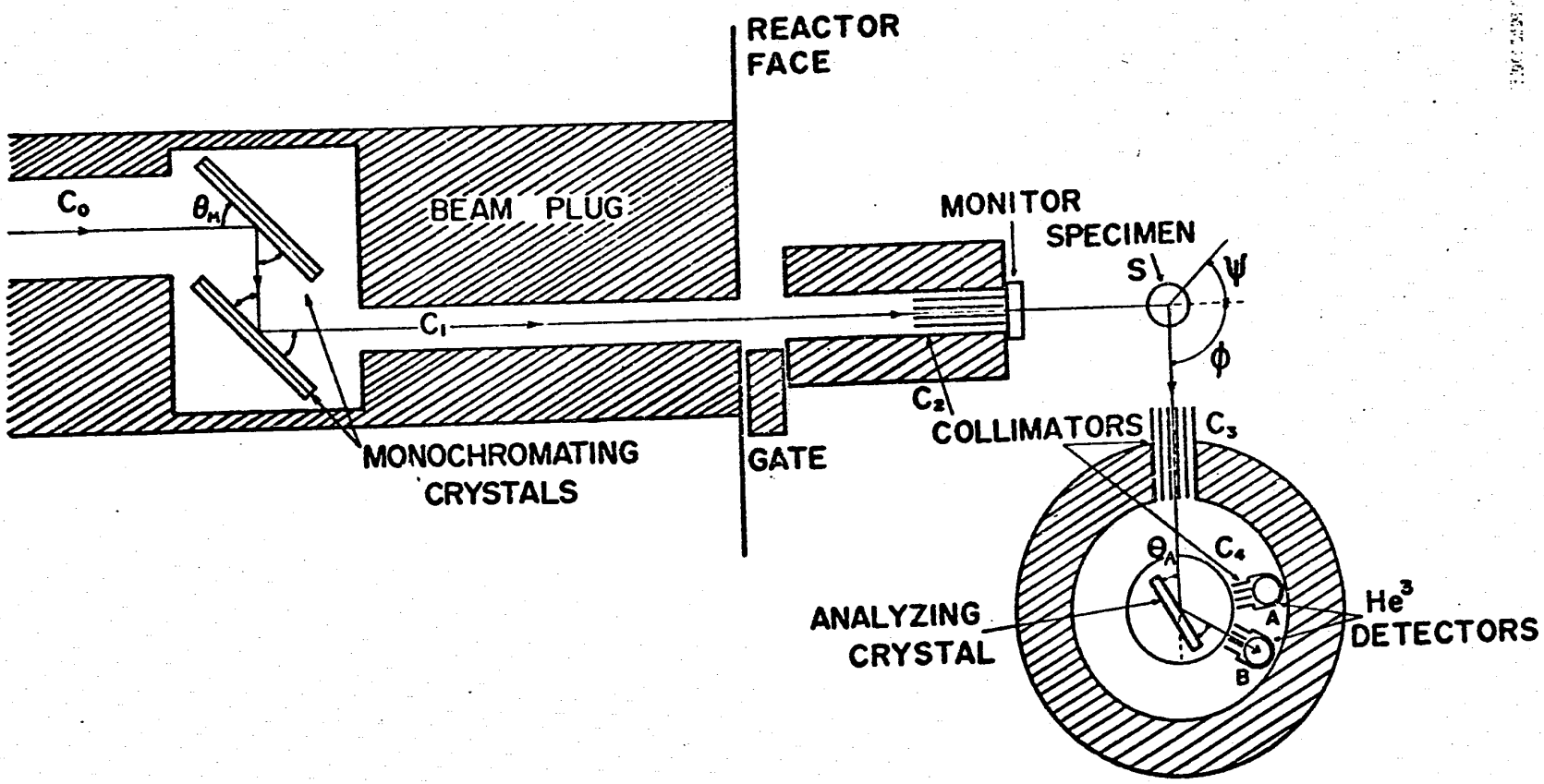

Fig. III-3 Schematic diagram of the McMaster (E2) triple-axis spectrometer at Chalk River.

their mosaic widths (Dymond and Brockhouse, 1970). The monoenergetic beam emerged parallel to but displaced from the incident beam so that fast neutron contamination should be greatly reduced. Since the direction of the monochromatic beam is independent of wavelength, the specimen position is fixed and, as a result, the design of the spectrometer is simplified.

A copper analysing crystal and two ^{3}He detectors are all mounted inside a boron/paraffin shielding drum. The analyser crystal was deformed in the same way as the monochromator crystals to increase its reflectivity. The detectors view the analysing crystal ; one counts the Bragg scattered neutrons giving the signal, the other the diffusely scattered neutrons and approximates the background. The angular acceptance of the Soller slit collimators before and after the specimen are variable depending on the resolution required. A fission counter situated before the specimen table is used to monitor the incident beam flux. The spectrometer control was semi-automatic employing an IBM 0-24 card punch as a card reader. The cards for the particular scans were produced by a large computer.

The spectrometer was operated in the constant $\underline{Q}$ mode (Brockhouse, 1961). This consists of fixing the scattering vector $\underline{Q}$ at a point in reciprocal space and varying ω to measure the energy distribution of scattered neutrons. A reciprocal lattice diagram showing a point on such a scan (in which $|\underline{k}|$ of the incident neutrons is varied) is given in Figure III-4.

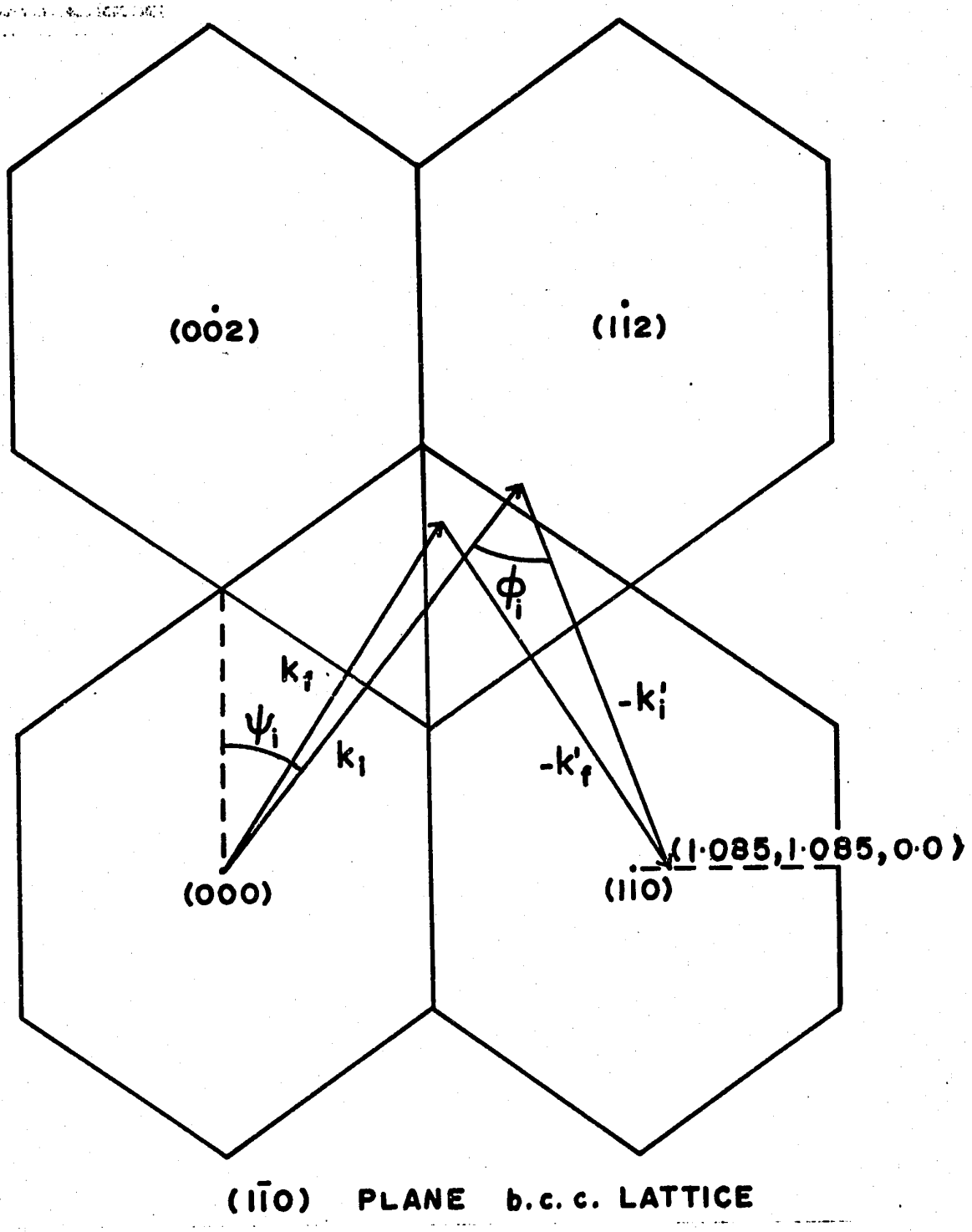

(1$\bar{1}$0) PLANE b.c.c. LATTICE

Figure III-4

Vector diagram of a Constant $\underline{Q}$ scan in reciprocal space. k_i, k_f and k_i', k_f' are the initial and final wave vectors of the incident and scattered neutrons respectively. It shows that in this scan only the direction of $\underline{k}'$ changes while both the direction and magnitude of $\underline{k}$ change .

If $\underline{Q}$ is along the [110] direction of the reciprocal lattice, then in the $\underline{k}$-$\underline{k}'$ plane Q is given by

$$Q = k \sin \psi + k' \sin (\phi+\psi)$$

where ϕ is the scattering angle and ψ is the angle between $\underline{k}$ and the [001] direction which defines the orientation of the specimen. If $|\underline{k}|$ is varied, then ψ and ϕ must be adjusted to keep $\underline{Q}$ fixed. This was calculated by means of a computer program.

C. Measurement of the Critical Temperature

The critical temperature T_c was determined by measuring the scattering as a function of temperature of the specimen (Figure III-5). T_c was taken to be the intersection of the lines of best fit to the scattered intensities at the two sides of the maximum intensity. The spectrometer was set at $\omega = 0$ and $q = 0.04\ A^{-1}$. The low value of q was chosen because at higher values the peak broadens out and shifts to higher temperatures (Bally et al., 1967). At $q = 0.04\ A^{-1}$ the temperature shift of the peak from true T_c should be less than 0.1°K (Als-Nielsen, 1970). Smaller wave vectors were not used because as q approaches zero the intensity of the (110) Bragg reflection becomes much greater than the critical scattering. T_c was measured this way several times during the experiment and no appreciable changes in its value were detected. It was reproducible to within 0.4°K every time.

It is clear that in experiments involving critical phenomena one is primarily interested in measuring the reduced

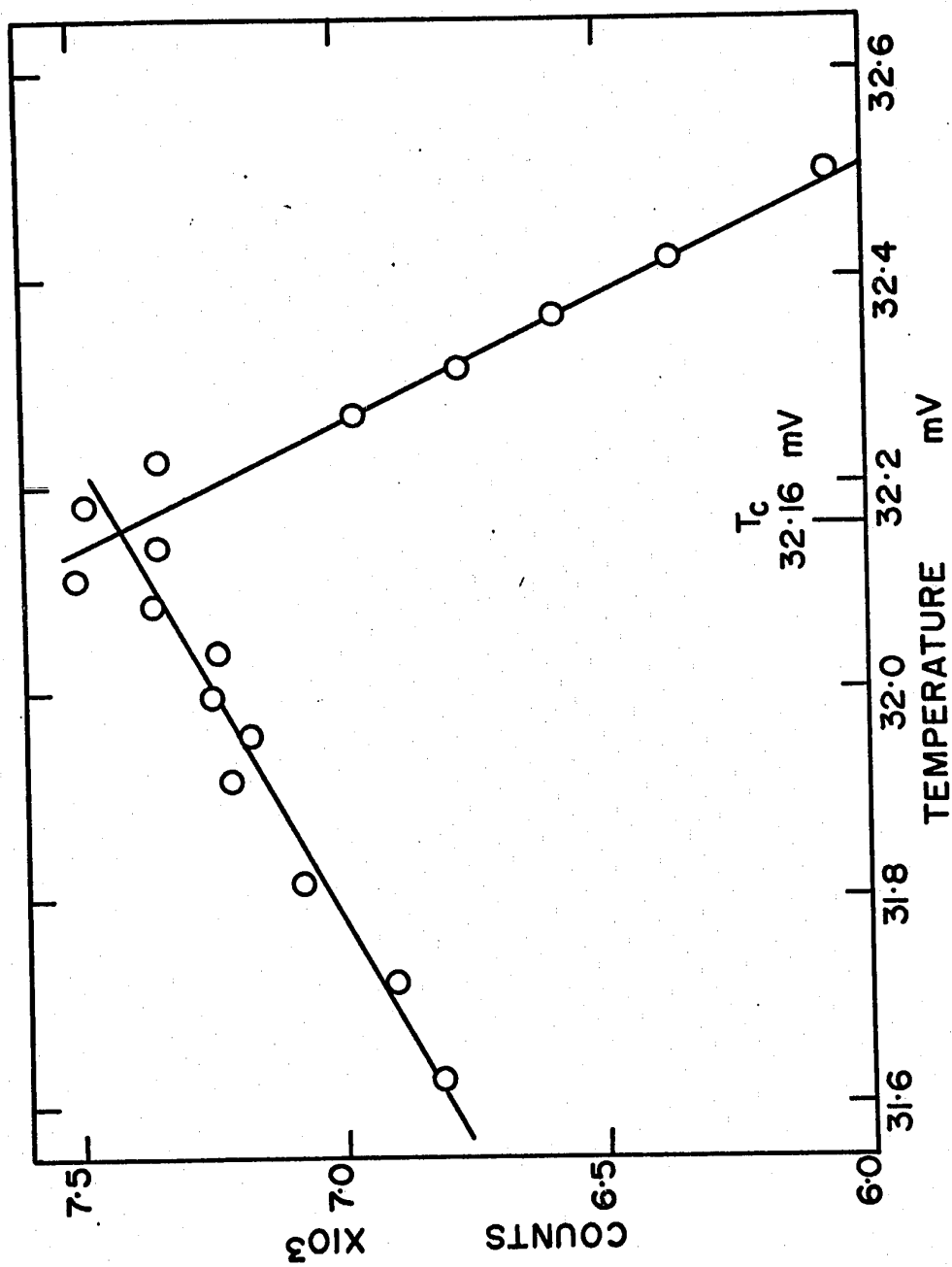

Figure III-5

The temperature dependence of the scattering at $q = 0.04\ A^{-1}$ and $\omega=0$. The peak in the scattering is taken to be the critical temperature.

temperature rather than the absolute temperature. Having calibrated the thermocouple at the critical temperature as described above, it was assumed that near T_c the change in temperature corresponding to a change in thermal emf. is the same as that given in the tables. Since most of the measurements were taken for the reduced temperature less than 0.03, this assumption should be reasonable and errors due to lack of absolute calibration of the thermocouples should be small compared to errors due to temperature fluctuations of the specimen. For measurements further away from T_c the accuracy in the temperature was not as important.

D. Instrumental Resolution

Neutron scattering experiments measure the intensity of scattered neutrons for a given momentum and energy transfer $\hbar\underline{Q}$ and $\hbar\omega$ respectively. This requires setting the monochromator, specimen, scattering and analyser angles θ_M, χ, ϕ, and θ_A (Figure III-3) respectively in such a way that the probability of detection of scattered neutrons is the highest at the point $\underline{Q}_o$, ω_o in $\underline{Q}$-ω space. $\underline{Q}_o$ and ω_o are given by the equations

$$k_o = \frac{\pi}{d_M \sin\theta_M} \quad , \quad k_o' = \frac{\pi}{d_A \sin\theta_A}$$

$$\underline{Q}_o = \underline{k}_o - \underline{k}_o' \quad , \quad \hbar\omega_o = (\hbar^2/2m)(k_o^2 - k_o'^2)$$

where d_M and d_A are the spacings between the atomic planes of the monochromator and analyser respectively from which the reflection occurs.

However the presence of finite collimation and finite mosaic spread of the monochromator and analyser crystals allows less probable neutrons to be detected at the same settings. The resolution function of the instrument is the probability of detection of neutrons as a function of $\Delta\underline{Q}$ and $\Delta\omega$, when the instrument has been set to measure a scattering process corresponding to the point $\underline{Q}_o$, ω_o in $\underline{Q}$-ω space.

Cooper and Nathans (1967) derived an analytic expression for the form of the instrumental resolution function $R(\underline{Q}_o, \omega_o; \Delta\underline{Q}, \Delta\omega)$ assuming that both the monochromator and analyser reflection probabilities and the collimator transmission probability can be approximated by Gaussian functions.

It is assumed that imperfect crystals have a Gaussian mosaic block distribution. The Gaussian mosaic spread parameter η is defined as the angle of mis-set of the crystal to give a probability of reflection of $\exp(-\frac{1}{2})$ times the optimum probability. The individual monochromator and analyser crystals had a mosaic spread of 0.0038 radians. Since the monochromator was two identical crystals in parallel orientation, its effective horizontal mosaic spread was smaller (Dymond) than that of the individual crystals. The Gaussian mosaic spread parameters of the monochromator (η_M) and of the analyser (η_A) were:

$$\text{Horizontal:} \quad \eta_{MH} = 0.0029 \text{ radians}$$
$$\eta_{AH} = 0.0038 \text{ radians}$$
$$\text{Vertical} \quad : \quad \eta_{MV} = \eta_{AV} = 0.0038 \text{ radians.}$$

The characteristic divergence angle α of the collimators is defined so that the probability of transmission of a neutron with a divergence angle of α radians is $\exp(-\frac{1}{2})$ times the optimum probability. The total acceptance angle α' of a collimator is the ratio of the slit opening to the length. The transmission function of an ideal collimator is triangular. However, because of imperfections in the Soller slit system and scattering from the walls, the transmission function is nearly a Gaussian (Sailor, Foote, Landon and Wood, 1956).

If a Gaussian is fitted to a triangular function at the center and at half widths one finds (Tucciarone et al., 1971) that the relation between the characteristic divergence angle α and the total acceptance angle α' is

$$\alpha = 0.425\ \alpha' \ . \qquad \text{(III-1)}$$

Using equation (III-1), the characteristic divergence angles for the four collimators C_0, C_2, C_3, C_4 (Figure III-3) that were used in the experiment are the following:

Horizontal: $\alpha_0 = 0.0425$ radians
$\alpha_2 = 0.0053$ radians
$\alpha_3 = 0.0053$ radians
$\alpha_4 = 0.0425$ radians

Vertical : $\beta_0 = 0.0425$ radians
$\beta_2 = 0.0071$ radians
$\beta_3 = 0.0106$ radians
$\beta_4 = 0.10$ radians

where the subscripts 0, 2, 3, 4 refer to the in pile, monochromator to specimen, specimen to analyser and analyser to

detector regions respectively (Figure III-3).

Using the theory of Cooper and Nathans (1967) and the above-mentioned parameters of the E2 spectrometer, the resolution ellipsoid was calculated near the (110) reciprocal lattice point in the region of $\underline{Q}$ and ω at which the experiments were performed, for the case of almost elastic scattering. It was found to have one of its larger axes in the $q_{[001]}$-ω plane, inclined with respect to the [001] and ω directions (cf. Figure III-6). One of the smaller axes was along the [110] direction and the second long axis was along the z direction.

For the resolution correction to be carried out meaningfully, it is necessary to know the resolution ellipse with some precision. The theoretical form of the resolution function for the parameters of the E2 spectrometer was compared with the experimental form, as mapped out at the (110) reflection in the $q_{[110]}$-ω and $q_{[001]}$-ω planes. They fitted well in both planes. Figure III-6 shows the experimental resolution function in the $q_{[001]}$-ω plane and the comparison with the theoretical form at half-height. All the measurements of the critical scattering from iron were at non-zero but small q and ω. It seems most reasonable to assume that if the calculated resolution function is correct at the Bragg position, then it should also be correct for small q and ω thus giving confidence to the accuracy of the resolution corrections.

The effect of the finite resolution is that if the cross-section is expressed in terms of $S(\underline{Q},\omega)$ (equation (II-3)), then the scattering intensity $I(\underline{Q},\omega)$ at the instrumental setting $\underline{Q}_o$, ω_o is given by the integral

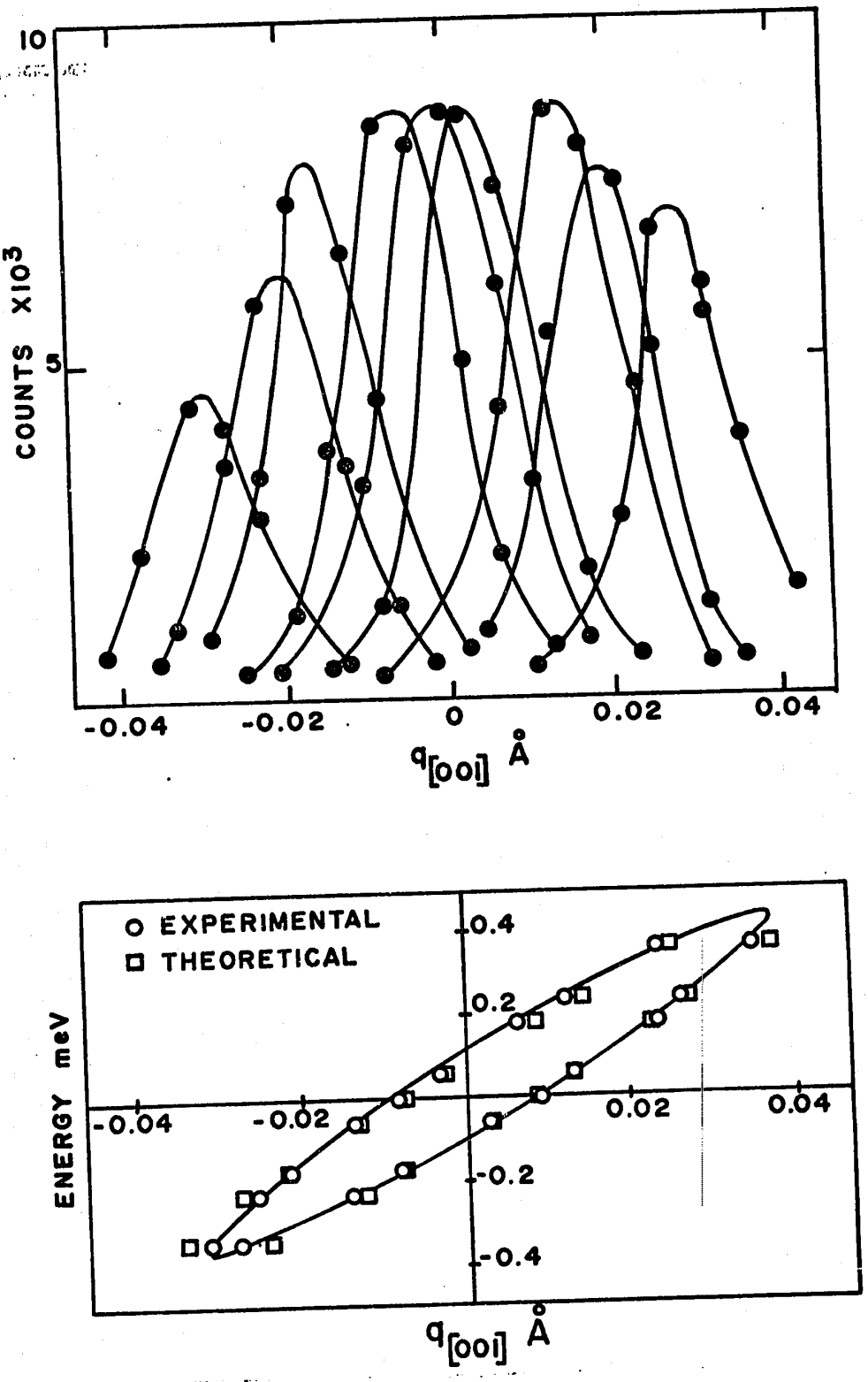

Figure III-6

Constant E scans to measure the extent of the resolution ellipse in the q[001]-ω plane at the (110) Bragg peak (top). Comparison of the experimental and theoretical half-height contours of the resolution ellipse (bottom).

$$I(\underline{Q}_o,\omega_o) = \int S(\underline{Q},\omega)R(\underline{Q}_o,\omega_o;\ (\underline{Q}-\underline{Q}_o),(\omega-\omega_o))d\underline{Q}d\omega.$$

The resolution correction of the data involved the prediction of the experimental line shape by numerical integration of the cross-section over the resolution function. This was performed using a large computer. The computer program calculated the resolution function at each value of $\underline{Q}$ and ω where the data was obtained. The numerical integration was performed with the limits placed at some appropriate low contour of the resolution ellipse, to make the integration just over the values that contribute significantly to the intensity. Detailed least squares fits were made to compare the predicted and experimental intensities. Figure III-7 shows the best fit of the resolution broadened theoretical cross-section (solid line) to the experimental data (open circles). The dashed line is the theoretical cross-section (equation (II-3)) before the numerical integration over the resolution ellipse. The filled circles represent a magnon of zero width broadened by the instrumental resolution. The solid line was obtained by convoluting curves denoted by the dashed line and the full circles.

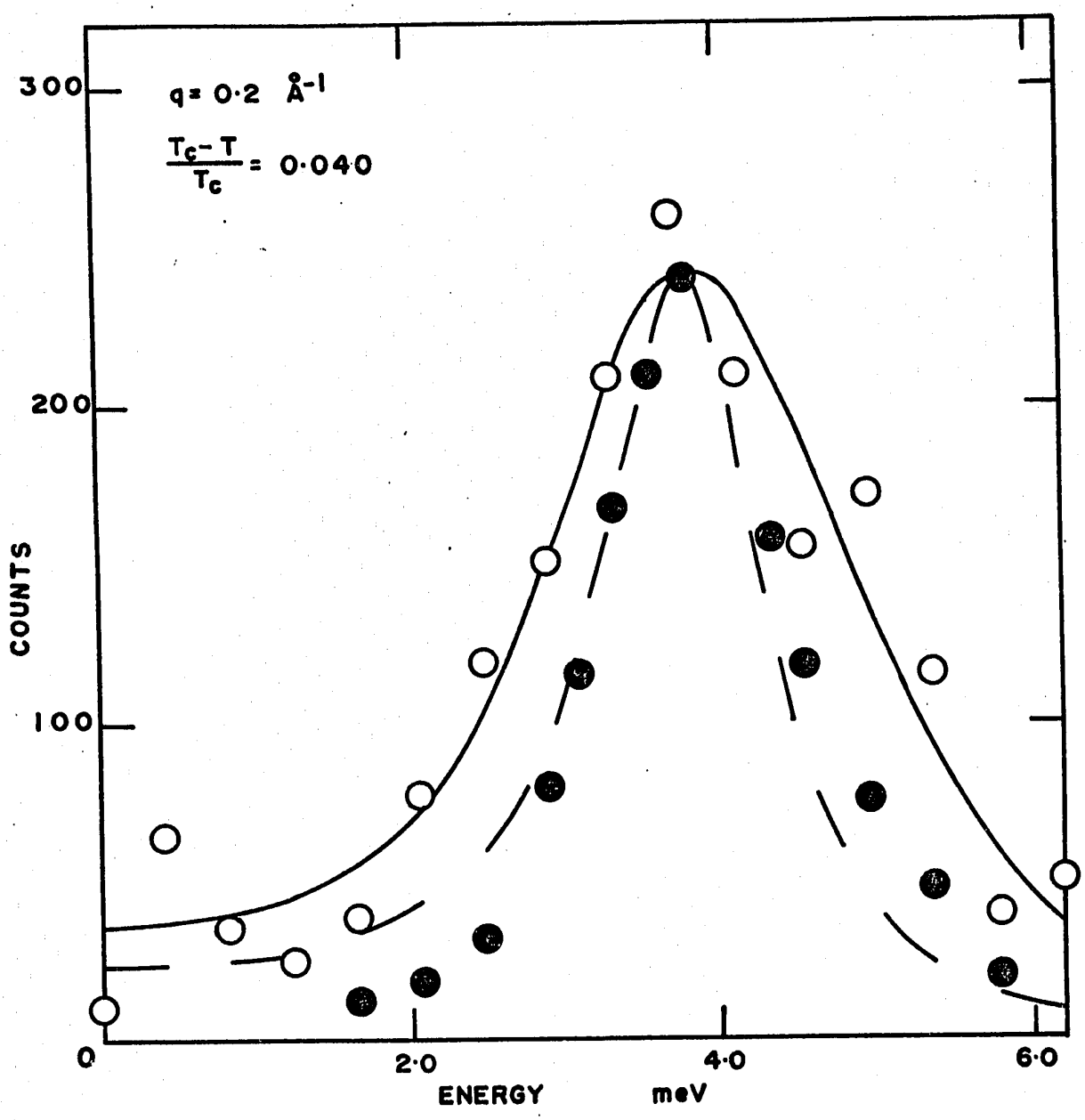

Figure III-7

The best fit of the resolution-broadened theoretical cross section (solid line) to the data points (open circles). The solid line can be obtained by convoluting the dashed line (theoretical cross-section) with the filled circles (magnon of zero width broadened by the instrumental resolution).

CHAPTER IV

EXPERIMENTAL RESULTS AND DISCUSSION

A. General Considerations

The measurements of the energy distribution of magnetically scattered neutrons from iron were taken at wave vectors near the (110) crystal reflection, along the [110] direction.

Since the magnon dispersion surface is periodic in reciprocal space, in principle it could be measured about any reciprocal lattice point. The measurements were not taken in the forward direction (i.e. about the $\underline{\tau} = 0$ reciprocal lattice vector) because there, at a given wave vector q, the maximum energy transfer that can be realized by neutron scattering is 2Eq/k, so that parts of the frequency spectrum of the scattering cannot be observed. The iron crystal studied had a body centered cubic structure so that the closest reciprocal lattice point to the origin is (110). The neutron scattering cross-section given by equation (II-2) is proportional to the square of the magnetic form factor F(Q). F(Q) decreases rapidly with increasing Q,hence it is not desirable to measure the scattering about a reciprocal lattice point further than (110) from the origin.

Shirane, Minkiewicz and Nathans (1968) found the magnon dispersion curves of iron to be isotropic at room temperature up to the largest wave vector measured, $q = 0.6\ A^{-1}$. The [110] direction was chosen in preference to the other symmetry directions for the reasons that follow. Near T_c the magnon and transverse phonon energies in the wavelength range covered in the present measurements are approximately equal. Thus, it is highly desirable to use a method of measurement that is not sensitive to scattering by the transverse phonons. This can be accomplished by using the fact that the cross-section for phonon scattering contains the term $(\underline{Q}\cdot\underline{\xi})^2$ where $\underline{\xi}$ is the polarization vector of the phonon mode. By definition, transverse modes have their polarization vector $\underline{\xi}$ perpendicular to their wave vector $\underline{q}$ along symmetry directions. Therefore, when $\underline{Q}$ is parallel to $\underline{q}$, which for the present measurements corresponds to $\underline{Q}$ along [110], the scattering cross-section for transverse phonons is zero.

It was shown in Chapter III that the resolution ellipsoid has one of its smaller axes along the [110] direction, so that even at the smallest wave vectors measured, it was effectively zero at the (110) reciprocal lattice point. Consequently the observed spectra did not have any contribution to their intensity from the Bragg peak.

B. Method of Data Analysis

After correcting for the instrumental resolution the experimental results were analysed using the spectral shape

functions given by equations (II-36) and (II-37) with the spin-wave energy E_q replaced by Dq^2 (equations (II-38) and (II-41)). The spin-wave damping parameter γ_q was included both as a constant and as $\gamma' q^4$ (equation (II-42)). For the latter case the damping varies over the resolution volume and the numerical integration does not yield exactly the same parameters as in the former case.

The spectral shape functions were designated as A1 and A2 for the Halperin and Hohenberg form with and without the explicit wave-vector dependence of the damping respectively and similarly as B1 and B2 for the double-Lorentzian form. Substituting in equations (II-36) and (II-37) for the spin-wave energy and damping, the mathematical expressions for the four spectral shape functions are as follows:

A1
$$F_q^{xx}(\omega) = \frac{\gamma' q^4 D^2 q^4}{(\omega^2 - D^2 q^4)^2 + \gamma'^2 q^8 D^2 q^4}$$

A2
$$F_q^{xx}(\omega) = \frac{\gamma_q D^2 q^4}{(\omega^2 - D^2 q^4)^2 + \gamma_q^2 D^2 q^4}$$

B1
$$F_q^{xx}(\omega) = \frac{0.5\ \Gamma' q^4}{(\omega - Dq^2)^2 + \Gamma'^2 q^8} + \frac{0.5\ \Gamma' q^4}{(\omega + Dq^2)^2 + \Gamma'^2 q^8}$$

B2
$$F_q^{xx}(\omega) = \frac{0.5\ \Gamma_q}{(\omega - Dq^2)^2 + \Gamma_q^2} + \frac{0.5\ \Gamma_q}{(\omega + Dq^2)^2 + \Gamma_q^2} .$$

Before the cross-section could be fitted to the experimental data, the magnitude of the background scattering had to be determined. Since it was sometimes an appreciable fraction of the intensity of the observed spectra of scattered neutrons, its estimation had to be made with care.

At most temperatures the spin-wave spectrum was broad so that the magnon creation and annihilation peaks merged and the wings on the high energy side of the peak had not levelled out completely before disappearing under the longitudinal acoustic phonon (Figure IV-1). This precluded an accurate determination of the background at each of the temperatures.

It was determined at lower temperatures where the creation and annihilation spin-wave peaks are quite narrow and well separated. The energy spectra of scattered neutrons were measured starting at negative energies so that the background could be the average over the largest possible number of data points. The counts between the creation and annihilation peaks were constant except for statistical fluctuations and the intensity was approximately the same as at the wings of the magnon peaks at the higher temperatures. This gave confidence that the true background was being measured and that it did not change significantly with temperature. The background was measured for each wave vector at which the spin dynamics were studied and was found to decrease with increasing wave vector.

As well as a background independent of energy transfer, there was a small narrow peak centered at $\omega=0$ with full width at half maximum intensity less than 1 meV. This scattering is independent of wave vector and of specimen temperature and is believed to arise from incoherent elastic scattering in the iron specimen. Its intensity could be most accurately determined at low temperatures where it was well separated from the spin

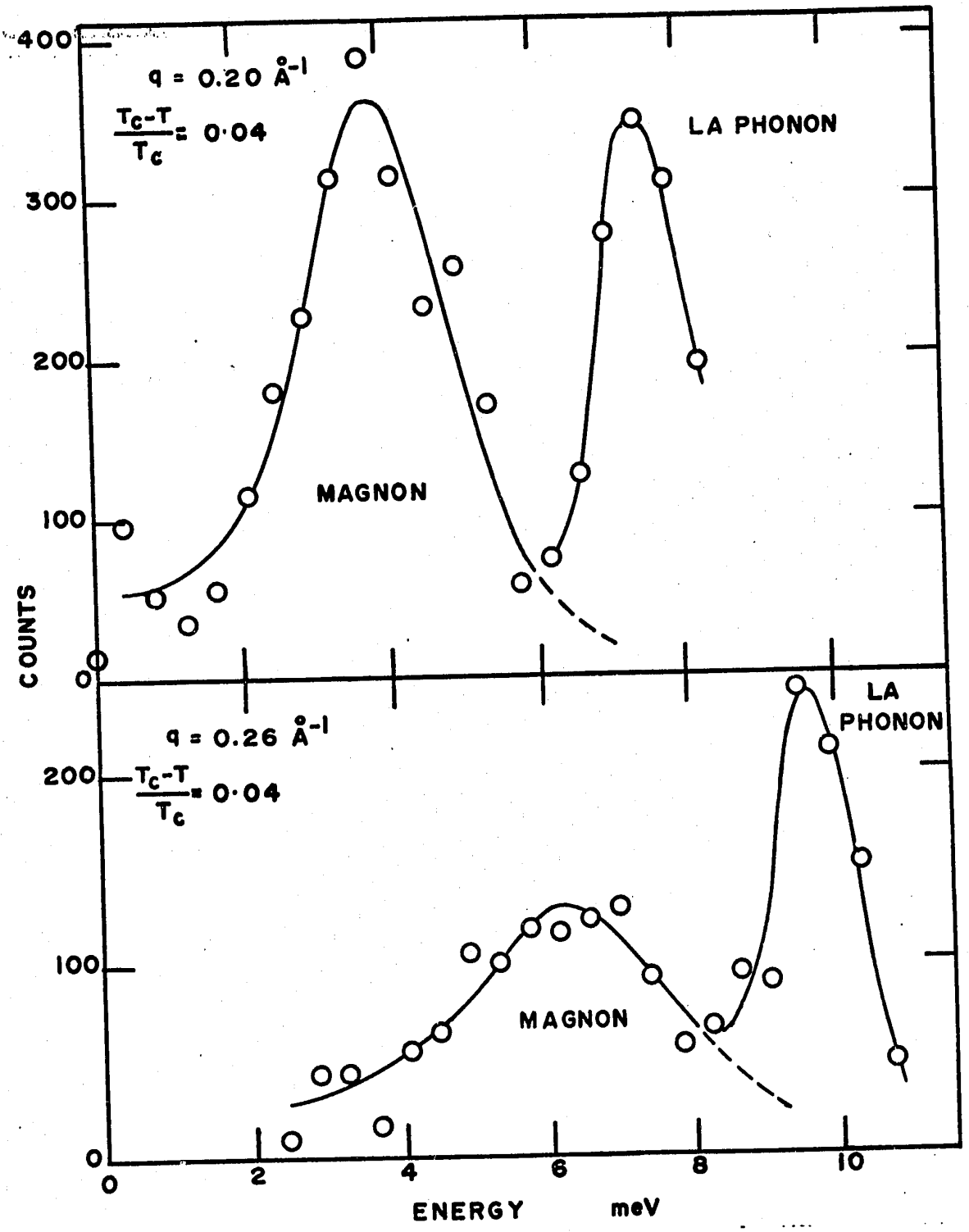

Figure IV-1

The energy spectra of scattered neutrons at q = 0.20 A^{-1} and 0.26 A^{-1} showing the position of the longitudinal acoustic phonon peak (labelled LA phonon) with respect to the magnon peak.

waves. Both these "background" scattering contributions were subtracted from the scattering before detailed quantitative analysis was performed on the data.

The fitting of the theoretical cross-section to the experimental data will now be described. For each of the spectral shape functions there were two adjustable parameters, corresponding to the spin-wave energy and the damping e.g. D and γ' for the form A1. For each spectrum the initial values of these parameters were estimated from the raw data. Using these values a resolution-corrected cross-section was computed and its area normalised to the observed spectral distribution. A goodness of fit parameter F can be defined by the equation:

$$F = \frac{1}{N-M} \sum_{n=1}^{N} \frac{[I_o(n)-I_B-I_c(n)]^2}{I_o(n)} \quad . \qquad \text{(IV-1)}$$

for the N data points of the spectrum. $I_o(n)$ and $I_c(n)$ are the individual observed and calculated intensities, I_B is the background and M is the number of fitted parameters (three in this case). Best values of the spin-wave parameters were obtained by minimizing F. The minimization was performed separately at each temperature and at each wave vector. The total range of F for the optimum parameters of the spin-wave energy and damping was from 0.4 to 0.2 and its value showed no systematic variation with temperature. The average values of F for the four spectral shape functions with which the data were analysed are as follows.

A1	F = 0.96	B1	F = 1.23
A2	F = 1.00	B2	F = 1.08.

The average value from all the spectral forms was F = 1.07.

A perfect fit of a theoretical curve to the data for a counting experiment is expected to give F = 1.0 since the errors are random and the standard error in an individual intensity is equal to its square root. The average values of F from each of the four spectral forms are not different from 1.0 at the .05 significance level, which indicates that the basic cross-sections we have used (equations (II-36) and (II-37)) are satisfactory descriptions of the experimental data. Also the difference between the individual values of F from the spectral forms A1, A2 and B1, B2 is not statistically significant at the 0.05 level so that it has not proved possible on this basis alone to discriminate between them.

The estimation of the errors of the fitted parameters was based on the Snedecor F test for equality of variance. When the F value of a particular fit for about 25 degrees of freedom is 5/3 times the minimum value then, assuming that the errors are normally distributed, at the .05 level of significance the error in the fit is two standard errors. If it is assumed also that the error in the fit varies linearly with the ratio of the values of F, then when F is 4/3 times the minimum value the error in the fitted parameters is one standard error. The errors in the parameters of the spin-wave energy and damping were determined by setting one of them at its optimum value and varying the other. The deviation of the varied parameter from its optimum value for which F is 4/3 times its minimum value was taken to be the standard

error of the parameter.

Since all the four spectral shape functions could be fitted to the experimental line shapes equally satisfactorily, emphasis will be placed on the results obtained using the form A1 and the differences where significant will be pointed out with the results from the other forms.

C. Spin Dynamics Below the Critical Temperature

(i) General description of the results

Extensive measurements of the energy distribution of scattered neutrons were carried out at the wave vectors $q = 0.20\ A^{-1}$ and $0.26\ A^{-1}$ for reduced temperatures between $\varepsilon = 0.067$ and $\varepsilon = 0.005$. In addition, measurements were also made at $q = 0.14$, 0.17 and $0.23\ A^{-1}$ at selected temperatures.

In Figure IV-2 is given the temperature variation of the measured energy spectra at $q = 0.20\ A^{-1}$ for reduced temperatures between $\varepsilon = 0.0407$ and $\varepsilon = 0.0067$. As the critical temperature is approached, the spin-wave energy decreases and the width increases until the magnon creation and annihilation peaks merge into a single broad peak centered at $\omega=0$. Figure IV-3 shows the wave-vector variation of the measured energy spectra at $\varepsilon = 0.018$. Included in the diagrams are the theoretical lines of best fit using the spectral shape function A1.

From Figure IV-3 it can be seen that the integrated intensity decreases while the spin-wave energy and width increases rapidly with increasing wave vector q. This tends to smear out

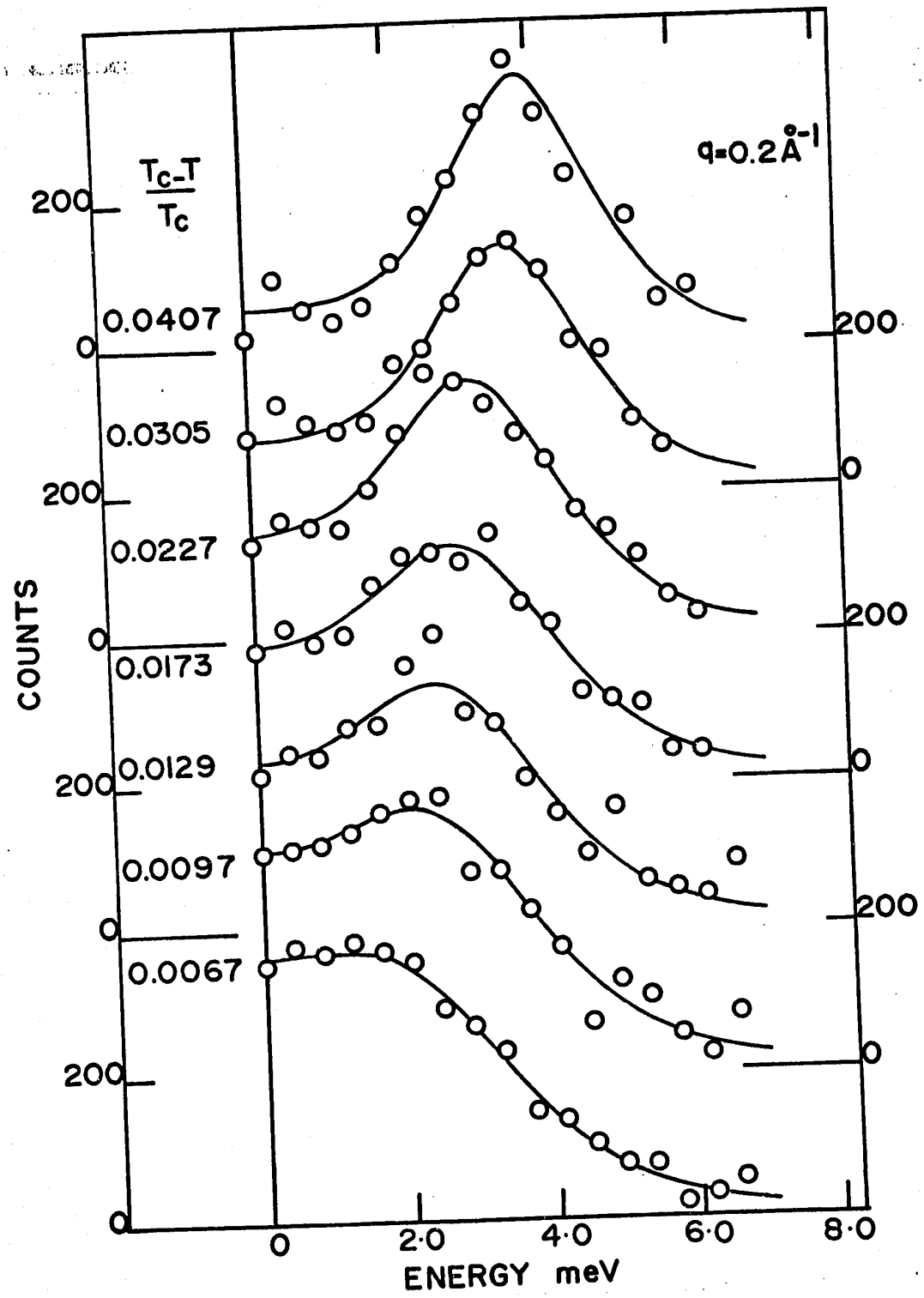

Figure IV-2

The scattering of neutrons at q = 0.20 A^{-1} plotted as a function of temperature below T_c. It shows that the magnon is well defined at the lowest temperature and that its energy decreases and its width increases with increasing temperature. The solid lines represent the fitted line shape.

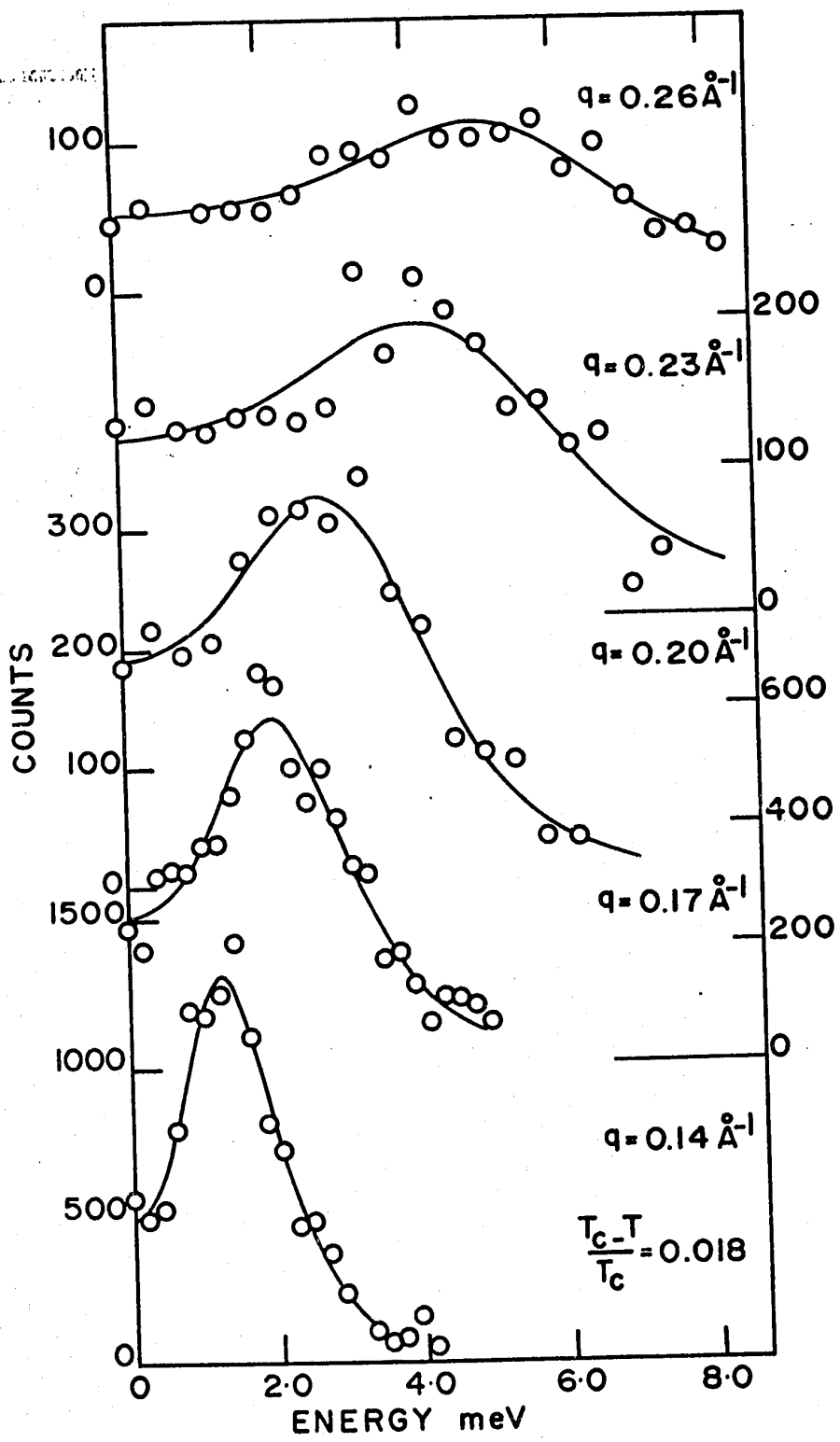

Figure IV-3

The scattering at $\varepsilon = 0.018$ as a function of wave vector q. The spin-wave energy and width increase rapidly while the integrated intensity decreases with increasing q. The solid lines represent the fitted line shape.

the magnon peak for the largest wave vectors. In fact, no accurate measurements were made for q greater than 0.26 A^{-1} because the scattered intensity was too low. Figure IV-1 shows the energy spectra at q = 0.20 and 0.26 A^{-1} for ε approximately equal to 0.04 including the longitudinal acoustic phonon peaks (labelled LA). Since in Figure IV-2 it was seen that the magnon peaks increase in energy with decreasing temperature, no measurements were made for ε greater than 0.07 because the magnon would merge with the phonon peak and the location of the magnetic scattering could not be determined accurately enough to provide useful information.

(ii) Spin-wave energy

It was found that the data could be fitted satisfactorily assuming that the spin-wave energy is given by $E_q = Dq^2$. The variation of the spin-wave energy with temperature is shown in Figure IV-4. The values of the spin-wave constant D were obtained using the spectral shape function A1. A complete list of the spin-wave energy and damping parameters found using the four different spectral shape functions is given in Tables IV-1 and IV-2. Figure IV-4 shows that at each wave vector the spin-wave energy tends towards zero as the critical temperature T_c is approached.

It is perhaps more illuminating to plot the spin-wave constant D against the reduced temperature ε on a log-log scale (Figure IV-5). In the temperature range ε = 0.067 to ε = 0.005 the values of D fell on the same straight line of slope 0.36±0.03 for all the wave vectors measured. This shows

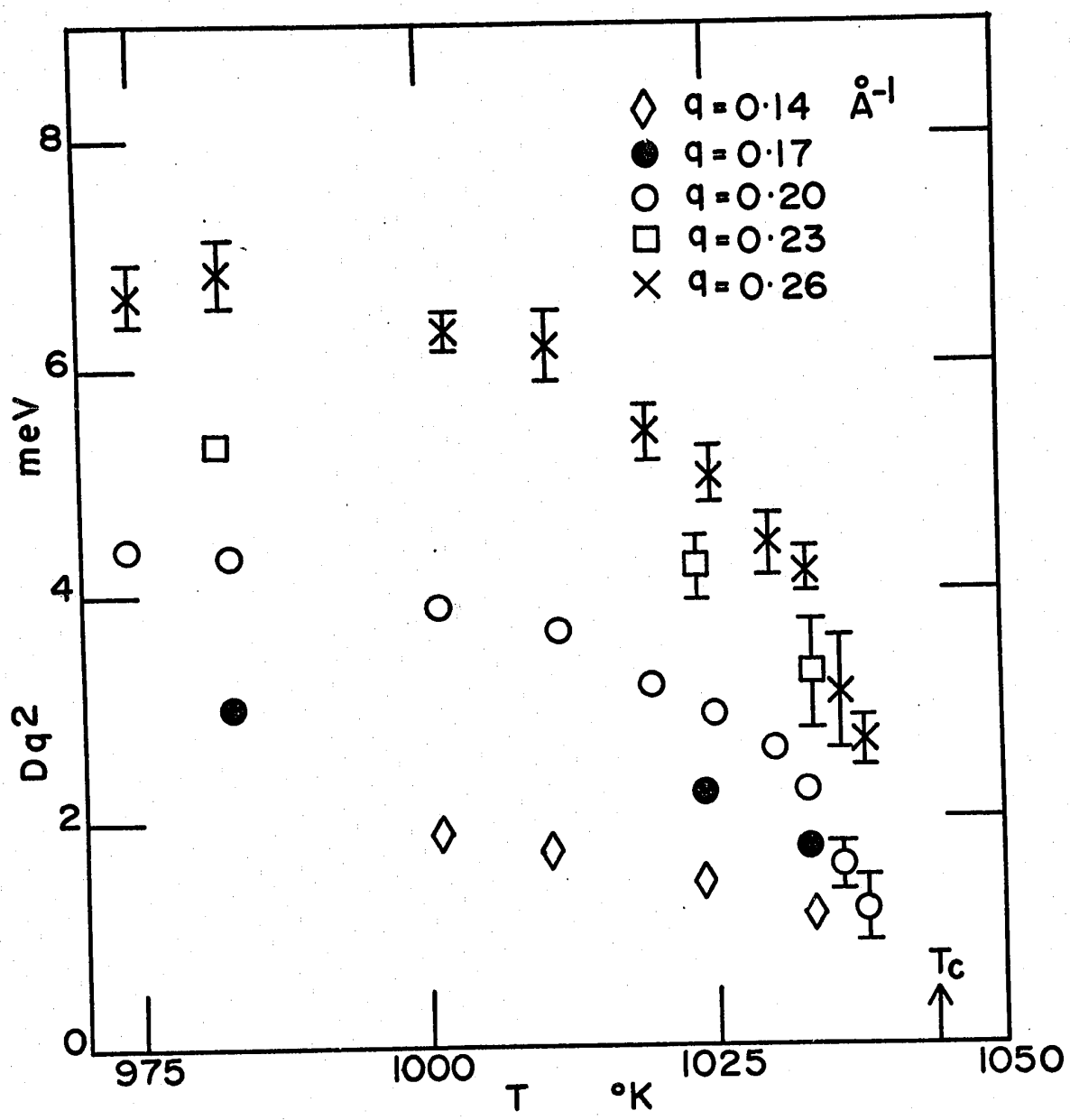

Figure IV-4

The variation of the spin-wave energy Dq^2 with temperature in the vicinity of T_c at the different wave vectors measured.

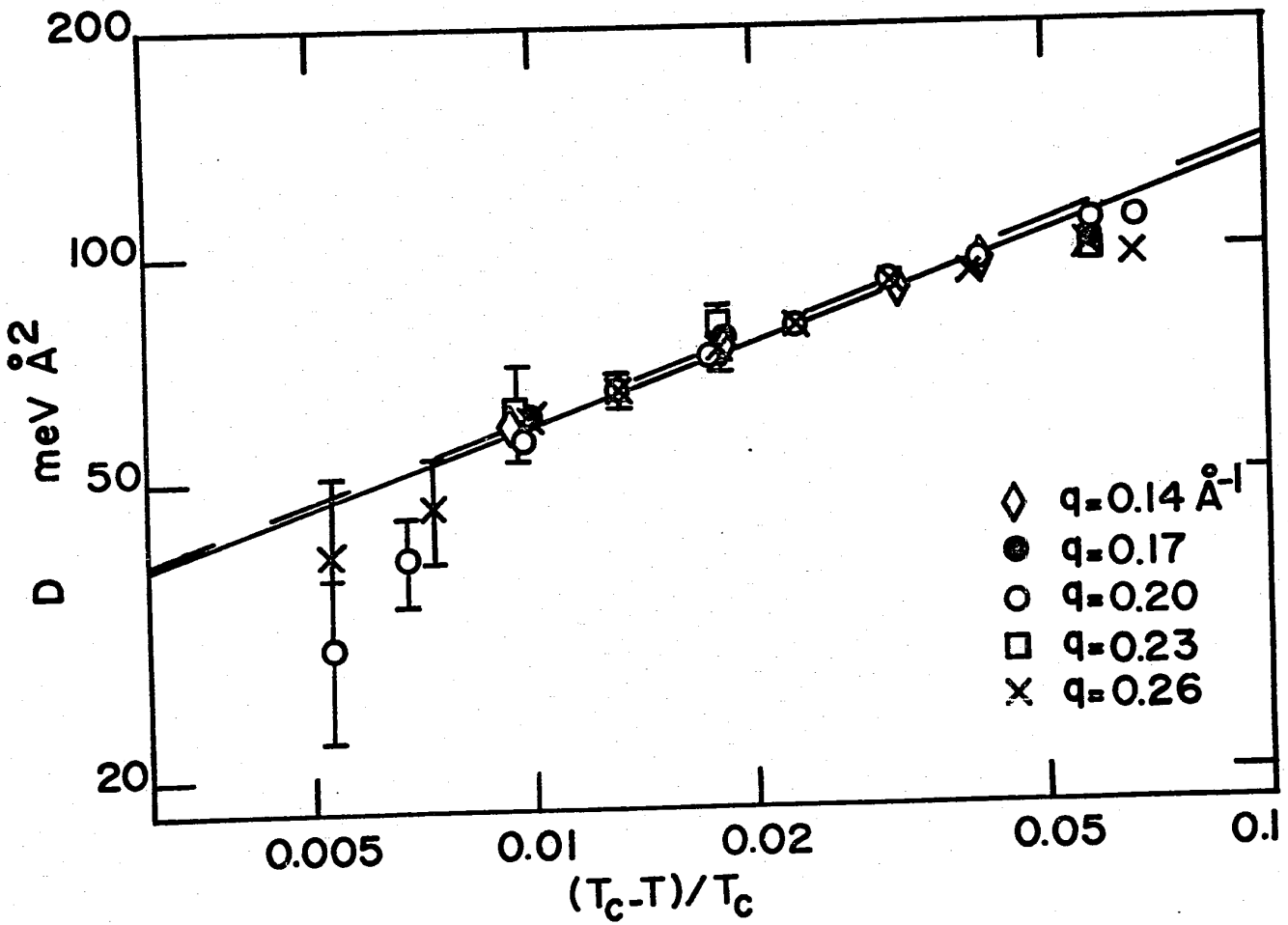

Figure IV-5

The spin-wave constant D plotted against the reduced temperature ε on a log-log scale. The linear fit (solid line) shows that the spin-wave energy is being renormalized to zero at T_c. The dashed line is the line of best fit to the values of D found by Collins et al. at smaller wave vectors.

Table IV-1. Resolution-corrected values of the spin-wave constant and the spin-wave damping parameter found using the spectral shape functions A1 and A2

		A1		A2	
$q(A^{-1})$	ε	$D(meV\ A^2)$	$\gamma'(meV\ A^4)$	$D(meV\ A^2)$	$\gamma_q(meV)$
0.14	0.0409	96.7±3.3	910± 372	94.3± 3.7	0.35±0.17
0.14	0.0314	88.9±2.9	1241± 372	85.8± 3.1	0.48±0.17
0.14	0.0182	74.4±2.9	1760± 370	70.7± 2.9	0.66±0.17
0.14	0.0093	59.1±2.3	2792± 310	55.4± 2.5	1.16±0.29
0.17	0.0577	103.8±2.9	360± 236	102.4± 2.9	0.29±0.21
0.17	0.0183	77.1±3.1	1740± 410	73.6± 3.7	1.55±0.41
0.17	0.0099	60.4±3.7	2895± 744	56.2± 3.7	2.69±0.66
0.20	0.0667	110.0±2.1	232± 145	108.8± 2.1	0.37±0.29
0.20	0.0580	108.4±3.5	517± 186	106.3± 3.7	0.79±0.35
0.20	0.0407	97.2±3.1	744± 160	95.1± 3.3	1.24±0.29
0.20	0.0305	91.8±2.3	943± 149	89.3± 2.1	1.57±0.25
0.20	0.0227	79.4±2.5	1323± 186	76.9± 2.9	2.23±0.37
0.20	0.0173	72.8±2.9	1760± 270	70.1± 2.7	2.98±0.50
0.20	0.0129	65.3±1.9	1861± 207	62.5± 2.5	3.31±0.41
0.20	0.0097	56.2±2.7	2600± 370	53.8± 2.9	4.47±0.62
0.20	0.0067	39.3±5.3	3528± 614	34.3± 4.1	7.03±1.00
0.20	0.0053	29.8±7.4	5500±1200	26.9±15.5	10.2 ±5.5
0.23	0.0580	100.5±2.5	314± 91	99.3± 2.1	0.90±0.3
0.23	0.0181	79.8±5.4	1613± 455	76.9± 5.0	4.90±0.6
0.23	0.0095	62.0±9.1	2399± 993	60.0± 8.3	7.00±2.5

(continued next page)

Table IV-1 (continued)

$q(A^{-1})$	ε	$D(\text{meV } A^2)^{A1}$	$\gamma'(\text{meV}) A^4)$	$D(\text{meV } A^2)^{A2}$	γ_q(meV)
0.26	0.0659	98.4± 4.1	310±110	97.0±4.0	1.41±0.12
0.26	0.0580	101.0± 4.5	455±165	98.5±4.5	1.98±0.83
0.26	0.0398	93.5± 2.5	540±124	92.0±2.5	2.44±0.58
0.26	0.0308	91.4± 4.5	600±165	85.0±4.0	2.65±0.83
0.26	0.0229	80.2± 3.7	703±174	79.0±4.0	3.31±0.79
0.26	0.0175	74.4± 3.7	930±186	72.5±3.5	4.30±0.91
0.26	0.0128	65.3± 4.1	1035±250	63.7±4.1	4.76±1.24
0.26	0.0098	62.0± 2.9	1260±250	60.2±3.1	5.46±0.62
0.26	0.0073	46.0± 7.4	1640±620	46.3±4.6	7.20±1.50
0.26	0.0053	39.7±10.6	2006±827	43.0±5.4	7.90±2.28

Table IV-2 Resolution-corrected values of the spin-wave constant and the spin-wave damping parameter found using the spectral shape functions B1 and B2

		B1		B2	
$q(A^{-1})$	ε	$D(meV\ A^2)$	$\Gamma'(meV\ A^4)$	$D(meV\ A^2)$	$\Gamma_q(meV)$
0.14	0.0409	93.5± 3.3	488±215	91.0± 2.9	0.20±0.08
0.14	0.0314	84.8± 3.5	703±281	81.7± 3.3	0.27±0.12
0.14	0.0182	67.0± 3.3	889±186	64.1± 3.1	0.37±0.08
0.14	0.0093	49.8± 2.5	1005±186	47.1± 2.1	0.43±0.04
0.17	0.0577	102.6± 2.9	207±120	101.3± 3.1	0.19±0.12
0.17	0.0183	69.5± 4.8	893±223	66.2± 4.1	0.79±0.16
0.17	0.0099	53.8± 4.4	1249±289	50.0± 3.7	1.07±0.25
0.20	0.0667	-	-	107.9± 2.0	0.25±0.17
0.20	0.0580	106.3± 2.9	294± 87	104.2± 3.3	0.48±0.19
0.20	0.0407	93.9± 3.3	443±103	91.8± 3.3	0.72±0.19
0.20	0.0305	87.7± 3.3	546±120	84.8± 2.9	0.87±0.17
0.20	0.0227	72.6± 3.3	695±116	69.9± 2.9	1.18±0.17
0.20	0.0173	64.9± 4.1	885±165	62.0± 3.5	1.45±0.21
0.20	0.0129	56.9± 3.5	848±137	54.6± 2.5	1.43±0.17
0.20	0.0097	50.9± 3.3	972±145	48.4± 2.9	1.61±0.17
0.20	0.0067	39.9± 2.7	918±116	38.3± 3.1	1.55±0.19
0.20	0.0053	40.1± 3.7	918±157	38.3± 2.5	1.55±0.21
0.23	0.0580	99.2± 2.1	182± 58	97.8± 2.1	0.52±0.14
0.23	0.0181	74.0± 4.1	893±256	70.7± 6.2	2.5 ±0.7
0.23	0.0095	57.1±11.6	1117±393	55.8±10.3	3.0 ±1.2

(continued next page)

Table IV-2 (continued)

		B1		B2	
$q(A^{-1})$	ε	$D(meV\ A^2)$	$\Gamma'(meV\ A^4)$	$D(meV\ A^2)$	$\Gamma_q(meV)$
0.26	0.0659	97.6±3.9	186± 70	96.4±4.1	0.91±0.37
0.26	0.0580	99.2±4.6	261± 91	97.1±4.6	1.20±0.46
0.26	0.0398	91.0±2.5	290± 62	89.3±2.5	1.36±0.66
0.26	0.0308	84.0±4.8	347± 91	81.9±5.0	1.61±0.45
0.26	0.0229	76.1±4.6	426±128	74.0±4.1	1.94±0.54
0.26	0.0175	68.9±4.8	496± 99	67.0±4.1	2.32±0.45
0.26	0.0128	58.9±5.2	509±108	57.5±4.5	2.40±0.50
0.26	0.0098	56.2±5.0	567±137	54.6±2.5	2.32±0.37
0.26	0.0073	43.8±5.8	562±137	42.6±5.4	2.65±0.62
0.26	0.0053	41.4±5.6	546±165	40.1±5.4	2.65±0.66

that the effect of the ferromagnetic phase transition on the spin dynamics is to renormalize the spin-wave energy to zero as T_c is approached and that the temperature variation of D is given by a simple power law with critical exponent 0.36±0.03.

The dynamic scaling hypothesis of Halperin and Hohenberg (1969) predicts that in the hydrodynamic region (q much smaller than the inverse correlation length κ_1) below T_c, D varies as ε to the power $(\nu'-\beta)$ (equation (II-43)), where ν' and β represent respectively the critical exponents describing the temperature dependence of the spin-spin correlation range ξ and the magnetization. The experimental values for β in iron are 0.389±0.005 from magnetization measurements (Arajs, Tehan, Anderson and Stelmach, 1970) and 0.342±0.004 using Mössbauer effect (Preston, 1968). Since Arajs et al. measured the magnetization directly, their value of the critical exponent β is used in the comparison of the dynamic scaling prediction with our result. As yet, there exists no experimental determination of ν'. Assuming the result of the static scaling hypothesis, namely that $\nu' = \nu$ and taking the average of the experimental values of ν determined by Passell et al. (1965), Bally et al. (1967) and by Parette and Kahn (1971) which is $\nu = 0.70\pm0.10$, then $\nu'-\beta = 0.31\pm0.10$. This agrees with our experimental result. Using the value of β by Preston, $\nu'-\beta = 0.36\pm0.10$ which also agrees with our result.

The line of best fit to the values of the spin-wave constant D (dashed line) found by Collins et al. (1969), at smaller wave vectors than were used in the present experiment is in-

cluded in Figure IV-5. Both their critical exponent 0.37±0.03 and their absolute values of D agree very well with our results. This indicates that to at least $q = 0.26\ A^{-1}$ in iron the spin-wave energy can be expressed as Dq^2 to within a few degrees below the critical temperature. The temperature variation of D does not follow the prediction of spin-wave theory (equation (II-39)). This is only to be expected since the temperatures used were higher than those where spin-wave theory is applicable.

Fitting the data with the four different spectral shape functions resulted in small differences in the corresponding values for D (Figure IV-6, Tables IV-1 and IV-2). The observed difference was systematic, the greatest being the spectral shape functions A1 and B2 where the average difference was 1.5 times the standard error. In particular, a) the spin-wave energies found using the spectral forms B1 and B2 were smaller by about one standard error than those found using the corresponding forms A1 and A2 and b) The slope of D plotted against ε was steeper (0.39±0.03) for the log-log plot from the former compared to (0.36±0.03) obtained from the latter (Figure IV-6).

However, the values of D from each of the four spectral forms fell on the same straight line for all the wave vectors measured. Thus the general conclusions concerning the temperature and wave-vector variation of D given above apply to all the different spectral forms used.

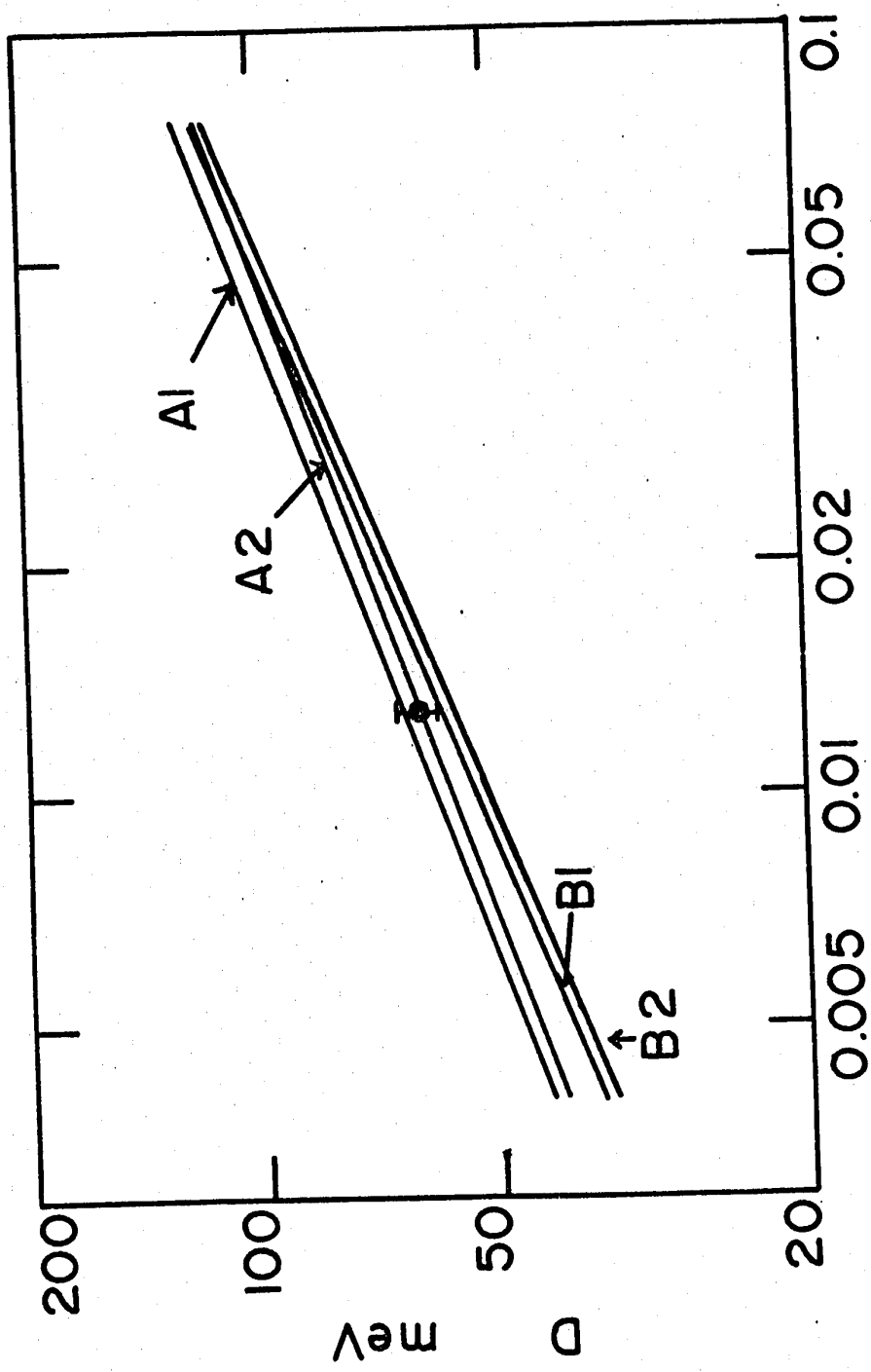

Figure IV-6

Comparison of the lines of best fit of D, plotted against ε on a log-log scale, found using the four different spectral shape functions described in the text.

This behaviour is similar to that found by Passell et al. (1972) for EuO when they analysed their data in a similar fashion using the forms A2 and B2.

As the critical temperature is approached, the values of D become less accurate because of the increasing ratio of the magnon width to its energy. When the magnons were almost over-critically damped, D and γ were highly correlated for the spectral shape functions A1 and A2 and the fitting was more sensitive to the product $D\gamma$ than to their individual values. However for ε greater than 0.01, the correlation was much less and D and γ could be separated more satisfactorily. The correlation was much less pronounced using the forms B1 and B2. For ε less than 0.005 the magnons were over-critically damped at q = 0.20 and 0.26 A^{-1} and it was no longer possible to extract any physically meaningful values of D and γ.

Our critical index of D (0.36±0.03) is equal within experimental errors to that found in Ni (0.39±0.04) by Minkiewicz et al. (1969) and in EuO (0.33) by Passell et al. (1972).

(iii) Spin-wave damping

The second parameter determined from the data below T_c was that of the spin-wave damping. The damping parameter gives the energy width of the magnon spectra. When the spin-wave energy is much greater than its width, the damping term is equal in magnitude to the width. However the dependence is complicated when the magnons start to become critically damped since the energy spectra become asymmetric (Figure II-2).

The variation of the spin-wave damping $\gamma' q^4$ with temperature is shown in Figure IV-7. The values of the spin-wave damping parameter γ' were obtained using the spectral shape function A1 and are given in Table IV-1. Figure IV-7 shows that the damping tends to diverge at the critical temperature.

In Figure IV-8, the spin-wave damping parameter γ' is plotted against the reduced temperature ε on a log-log scale. Of interest is the temperature variation of γ', at $q = 0.20\ A^{-1}$ for ε between 0.06 and 0.005, to which a straight line of slope -0.96 ± 0.10 can be fitted. Thus γ' tends to diverge at the critical temperature T_c with critical exponent -0.96 ± 0.10

Halperin and Hohenberg predicted, using dynamic scaling, that in the hydrodynamic region the critical exponent of the damping parameter γ' is $-(\nu'+\beta)$ (equation (IV-44)). The experimental values of ν and β, with β from Arajs et al. (1970), yield $-(\nu'+\beta) = -1.09\pm0.10$ which agrees within experimental error with our result. If β is taken from Preston (1968), then $-(\nu'+\beta) = 1.04\pm0.10$ which is also in agreement with our result. However, for $q = 0.26\ A^{-1}$ in the same temperature range, γ' varies only as ε to the power -0.67 ± 0.12. Although it seems that at this wave vector the divergence of γ' can still be described by a simple power law, the value of the resulting critical exponent is smaller than that predicted by dynamic scaling.

In Figure IV-9 the spin-wave damping parameter Γ' is plotted against the reduced temperature ε on a log-log scale. The values of Γ' were found using the spectral shape function B1 and are listed in Table IV-2. The temperature variation of Γ',

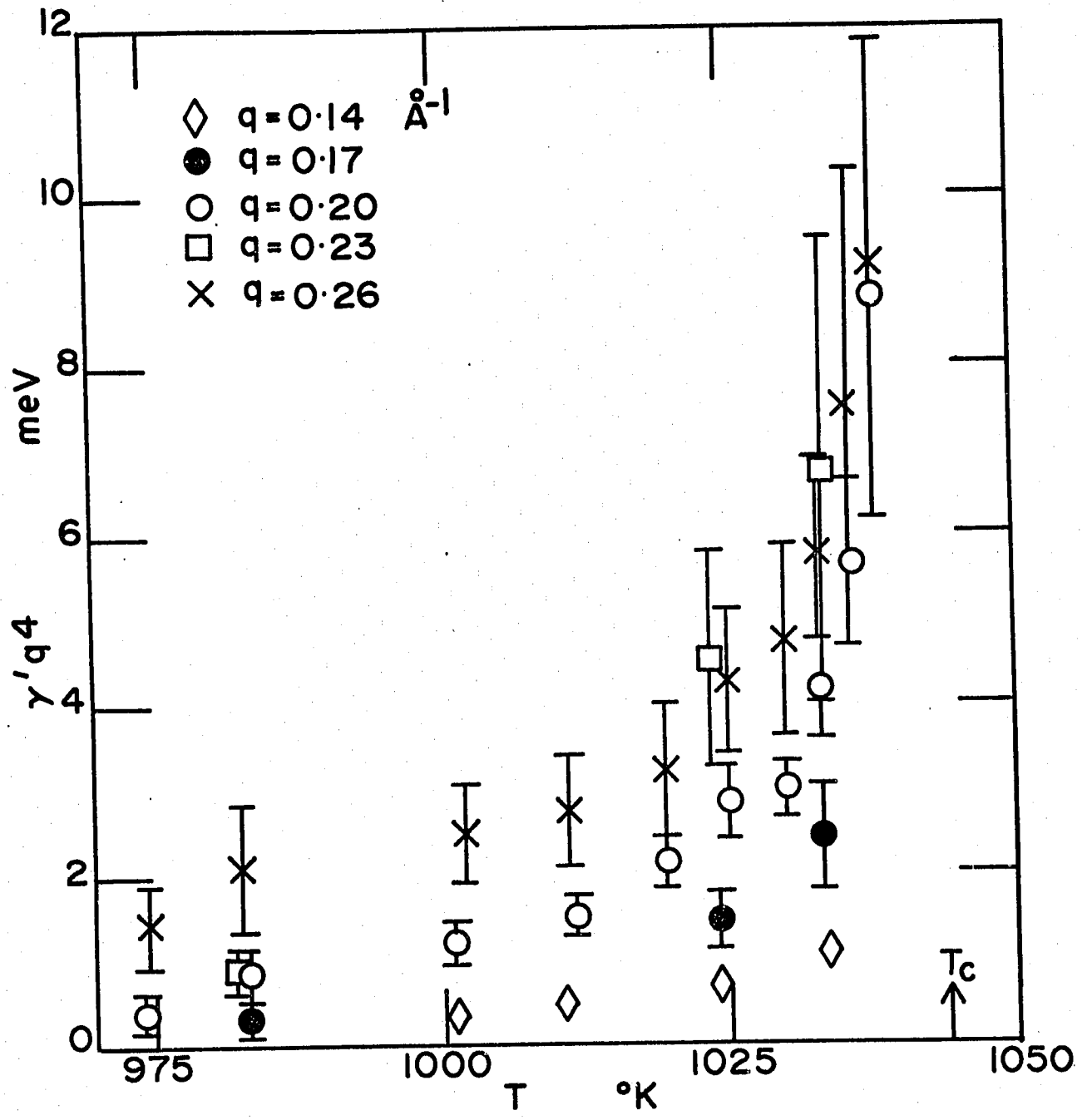

Figure IV-7

Variation of the spin-wave damping $\gamma' q^4$ with temperature in the vicinity of T_c at the different wave vectors measured.

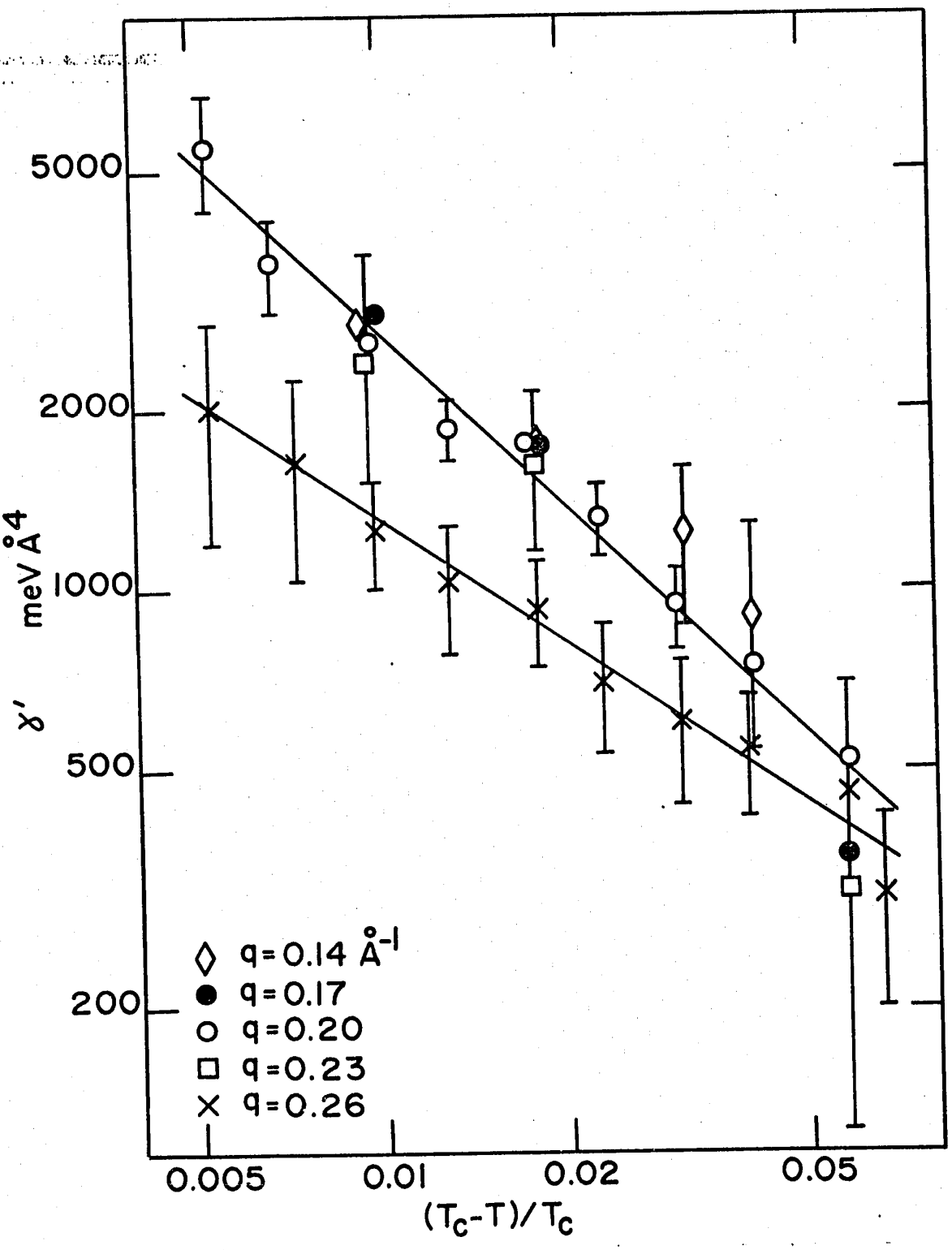

Figure IV-8

The spin-wave damping parameter γ' plotted against ε on a log-log scale. The linear fit shows that γ' diverges at T_c with different critical exponents at $q = 0.20\ A^{-1}$ and $0.26\ A^{-1}$. The critical exponent of γ' at $q = 0.20\ A^{-1}$ is -0.96 ± 0.10.

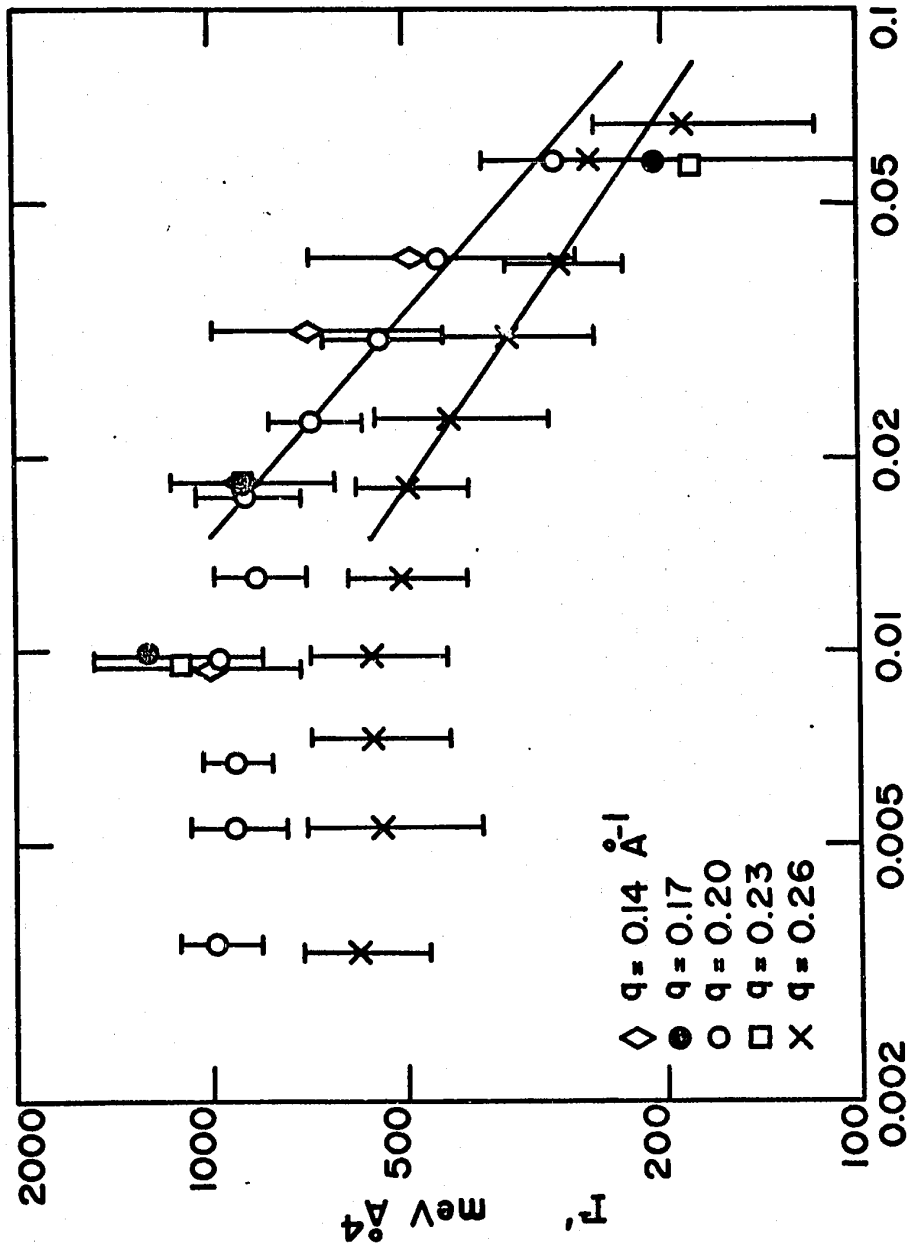

Figure IV-9

The spin-wave damping parameter Γ' plotted against ε on a log-log scale. It shows that there is a change in the temperature variation of Γ' at approximately $\varepsilon = 0.015$. Since the other analytic form for the damping gives straight-line temperature variation on a similar plot (Fig. IV-8), it is likely that the double Lorentzian form used in the present figure is not an appropriate form for describing spin-wave damping.

for $q = 0.20\ A^{-1}$, appears to have a change in slope when ε equals approximately 0.015 which is close to the temperature where the spin waves start to become critically damped (Figure IV-2). There also seems to be a change in slope at about the same temperature for $q = 0.26\ A^{-1}$; however it is less definite. A possible explanation is that the form B1 is sensitive to the boundary between the hydrodynamic and the critical regions (Figure II-1) and the change in slope corresponds to this boundary. From the definitions of the hydrodynamic and critical regions in Chapter II it seems reasonable to take the boundary between them at q approximately equal to κ_1. Since the inverse correlation range κ_1 is proportional to the reduced temperature ε raised to the power ν' (equation (II-26a)), one would expect the change in slope to occur at a larger value of ε for $q = 0.26\ A^{-1}$ than for $q = 0.20\ A^{-1}$. Because of the experimental uncertainties in Γ', this possibility cannot be ruled out.

Another possibility is that the description of the data given by spectral form B1 is not as satisfactory as that given by the form A1. This, in fact, is the simplest interpretation of the data and so must be looked upon in the first instance as the most likely interpretation. This is discussed further in Chapter V.

Figure IV-9 shows that when the reduced temperature ε is greater than 0.015, the slope of the spin-wave damping parameter Γ' plotted against ε on a log-log scale is -0.87 ± 0.12 for $q = 0.20\ A^{-1}$ and -0.69 ± 0.12 for $q = 0.26\ A^{-1}$. These critical exponents

agree within experimental errors with those obtained using the spectral form A1 for the corresponding wave vectors, however they are smaller than $-(\nu'+\beta) = 1.09$ predicted by dynamic scaling. When ε is less than 0.015, there was a marked difference in the temperature variation of the spin-wave damping obtained from the spectral shape functions A1 and B1. While γ' continued to diverge with the same critical exponent as for ε greater than 0.015, Γ' remained approximately constant as the spin waves were becoming critically damped. As expected the temperature variation of the damping did not follow the prediction of spin-wave theory, given in equation (II-40). However, as shown below, spin-wave theory is correct in assigning the q^4 term as the dominant wave-vector dependence.

Figure IV-8 shows that at q = 0.14, 0.17, 0.20 and 0.23 A^{-1}, γ' determined using the spectral shape function A1 was the same within experimental error at each of the temperatures measured, indicating that the spin-wave damping is proportional to q^4 in accordance with the predictions of hydrodynamic theory (equation (II-42)). Similarly, using the form B1 the damping was found to be proportional to q^4 for q between 0.14 and 0.23 A^{-1}. However this wave-vector dependence breaks down suddenly at q = 0.26 A^{-1} for both spectral shape functions because the values of γ' and Γ' determined at 0.26 A^{-1} were significantly lower than at the smaller wave vectors. Thus, at q = 0.26 A^{-1} neither the wave-vector nor the temperature dependence of the spin-wave damping follows the predictions of the hydrodynamic theory or of dynamic scaling.

A possible source of the sudden change in the wave-vector dependence of the damping at $q = 0.26\ A^{-1}$ is a change in the screening of the electrons when the magnon wave vector equals twice an extremal Fermi surface radii in the same direction. Although the Fermi surface in iron is not completely known, several of the extremal radii were measured by Gold et al. (1971) using the de Haas-van Alphen effect.

Since all the spin waves were measured in the [110] direction we are only interested in the projection of the Fermi surface on the (110) plane. Of the several pairs of Fermi surfaces perpendicular to the (110) plane, there was one with an extremal diameter of $0.25\ A^{-1}$. This was the neck of the minority spin surface VIb (notation of Gold et al.) whose axis is along the [001] direction. Our results suggest that for wave vectors q less than $0.25\ A^{-1}$, these electrons contribute significantly to the spin-wave damping, but for larger wave vectors they are unable to follow the spin-wave motion and do not contribute towards the damping.

The values of γ_q and Γ_q found using the spectral forms A2 and B2 were equal within experimental error to the corresponding $\gamma' q^4$ and $\Gamma' q^4$ (Tables IV-1 and IV-2). Hence, none of the above conclusions, regarding spin-wave damping, were altered when the results were analysed using the spectral shape functions in which the wave-vector dependence of the damping was not explicitly included.

It was seen in Chapter II that the predictions of dynamic scaling for the spin-wave energy and damping were only applicable in the hydrodynamic region. As yet the boundary for the hydrodynamic region below T_c is not known. It could be tentatively assumed that the boundary between the hydrodynamic and the critical regions is at q approximately equal to κ_1 and that κ_1 has the same values below T_c as above. Thus $q = \kappa_1$ when $\varepsilon \sim 0.035$ for $q=0.14\ A^{-1}$, $\varepsilon \sim 0.06$ for $q=0.20\ A^{-1}$ and $\varepsilon \sim 0.08$ for $q=0.26\ A^{-1}$. On this basis, it appears that most of the measurements were made outside the hydrodynamic region. Thus, the experimental results indicate that the spin dynamics of iron follow the predictions of hydrodynamic theory even outside the expected range of validity of that theory. There is in fact no breakdown of the hydrodynamic predictions for q less than $0.26\ A^{-1}$, at least until the spin waves become over-critically damped.

It is interesting to compare our observations with those of Passell, Als-Nielsen and Dietrich (1972) for the Heisenberg ferromagnet EuO. They analysed their data using the spectral shape functions A2 and B2, but for the spin-wave damping they only presented their results obtained with the form A2. Their findings are substantially the same as ours, namely that the temperature variation of the spin-wave energy and damping is not very different from what is expected in the hydrodynamic region. However they found that the wave vector variation of the damping was considerably less than q^4.

(iv) Susceptibility

The intensity at a given q integrated over all ω is proportional to the wave-vector-dependent susceptibility $\chi(q)$ (equation (II-17)). The integrated intensity was determined for all the spin waves measured and the calculation of errors considered the statistical fluctuation of the individual counts as well as the error in the background. The integration was over the resolution-broadened spectrum; however the effect of the resolution is only expected to change the areas under the spectrum by a small amount.

In Figure IV-10 the wave-vector-dependent transverse susceptibility $\chi(q)$ is plotted against the reduced temperature ε. It shows that $\chi(q)$ increases with increasing temperature for all wave vectors up to $\varepsilon = 0.005$. However at all temperatures $\chi(q)$ decreases rapidly with increasing q.

In Chapter II there were two different predictions for the form of $\chi(q)$. Firstly, the low-temperature form for the neutron scattering cross-section for a Heisenberg ferromagnet gives a susceptibility $\chi(q)$ which varies as k_BT/Dq^2 (equation (II-52)) when the thermal energy k_BT is very much greater than the spin-wave energy Dq^2. In the vicinity of T_c, k_BT is approximately 80 meV. The spin waves measured had energies less than 7 meV; hence the above condition is satisfied for all the data. If the above form of $\chi(q)$ was valid at temperatures approaching T_c, then the intensity should increase rapidly since D is being renormalized to zero.

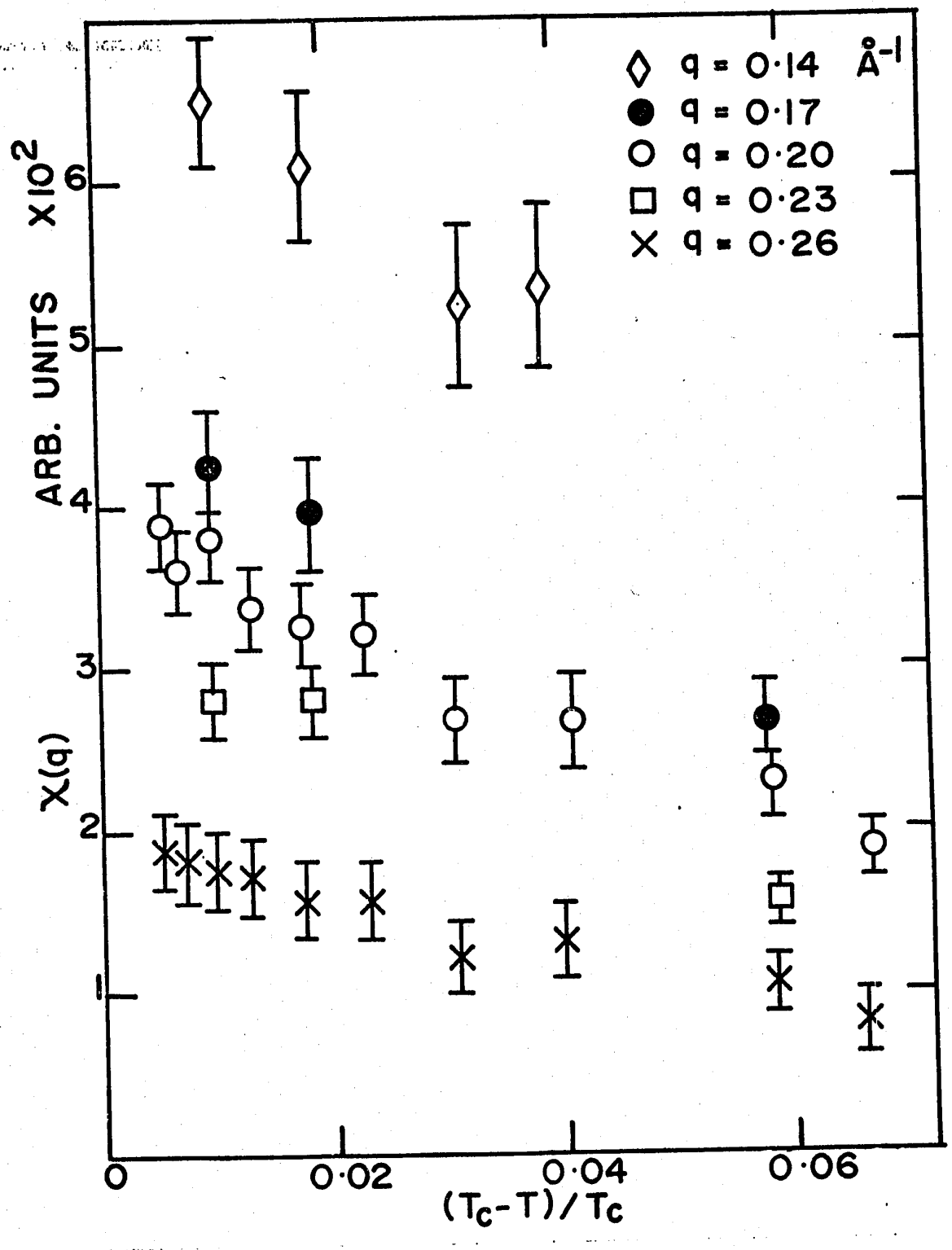

Figure IV-10

The transverse susceptibility $\chi(q)$ plotted against ε below T_c. $\chi(q)$ increased with increasing temperature at all wave vectors up to the highest temperature measured.

Secondly, Marshall and Murray (1968) predicted that $\chi(q)$ varies as $\langle S^z \rangle kT/Dq^2$ (equation (II-53)). $\langle S^z \rangle$ is proportional to the magnetization which in a zero magnetic field varies as ε^{β} near T_c and D varies as $\varepsilon^{\nu'-\beta}$ (equation (II-43)). Both theory and experiment give that β equals approximately $(\nu'-\beta)$, hence $\langle S^z \rangle$ is expected to have almost the same temperature variation as D so that in this case $\chi(q)$ should depend on the temperature only weakly.

Plotting $\chi(q)\,Dq^2/T$ against ε on a log-log scale (Figure IV-11) shows that when ε is geater than 0.01 data points appear to be independent of temperature within experimental error so that $\chi(q)$ appears to have a form similar to that predicted by the low-temperature theory (equation II-52)). However for temperatures closer to T_c this behaviour changes and the curve turns downwards. This change corresponds to the temperature region where the spin waves are becoming critically damped. Figure IV-11 also shows that up to the wave vector $q = 0.23$ $\mathring{A}^{-1}$ $\chi(q)$ is proportional to q^{-2} within experimental errors as expected, but at $q = 0.26$ $\mathring{A}^{-1}$ $\chi(q)$ appears to have a value somewhat lower than would be predicted by the q^{-2} law. This could possibly be related to the anomaly observed in the spin-wave damping.

$\chi(q)$ in iron was measured below $0.7\ T_c$ by Collins et al. (1969) and by Stringfellow (1968). They also observed that $\chi(q)$ increased with increasing temperature; however their measurements were somewhat different from those of our experiment.

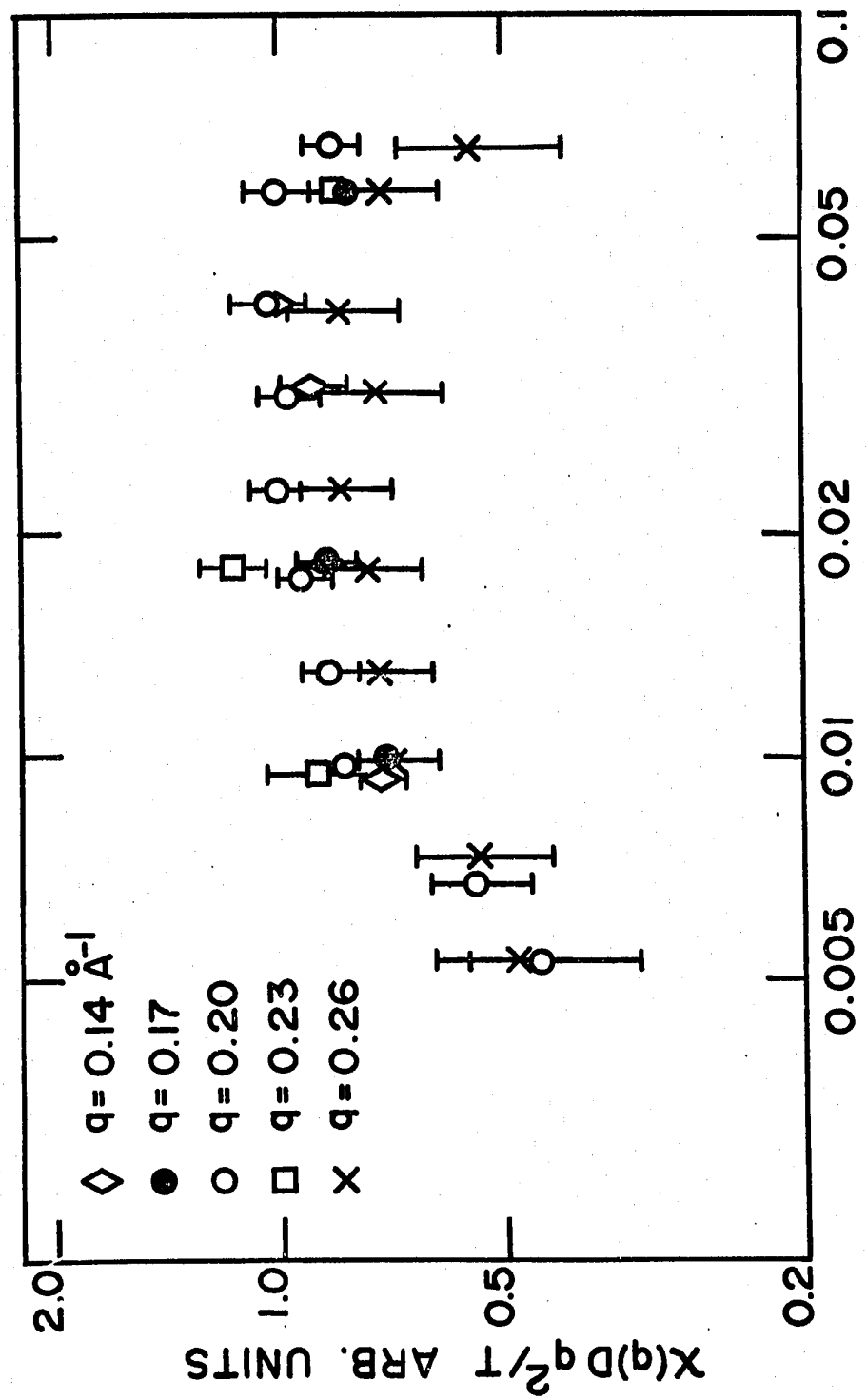

Figure IV-11

$\chi(q)Dq^2/T$ plotted against ε on a log-log scale. When ε is greater than 0.01 the data points appear to be independent of temperature within experimental error.

The measurements of Collins et al. were similar to ours, but at smaller wave vectors. They found that $\chi(q)$ appeared to be proportional to T/q^2 below 0.7 T_c, which is similar to the temperature behaviour of the form of $\chi(q)$ predicted by Marshall and Murray (equation (II-53)), and is close to our observations.

Stringfellow, used a scattering-surface technique to measure the spin-wave scattering cross-section below 0.7 T_c. He found that $\frac{\chi(q)Dq^2}{T<S^z>}$ decreased linearly with increasing temperature. Since the slope was quite small, his result was close to the prediction of Marshall and Murray and to the observation of Collins et al.

The approximate limit of validity of the theory of Marshall and Murray is 0.7 T_c and it appears that it is in satisfactory agreement with the experiments. However, it has already been seen that neither predictions of spin-wave theory concerning the temperature dependence of the magnon energy and damping are in accord with the experiments near T_c. Thus it is not entirely surprising that our observation of the temperature variation of $\chi(q)$ is somewhat different from the prediction of Marshall and Murray and from the experiments at lower temperatures.

There was no evidence of a zero energy diffusive peak below T_c. The theoretical spectral shape functions fitted well the complete spectrum at all temperatures with no systematic difference at zero energy that may be expected if there was a narrow unresolved central peak present (Figures IV-2 and IV-3).

From the accuracy of the experiment it was estimated that if a diffusive peak does exist, its intensity is less than 3% at $q = 0.20\ \mathring{A}^{-1}$ and less than 5% at $q = 0.26\ \mathring{A}^{-1}$ of the intensity of the magnon peak, assuming that it extends no further than 2.0 meV.

It is of course entirely possible that an extremely broad central peak exists at all temperatures; we would have no way of observing such a peak. The absence of the diffusive peak agrees with the observations of Collins et al. (1969) at very small wave vectors in Fe, Minkiewicz et al. (1969) in Ni and Passell et al. (1972) in EuO. Hence, this feature appears to be characteristic of isotropic ferromagnets which differentiate them from antiferromagnets and from anisotropic ferromagnets.

D. Spin Dynamics Close to and Above the Critical Temperature

Extensive measurements of the energy distribution of scattered neutrons were carried out for the temperature range $(T_c-1.7)°K$ to $(T_c+118)°K$ at the same wave vectors as below T_c, namely at $q = 0.20$ and $0.26\ A^{-1}$. In addition measurements were also made at $q = 0.23\ A^{-1}$ at several temperatures similar to below T_c. The scattering at wave vectors greater than $q = 0.26\ A^{-1}$ was only measured at T_c for $q = 0.29\ A^{-1}$ where already the peak intensity of the spectrum was less than the background, and in order to obtain an accuracy that was comparable with that at $q = 0.26\ A^{-1}$ the counting time required was twice as long.

Figure IV-12 shows the variation of the spectrum of scattered neutrons with temperature above T_c at $q = 0.20\ A^{-1}$ which

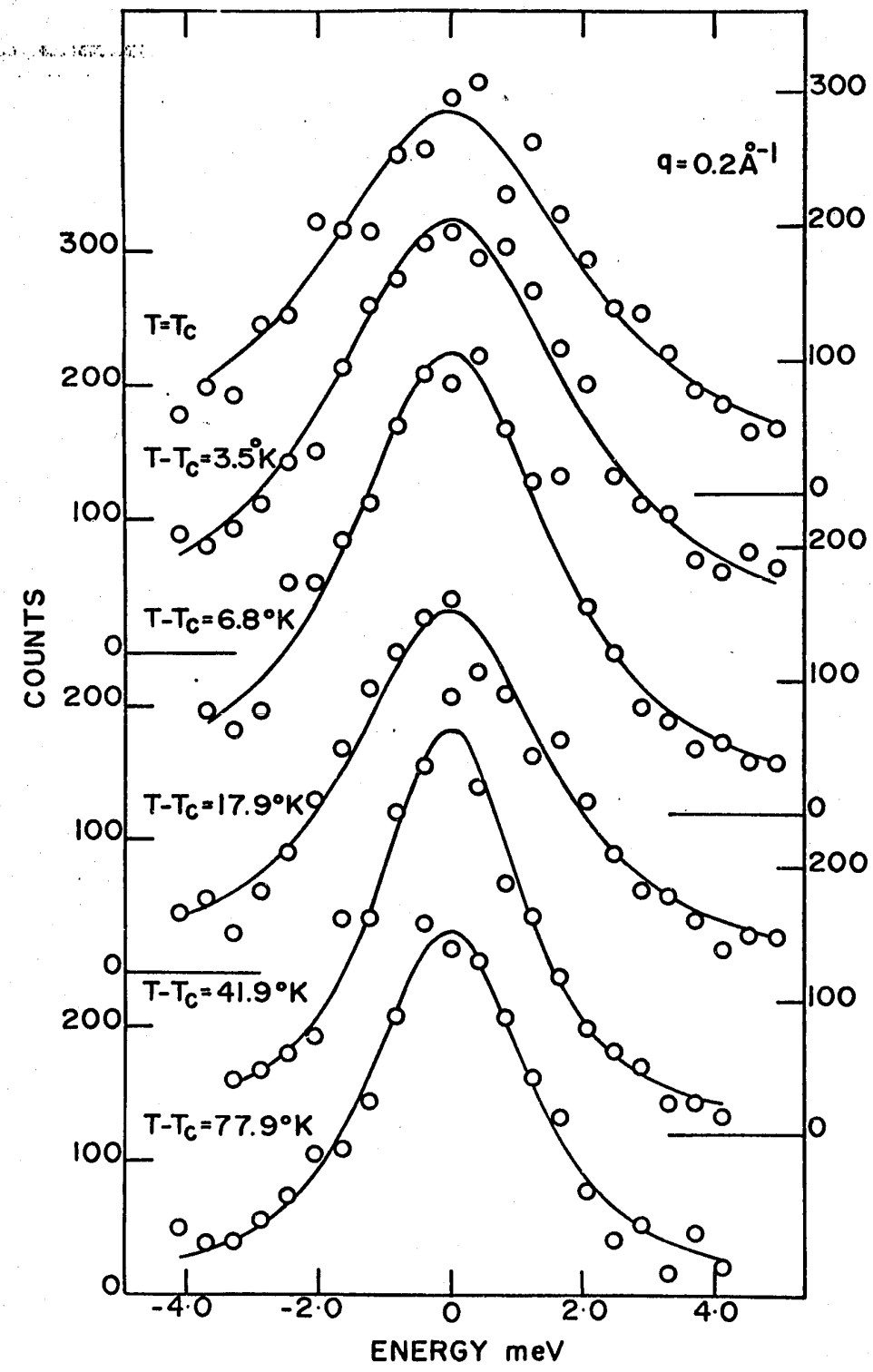

Figure IV-12

The scattering at q = 0.20 A^{-1} plotted as a function of temperature above T_c. The solid lines represent calculated peak shapes using the Lorentzian spectral form given in equation (IV-2). There does not appear to be any shoulders that could be attributed to remnant spin waves.

was representative of the data at the other wave vectors. The energy spectra showed a broad peak, centered about $\omega = 0$, and even near T_c there was no definite shoulder that could be attributed to remnants of spin-wave excitations.

The frequency dependence of the scattering could be fitted satisfactorily over the entire temperature range with a Lorentzian spectral shape function (equation (II-45))

$$F_q(\omega) = \frac{\Gamma_T(q)}{\omega^2+\Gamma_T^2(q)} \qquad \text{(IV-2)}$$

where $\Gamma_T(q)$ is the characteristic frequency or the width parameter. The fitting procedure was exactly the same as for the scattering below T_c. The background was taken into account in the same way as for the data at lower temperatures. The intensity at the wings of the distribution went smoothly down to a level equal to that assigned as the background level, indicating that the assumption of a temperature-independent background introduced earlier is in fact quite satisfactory. The wave-vector dependence of the width parameter $\Gamma_T(q)$ was not included explicitly when fitting the resolution-corrected cross-section (equation (IV-2)) to the observed intensity. Theories given in Chapter II predict that the q dependence of $\Gamma_T(q)$ changes from $\Gamma_T(q) = c\, q^{5/2}$ (equation (II-47)) on going from the critical region to $\Gamma_T(q) = c\, \kappa_1^{1/2} q^2$ (equation (II-49)) in the hydrodynamic region. According to Résibois and Piette (1970) and verified experimentally by Parette and Kahn (1971) the hydrodynamic region does

not start until the ratio κ_1/q is greater than 4. At the highest temperature where the scattering was measured, $(T_c+118)°K$, $\kappa_1 = 0.34$ $\mathring{A}^{-1}$ which for $q = 0.20$ $\mathring{A}^{-1}$ yields the ratio $\kappa_1/q = 1.7$. Hence, although our measurements start in the critical region, they do not extend into the hydrodynamic region. Nevertheless there still could be a change in the q dependence of $\Gamma_T(q)$ and although it would be possible to use some iterative method to make (at least approximately) such a correction to the spectral shape function, the data of part C indicates that the use of a constant $\Gamma_T(q)$ over the resolution function does not introduce any large errors. The values of $\Gamma_T(q)$ are given in Table IV-3.

The F value, the statistical measure of the quality of fit (equation (IV-1)) was on the average 1.2 . The total range of F was from 0.6 to 2.0 and it varied randomly with temperature. We observed no shoulders in the spectra at or just above T_c which could be due to remnants of spin waves. Collins et al. observed weak shoulders at $q = 0.15$ A^{-1} up to $(T_c+3)°K$ however they were not statistically significant. Thus it appears that there are no propagative excitations above T_c in iron.

It should be noted that we observed that the scattering changed its character from a critically-damped spin wave at $(T_c-5)°K$ to a mode that, within the accuracy of the experiment, appeared completely diffusive at $(T_c-1.7)°K$. In between the scattering was a broad peak centered at $\omega = 0$ with definite shoulders indicating a propagative nature. It was not possible to assign meaningfully to the spectra a spin-wave energy or damping

Table IV-3 Resolution-corrected values of the width of the diffusive peak found neglecting the wave vector dependence of the width

$q(A^{-1})$	$(T-T_c)°K$	$\Gamma_T(q)$ (meV)	$q(A^{-1})$	$(T-T_c)°K$	$\Gamma_T(q)$ (meV)
0.20	-1.7	2.40 ± 0.30	0.26	-1.6	5.75 ± 1.34
0.20	0.0	2.31 ± 0.30	0.26	-0.8	4.96 ± 1.24
0.20	0.2	2.11 ± 0.29	0.26	0.0	4.70 ± 1.45
0.20	3.2	2.13 ± 0.21	0.26	3.2	3.90 ± 0.80
0.20	6.8	1.72 ± 0.17	0.26	7.1	4.10 ± 0.45
0.20	12.3	1.55 ± 0.15	0.26	11.8	3.60 ± 0.70
0.20	17.4	1.65 ± 0.21	0.26	15.1	3.20 ± 0.60
0.20	29.4	1.37 ± 0.19	0.26	18.3	3.20 ± 0.80
0.20	41.9	1.12 ± 0.15	0.26	29.1	2.80 ± 0.60
0.20	56.4	1.12 ± 0.15	0.26	41.7	2.90 ± 0.60
0.20	77.9	1.28 ± 0.17	0.26	57.0	2.40 ± 0.35
0.20	118.8	1.20 ± 0.17	0.26	77.4	2.85 ± 0.40
			0.26	117.9	2.80 ± 0.45
0.23	-0.8	3.85 ± 0.87			
0.23	0.2	3.47 ± 0.50	0.29	-0.3	6.00 ± 0.83
0.23	11.4	2.73 ± 0.50			
0.23	27.9	2.34 ± 0.45			

and also the spectra could not be fitted satisfactorily by a Lorentzian form (equation (IV-2)).

Figure IV-13 shows $\Gamma_{T_c}(q)$ plotted against q on a log-log scale for q between 0.20 A^{-1} and 0.29 A^{-1}. $\Gamma_{T_c}(q)$ varies as q to the power 2.8±0.3 with a proportionality constant equal to $c' \sim 200$ meV $A^{2.8}$ (c.f. equation (II-47)). This critical exponent is equal within experimental error to the prediction of dynamic scaling (equation (II-47)) for Heisenberg (Halperin and Hohenberg) and itinerant (Hertz, 1971) ferromagnets. It also agrees favourably with the value of 2.7±0.3 found by Collins et al. in Fe at smaller wave vectors and is close to the value of 2.46±0.25 observed by Minkiewicz et al. (1969) in Ni. Als-Nielsen (1970) fitted the data of Collins et al. at T_c to a $q^{5/2}$ power law and came to the conclusion that their values of $\Gamma_{T_c}(q)$ could also be fitted satisfactorily by $c\,q^{5/2}$ where $c \sim 130$ meV $A^{5/2}$. This is shown on the dashed line in Figure IV-13; it also gives a satisfactory fit to our data.

In Figure IV-14 $\Gamma_T(q)$ is plotted against $(T-T_c)$ for q = 0.20, 0.23 and 0.26 A^{-1} and it shows that the width of the diffusive peak narrows markedly with increasing temperature in the vicinity of T_c, then it slowly levels out at the higher temperatures. This in fact is exactly the qualitative behaviour predicted by Résibois and Piette (1970). The dynamic scaling prediction (equation (II-46)) for the width of the zero energy peak above T_c was given in Chapter II. Résibois and Piette (1970) calculated theoretically that the scaling function $f(\kappa_1/q)$ de-

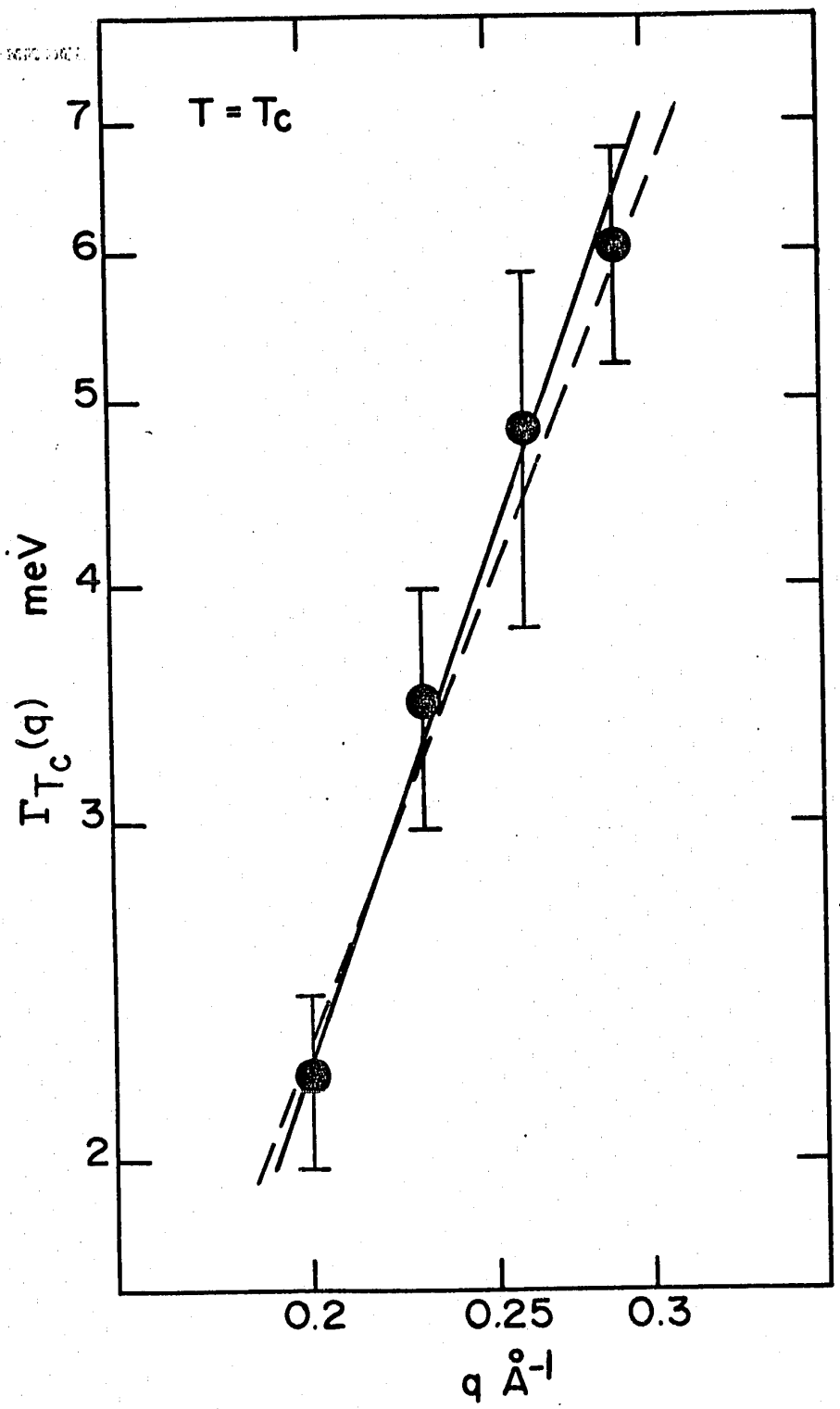

Figure IV-13

$\Gamma_{T_c}(q)$ plotted against q on a log-log scale. The data have been corrected for instrumental contributions to the width. The solid line is the best fit to the data and its slope is 2.8±0.3. The dashed line is the best fit to the data of Collins et al. Dynamic scaling predicts the slope to be 2.5.

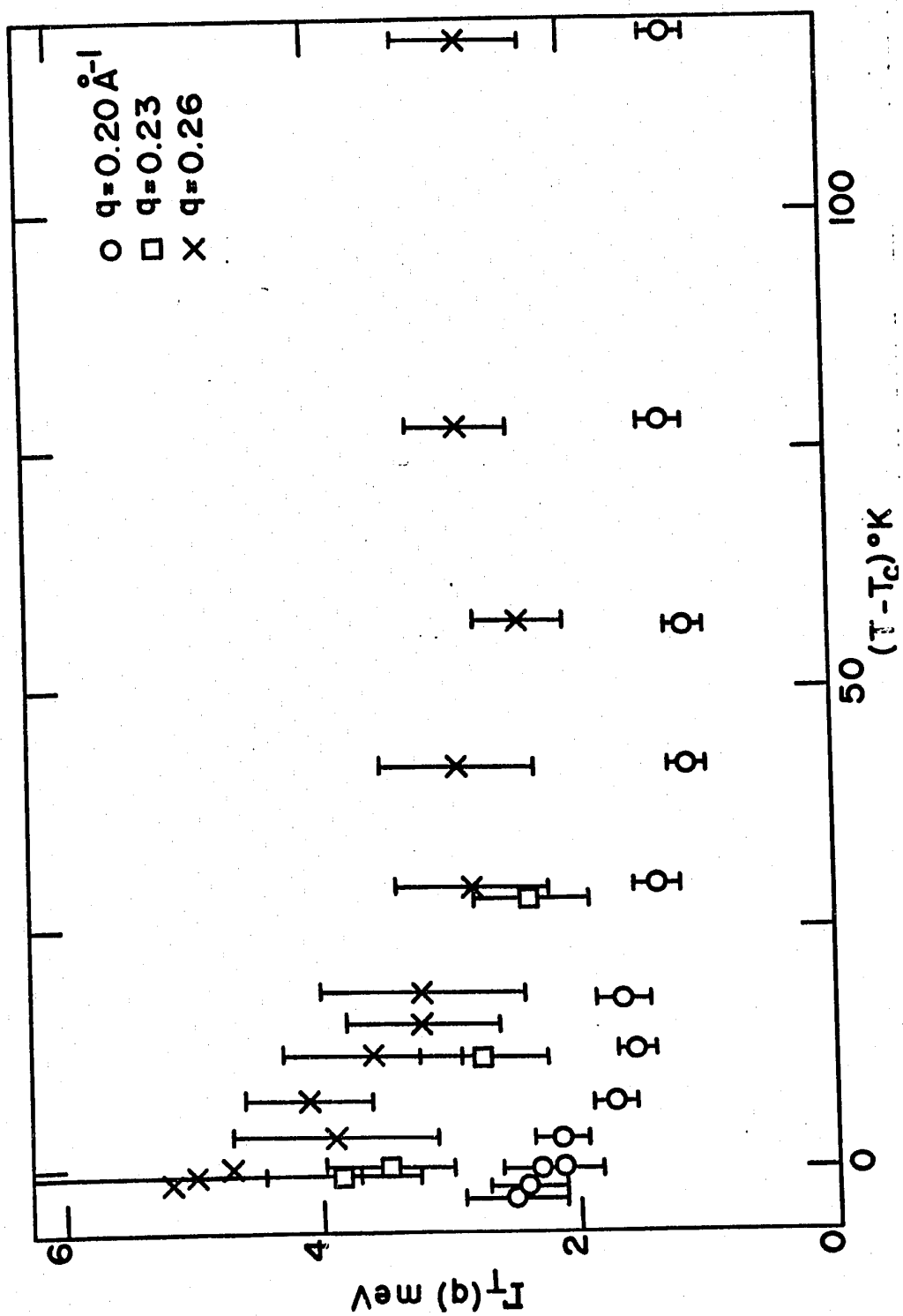

Figure IV-14

Γ_T (q) plotted against temperature at different wave vectors. The narrowing of the diffusive peak is the greatest near T_c. Above (T_c+40) °K the width is approximately constant.

creases with increasing κ_1/q from unity at $\kappa_1/q = 0$ until a minimum value is reached at κ_1/q equal to approximately 1.0. After this, it slowly increased until κ_1/q is equal to or larger than 4 when the asymptotic form $f(\kappa_1/q) \sim (\kappa_1/q)^{1/2}$ (equation II-48)) is attained.

Figure IV-15 shows $\Gamma_T(q)/\Gamma_{T_c}(q)$ plotted against κ_1/q where $\Gamma_{T_c}(q) = c'q^{2.8}$ is the width of the diffusive peak at T_c and the values of κ_1 are from the line of best fit to the experimental values found by Bally et al. (1967). The scaling function $f(\kappa_1/q)$ calculated by Résibois and Piette (1970) is also included in Figure IV-15, and the agreement with our experimental results is very good. Figure IV-16 shows $\Gamma_T(q)/\Gamma_{T_c}(q)$ plotted against κ_1/q with κ_1 from the line of best fit to the experimental values found by Passell et al. (1965) and Parette and Kahn (1971) respectively. Again, there is good agreement between our experimental values and the theoretical scaling function.

It should be noted that the spin dynamics at and above T_c were not anomalous at $q = 0.26\ A^{-1}$. The reason why there is an anomaly below T_c but not above is not understood.

Analysis of the data was also made at five different temperatures with a q^2 wave-vector dependence in the width parameter. The corresponding spectral shape function was

$$F_q(\omega) = \frac{\Gamma_T' q^2}{\omega^2 + \Gamma_T'^2 q^4} \quad .$$

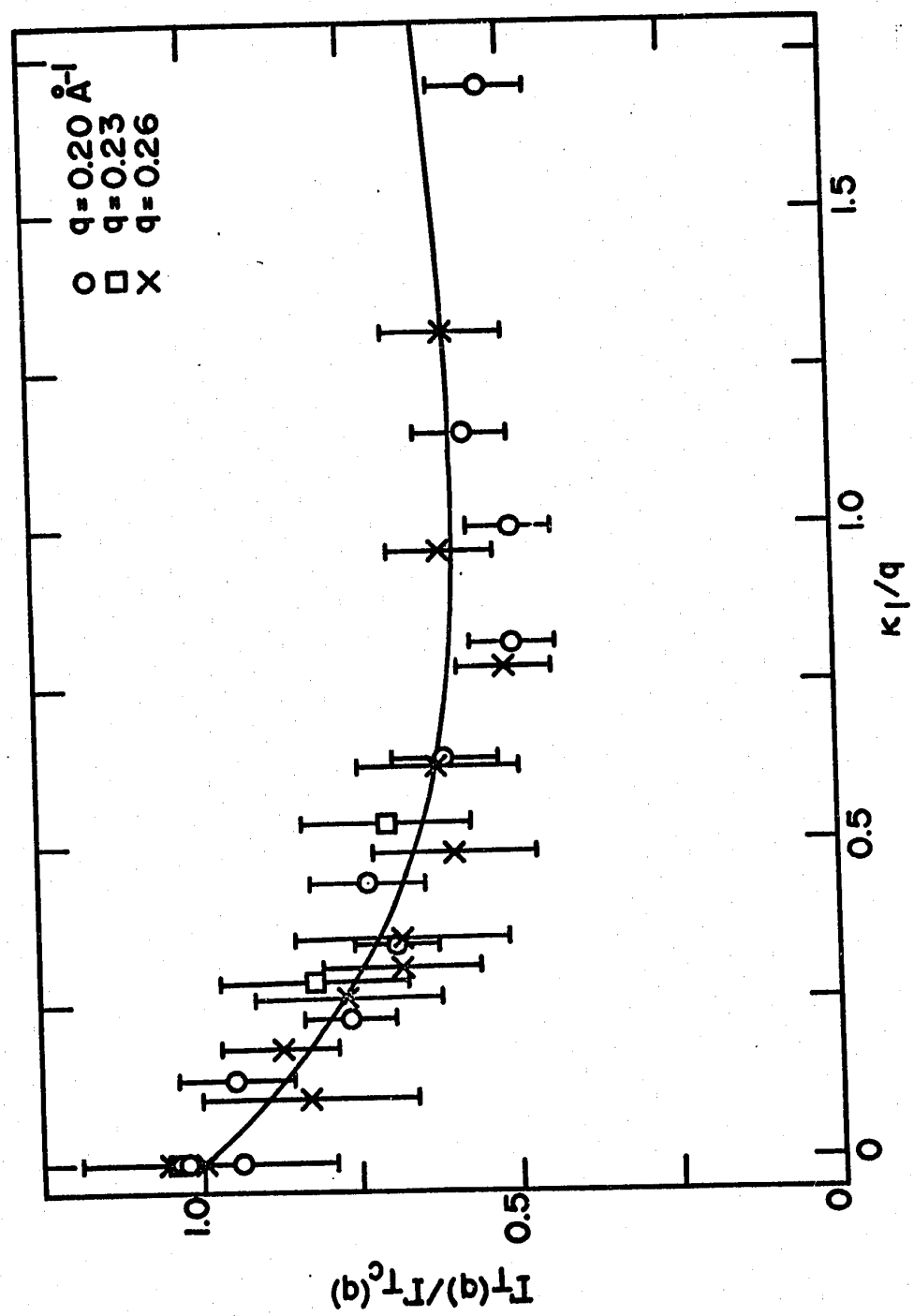

Figure IV-15

$\Gamma_T(q)/\Gamma_{Tc}(q)$ plotted against κ_1/q above T_c. $\Gamma_{Tc}(q)$ is the width of the diffusive peak at T_c. The values of κ_1 are from the line of best fit to the experimental values of Bally et al. The solid curve is the theoretical scaling function $f(\kappa_1/q)$ calculated by Résibois and Piette.

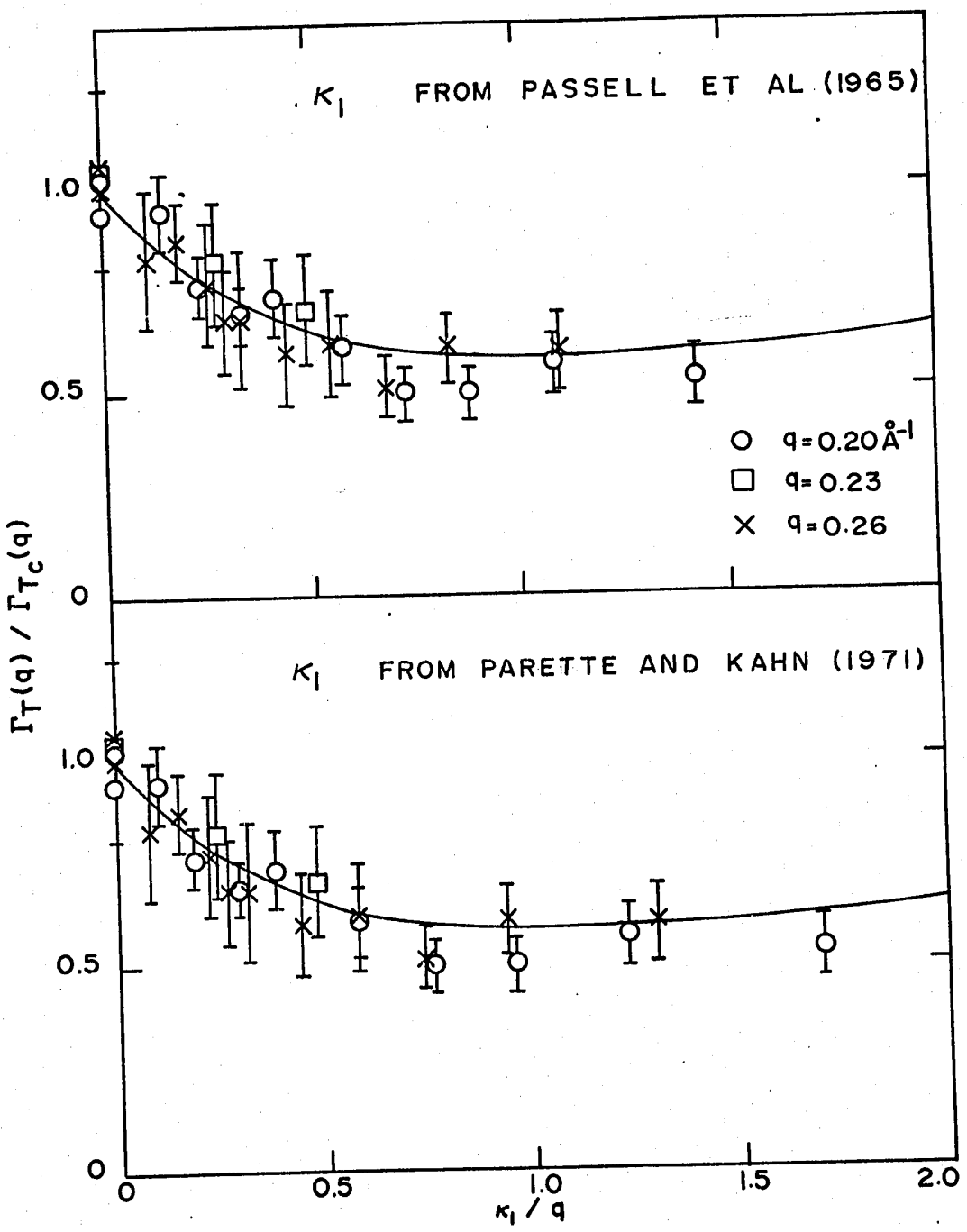

Figure IV-16

$\Gamma_T(q)/\Gamma_{T_c}(q)$ plotted against κ_1/q above T_c. The solid curve is the theoretical scaling function $f(\kappa_1/q)$ calculated by Résibois and Piette.

Table IV-4. Resolution-corrected values of the width parameter of the diffusive peak found assuming that the width is proportional to the square of the wave vector.

$q(A^{-1})$	$(T-T_c)°K$	Γ_T'(meV A^2)
0.20	0.0	55.8 ± 5.8
0.20	3.2	51.7 ± 5.8
0.20	29.4	31.8 ± 4.1
0.20	56.4	27.3 ± 3.7
0.20	118.8	28.9 ± 4.1
0.26	0.0	67.4 ± 16.5
0.26	3.2	55.8 ± 10.8
0.26	29.1	40.5 ± 9.0
0.26	57.0	34.3 ± 5.0
0.26	117.9	40.5 ± 6.2

The resulting cross-section when broadened by the instrumental resolution fitted the scattering equally well as the spectral form (equation (IV-2)) without the explicit wave-vector dependence of the width parameter. The optimum values of $\Gamma_T' q^2$ (Table IV-4) were on the average smaller by 25% of the standard error than the respective $\Gamma_T(q)$. Since the difference was independent of temperature our conclusions were left unchanged.

Figure IV-17 shows that $\chi(q)$ was the largest at $T = T_c$ and at all wave vectors decreased with increasing temperature, the decrease being the greatest near T_c. At all temperatures $\chi(q)$ decreased with increasing q. It is more instructive to plot the product $\chi(q)(q^2+\kappa_1^2)$ against temperature (Figure IV-18); the values of κ_1 are from Bally et al. (1967). The resultant products are equal within the experimental errors at the different wave vectors and have a weak temperature variation near T_c, but increase at a faster rate at higher temperatures. In Chapter II, it was shown that $\chi(q)(q^2+\kappa_1^2)$ is proportional to $\frac{1}{r_1^2}$ (equation (II-50)), where r_1 is the Ornstein-Zernike interaction range. Our result for the temperature variation of r_1 is consistent qualitatively with that of Bally et al. (1967) and of Passell et al. (1965). In Figure IV-19, $\chi(q)(q^2+\kappa_1^2)$ is plotted against temperature, with the values of κ_1 from Passell et al. (1965) and from Parette and Kahn (1971). The resulting temperature variation of r_1 agreed with that of the previous experiments of Passell et al. and Bally et al.

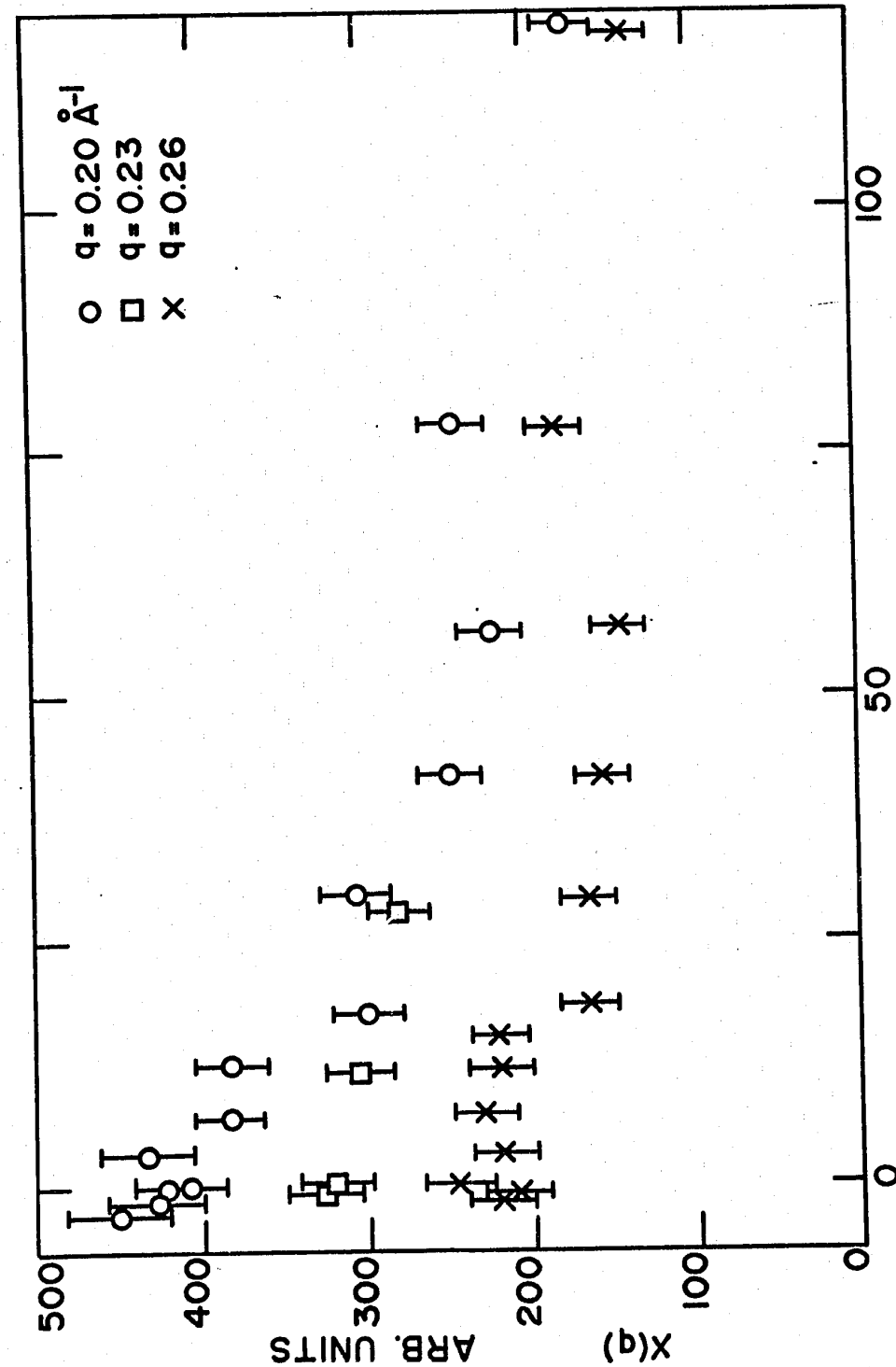

Figure IV-17

The susceptibility $\chi(q)$ plotted against temperature above T_c. The decrease in $\chi(q)$ with increasing temperature is the greatest near T_c.

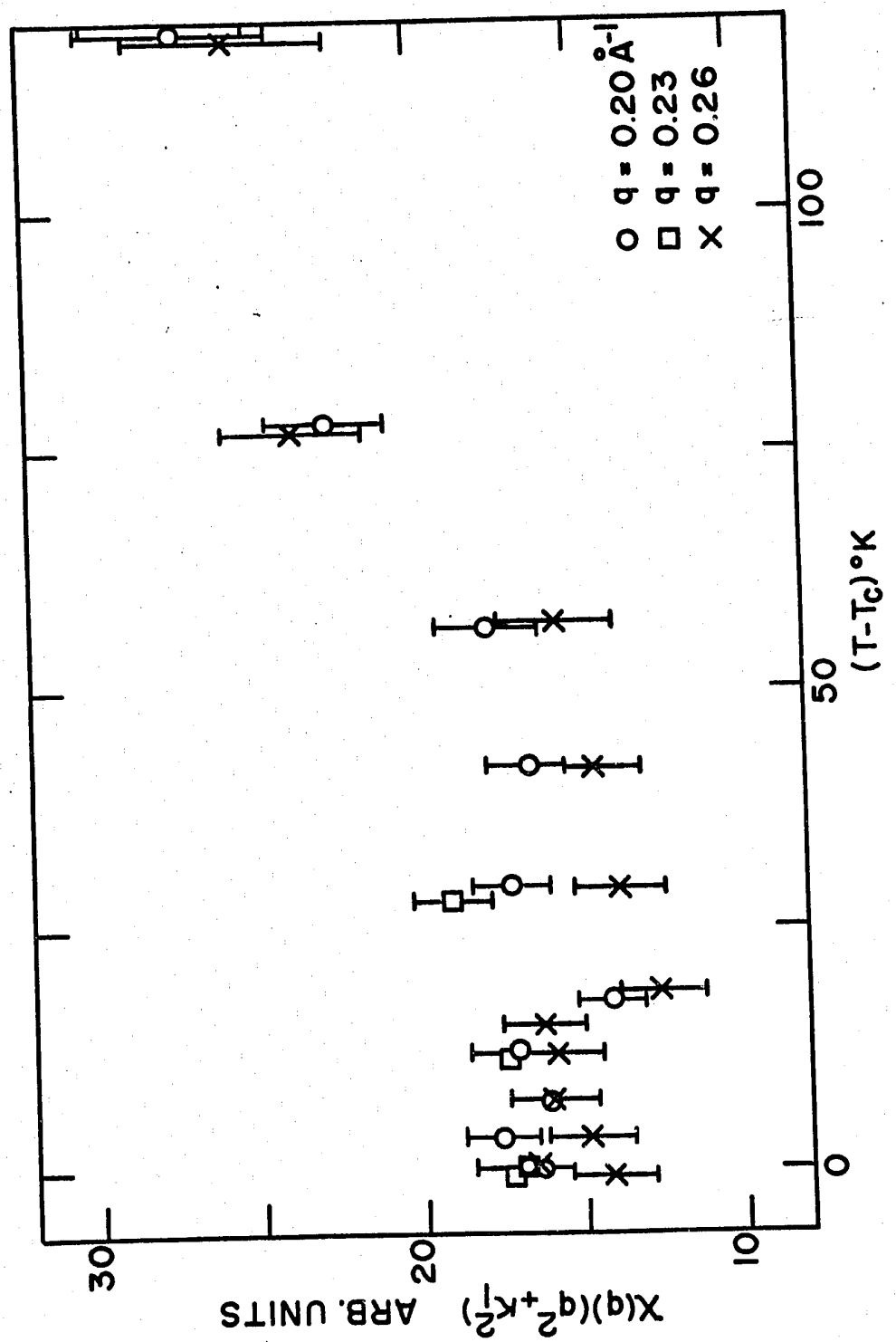

Figure IV-18

$\chi(q)(q^2+\kappa_1^2)$ plotted against temperature above T_c. The values of κ_1 are from Bally et al. $\chi(q)(q^2+\kappa_1^2)$ is directly proportional to $1/r_1^2$ where r_1 is the effective interaction range of the Ornstein-Zernike correlation function.

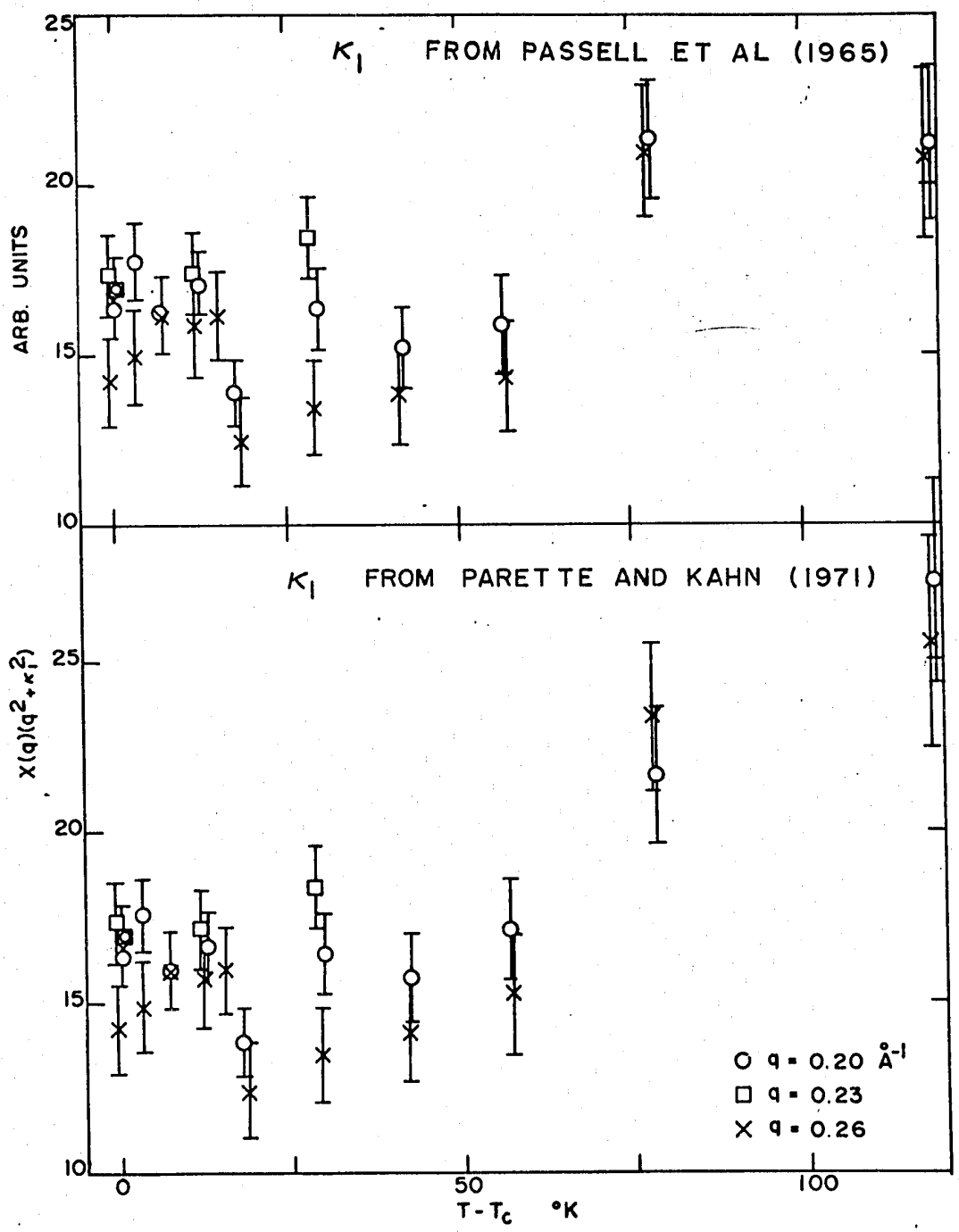

Figure IV-19

$\chi(q)(q^2+\kappa_1^2)$ plotted against temperature above T_c. The values of κ_1 are from Passell et al. (top) and from Parette and Kahn (bottom). $\chi(q)(q^2+\kappa_1^2)$ is directly proportional to $1/r_1^2$ where r_1 is the effective interaction range of the Ornstein-Zernike correlation function.

CHAPTER V
CONCLUSIONS

The spin dynamics of iron in the vicinity of the critical temperature was measured by the technique of neutron spectroscopy in order to study the magnetic phase transition.

It was found that most of the experimental results agreed with theory for the critical properties of a Heisenberg ferromagnet. This result is in accord with the empirical observations that in general the spin dynamics of iron at low temperatures behave in a manner that may be expected for a Heisenberg ferromagnet, and that the metallic properties are not evident.

Another important observation was that the behaviour of various quantities describing the critical spin dynamics could be interpreted in terms of simple power laws. The exponents extracted from these power laws can be used to describe the behaviour of dynamic as well as static quantities near the critical temperature. Hence our data tends to support the proposition that critical exponents are a powerful way of describing critical phase transitions.

Below the critical temperature the spin-wave energy and damping were studied extensively and the results indicate that they behaved as predicted in the long wavelength limit

even at wave vectors that were outside the expected range of validity of the theory.

The wave-vector variation of the spin-wave energy was in accord with the predictions of spin-wave and hydrodynamic theories. The spin-wave energy was observed to be renormalized to zero as the critical temperature was approached and its temperature variation could be described in terms of a power law. The critical exponent of the spin-wave constant was 0.36 ± 0.03, which agrees with the predicted value of 0.31 ± 0.10 from dynamic scaling hypothesis. Our value is the same within experimental error as has been observed for europium oxide and for nickel. Our data is also in accord with earlier measurements in iron.

In order to study the spin-wave damping, theoretical line shapes were fitted to the observed scattered neutron spectra. The damping was included as a parameter on which the width of the line depended. There were two such theoretical spectral shape functions fitted; one a double-Lorentzian form that has been commonly used in the past for interpreting experimental data, and another form derived by Halperin and Hohenberg from hydrodynamic theory.

When fitting to the experimental data the average of the minimum F values, which measures the goodness of fit, was smaller for the Halperin and Hohenberg spectral forms than for the double-Lorentzian form. However the difference was not

significant at the 0.05 level. Nevertheless for five out of the thirty magnons, to which the theoretical cross-section was fitted, the minimum value of F obtained using the Halperin and Hohenberg form was smaller, at 0.05 significance level, than that obtained using the double-Lorentzian form but never higher. This evidence from the least squares fitting is not overwhelming but it indicates that the Halperin and Hohenberg spectral form is somewhat better than the double-Lorentzian form in representing the experimental data.

The hydrodynamic theory prediction that the spin-wave damping is proportional to q^4 adequately described our results for both spectral shape functions for wave vectors between $0.14\ A^{-1}$ and $0.23\ A^{-1}$. However the temperature dependence of the damping of the two spectral shape functions was markedly different.

The temperature variation of the damping found using the Halperin and Hohenberg spectral form was continuous over the complete temperature range and could be described by a power law variation. In contrast the temperature variation of the damping found using the double-Lorentzian form was more complicated and it had a discontinuity of slope near the reduced temperature $\varepsilon = 0.015$. At temperatures below this value the damping varied similarly to that found using the Halperin and Hohenberg form, but at temperatures above the

damping remained approximately constant.

Generally in physics preference is given to the theoretical expression that gives the simplest description of the experimental results. Hence our results indicate that the spectral shape function predicted by Halperin and Hohenberg not only is somewhat better in representing the data,but is also more useful than the double-Lorentzian form in describing the critical properties of the spin dynamics of iron.

For the Halperin and Hohenberg spectral form at a wave vector of 0.20 A^{-1} the damping varied as the reduced temperature to the power -0.96±0.10. This critical exponent was in satisfactory agreement with the predicted value of -1.09±0.10 from dynamic scaling. Spin-wave damping in iron has not been previously measured and the results obtained for the wave-vector and temperature dependence constitute a notable success for the theory.

The spin waves became over-critically damped a few degrees below the critical temperature, so that it is not possible to measure the temperature variation of the spin-wave energy and damping right up to the critical temperature. However the simple power law variations were observed to hold over a range of reduced temperature of more than a decade.

The critical exponent ν' of the correlation range below the critical temperature can be determined from the experimental

critical exponent of the spin-wave energy and damping using a relation between critical exponents given by dynamic scaling hypotheses (equations (II-43) and (II-44)). It is found that

$$\nu' = 0.66 \pm 0.05 \ .$$

This is equal within error to both the experimental and theoretical values of the critical exponent ν of the correlation range above the critical temperature. The critical exponent ν' has not been found previously for iron and the equality with ν agrees with a prediction of static scaling.

Measurements at wave vector 0.26 A^{-1} show anomalous damping both with respect to wave-vector dependence and temperature dependence. This is believed to be caused by the change in the electron screening at the region of the Fermi surface where the extremal diameter is 0.25 A^{-1} in the [110] direction. This was the only observation which could not be explained without invoking the metallic properties of iron.

The transverse susceptibility below the critical temperature increased with increasing temperature. However at non-zero wave vectors the susceptibility did not seem to vary rapidly as the critical temperature was approached from below.

No evidence was found to support the existence of a diffusive mode below the critical temperature. It was estimated that if it does exist, it is very much less intense than the spin-wave modes. This is in accord with previous observations on isotropic ferromagnets.

At temperatures equal to and above the critical temperature there was only a diffusive peak present with no evidence of remnant spin waves. At the critical temperature the width of the diffusive mode was found to vary as the wave vector q to the power 2.8±0.3, in agreement with the predictions of dynamic scaling and with earlier measurements in nickel. Our data is also in satisfactory agreement with the earlier measurements in iron. Above the critical temperature the temperature and the wave-vector dependence of the width of the diffusive mode supported the theoretical scaling function of Résibois and Piette (1970). It was also found that the susceptibility was adequately described by the Ornstein-Zernike form.

The experimental results showed that the ferromagnetic phase transition in iron is reflected in a rapid change of the spin dynamics near the critical temperature. This is in accord with observations in other systems and indicates that a study of the dynamical properties of a spin system near the critical temperature will give useful information about the critical phase transition.

From the available experimental observations it appears that the detailed behaviour of the spin dynamics near the critical temperature is different for the various types of magnetic systems. This contrasts with the observation that in general the static properties of magnetic phase transitions

are system independent. Although the details are different, a common feature of the various magnetic systems studied so far is that in general the observed behaviour of the spin dynamics is in accord with dynamic scaling predictions for a Heisenberg Hamiltonian. The predictions of dynamic scaling are also consistent with the theory of critical spin fluctuations in magnetic systems, above the critical temperature, of Résibois and Piette. Although the underlying principles of the dynamic scaling hypothesis have not been justified theoretically, it is nevertheless useful in the study of the critical magnetic phase transitions.

BIBLIOGRAPHY

J. Als-Nielsen, Phys. Rev. Letters 25, 730 (1970).

J. Als-Nielsen and O. W. Dietrich, Phys. Rev. 153, 717 (1967).

J. Als-Nielsen, O. W. Dietrich, W. Kunmann, and L. Passell, Phys. Rev. Letters 27, 741 (1971).

S. Arajs and R. V. Colvin, J. Appl. Phys. 35, 2424 (1964).

S. Arajs, B. L. Tehan, E. E. Anderson, and A. A. Stelmach, Intern. J. Magnetism 1, 41 (1970).

A. S. Arrott, and B. Heinrich, and J. E. Noakes, paper presented at the 18th Annual Conference on Magnetism and Magnetic Materials, A.I.P., Denver, November 1972 (In press).

G. E. Bacon, Neutron Diffraction, 2nd ed., Oxford (1962).

D. Bally, B. Grabcev, A. M. Lungu, M. Popovici, and M. Totia, J. Phys. Chem. Solids 28, 1947 (1967).

R. G. Bowers and M. E. Woolf, Phys. Rev. 177, 917 (1969).

B. N. Brockhouse, Inelastic Scattering of Neutrons in Solids and Liquids (IAEA, Vienna, 1961) p. 113.

B. N. Brockhouse, G. A. deWit, E. D. Hallman, and J. M. Rowe, Neutron Inelastic Scattering, Vol. II. (IAEA, Vienna, 1968). p. 259.

M. F. Collins, V. J. Minkiewicz, R. Nathans, L. Passell, and G. Shirane, Phys. Rev. 179, 417 (1969).

M. F. Collins and D. H. Saunderson, J. Appl. Phys. 41, 1433 (1970).

M. J. Cooper and R. Nathans, Acta Cryst. 23, 357 (1967).

G. Develey, Compt. Rend. 260, 4951 (1965).

C. Domb and D. L. Hunter, Proc. Phys. Soc. (London) 86, 1147 (1965).

R. R. Dymond and B. N. Brockhouse, Instrumentation for Neutron Inelastic Scattering Research (IAEA, Vienna, 1970), p. 105.

R. R. Dymond, private communication.

F. J. Dyson, Phys. Rev. 102, 1217 (1956); 102, 1230 (1956).

M. Ericson and B. Jacrot, J. Phys. Chem. Solids 13, 235 (1960).

M. Ferer, M. A. Moore, and M. Wortis, Phys. Rev. B4, 3954 (1971).

M. E. Fisher, Rept. Progr. Phys. 30, 615 (1967).

A. V. Gold, L. Hodges, P. T. Panousis, and D. R. Stone, Intern. J. Magnetism 2, p. 357 (1971).

Y. V. Gulayev, Zh. Eksp. Teor. Fiz. Pis. Red. (JETP Letters 2, 1 (1965).

B. I. Halperin and P. C. Hohenberg, Phys. Rev. 177, 952 (1969); 188, 898 (1969).

A. B. Harris, Phys. Rev. 175, 674 (1968).

J. A. Hertz, Intern. J. Magnetism 1, 253 (1971).

T. Holstein and H. Primakoff, Phys. Rev. 58, 1098 (1940).

E. Ising, Z. Phys. 31, 253 (1925).

B. Jacrot, J. Konstantinovic, G. Parette, and D. Cribier, Inelastic Scattering of Neutrons in Solids and Liquids (IAEA, Vienna, 1963) p. 317.

L. P. Kadanoff, Physics 2, 263 (1966).

L. P. Kadanoff, W. Götze, D. Hamblen, R. Hecht, E. A. S. Lewis, V. V. Palciauskas, M. Rayl, J. Swift, D. Aspnes, and J. Kane, Rev. Mod. Phys. 39, 395 (1967).

R. Kubo, J. Phys. Soc. Japan 12, 570 (1957).

L. D. Landau and E. M. Lifshitz, Statistical Physics, 2nd ed. Pergamon Press, Oxford (1969).

W. Marshall and S.W. Lovesey, Theory of Thermal Neutron Scattering, Oxford Univ. Press (1971).

W. Marshall and G. Murray, J. Phys. C. (Sol. St.) 2, 539 (1969).

V.J. Minkiewicz, M. F. Collins, R. Nathans, and G. Shirane, Phys. Rev. 182, 624 (1969).

V. J. Minkiewicz, Intern. J. Magnetism 1, 149 (1971).

V. J. Minkiewicz, K. Gesi, and E. Hirahara, J. Appl. Phys. 42, 1374 (1971).

M.A. Moore, D. Jasnow, and M. Wortis, Phys. Rev. Letters 22, 940 (1969).

Neutron Cross Sections, BNL 325, Second edition, Supplement No. 2 Vol. II A.

J. E. Noakes and A. Arrott, J. Appl. Phys. 39, 1235 (1968).

J. E. Noakes, N. E. Tornberg, and A. Arrott, J. Appl. Phys. 37, 1264 (1966).

L. Onsager, Phys. Rev. 65, 117 (1944).

H. Palevsky and D. J. Hughes, Phys. Rev. 92, 202 (1953).

G. Parette and R. Kahn, J. de Phys. 32, 447 (1971).

L. Passell, K. Blinowski, T. Brun, and P. Nielsen, Phys. Rev. 139 , A1866 (1965).

L. Passell, J. Als-Nielsen, and O. W. Dietrich, Brookhaven National Laboratories, Report No. 16597 (1972).

W. B. Pearson, Vol. 2, A Handbook of Lattice Spacings and Structures of Metals and Alloys. Pergamon Press, (1967).

R. S. Preston, J. Appl. Phys. 39, 1231 (1968).

G. Reiter, Phys. Rev. Letters 20, 1170 (1968).

P. Résibois and C. Piette, Phys. Rev. Letters 24, 514 (1970).

N. Ridley and H. Stuart, J. Phys. D. (Appl. Phys.) 1, 1291 (1968).

V. L. Sailor, H. L. Foote, Jr., H. H. Landon, and R. E. Wood, Rev. Sci. Instr. 27, 26 (1956).

M. P. Schulhof, R. Nathans, P. Heller, and A. Linz, Phys. Rev. B4, 2254 (1971).

G. Shirane, V. J. Minkiewicz and R. Nathans, J. Appl. Phys. 39, 383 (1968).

S. Spooner and B. L. Averbach, Phys. Rev. 142, 291 (1966).

G. L. Squires, Proc. Phys. Soc. (London) A67, 248 (1954).

H. E. Stanley, Introduction to Phase Transitions and Critical Phenomena, Oxford Univ. Press (1971).

R. L. Stephenson and P. J. Wood, J. Phys. C. (Sol. St.) 3, 90 (1970).

M. W. Stringfellow, J. Phys. C. (Sol. St.) 1, 950 (1968).

A. Tucciarone, H. Y. Lau, L. M. Corliss, A. Delapalme, and J. M. Hastings, Phys. Rev. B4, 3206 (1971).

V. G. Vaks, A. I. Larkin and S. A. Pikin, Zh. Eksp. Teor. Fiz. (U.S.S.R.) 53, 1089 (1967) (Soviet Phys. JETP 26, 647 (1968)).

J. D. Van der Waals, Ph.D. Thesis, University of Leiden, (1873).

L. Van Hove, Phys. Rev. 95, 249 (1954); 95, 1374 (1954).

P. Weiss, J. Phys. Radium, Paris 6, 667 (1907).

B. Widom, J. Chem. Phys. 43, 3892 (1965); 43, 3898 (1965).

M. K. Wilkinson and C. G. Shull, Phys. Rev. 103, 516 (1956).

K. G. Wilson and M. E. Fisher, Phys. Rev. Letters 28, 240 (1972).

K. G. Wilson, Phys. Rev. Letters 28, 548 (1972).